Dynamics of Cold Atoms in High Quality Cavities

A THESIS

submitted for the Award of Ph.D degree of

Mohan Lal Sukhadia University

in the

Faculty of Science

BY

R. Arun

Under the Supervision of

Professor G.S. Agarwal
Director, Physical Research Laboratory

DEPARTMENT OF LASER PHYSICS AND QUANTUM OPTICS
PHYSICAL RESEARCH LABORATORY, AHMEDABAD.

MOHANLAL SUKHADIA UNIVERSITY, UDAIPUR

Year of submission: 2002

CERTIFICATE

This is to certify that the thesis entitled “Dynamics of Cold Atoms in High Quality Cavities” submitted for the award of the degree of Doctor of Philosophy of Mohanlal Sukhadia University in the faculty of Science is a record of bonafide investigations carried out by Shri. R. Arun under my supervision and guidance.

This is an original piece of work on which no one has been awarded a degree in this University or in any other University.

The literary presentation of the thesis is satisfactory and it is in a form suitable for publication. The work presented in the thesis has been done after registration in this University.

Further, the candidate has put in attendance of more than 200 days in my institution as required under rule 7(b) and thus completed the residential requirement.

Professor G.S. Agarwal
(SUPERVISOR)

to

My Parents & My Teachers

Contents

Acknowledgement

I take this opportunity to express my sincere gratitude to Prof. G. S. Agarwal for his excellent guidance, encouraging support and many valuable suggestions. I have benefited much from his clarity of physical ideas, working on fundamental problems and overall his clear approach in solving the problems. His professional, strict behavior and his exceptional capacity to work on many different areas of the subject always inspires me to take research as a serious part of life. I would also like to thank Dr. D. R. Kulkarni for teaching me a beautiful programming style in Fortran. It has been of great help to me in all my work.

I thank all my college teachers of master degree course for their excellent teaching of basic physics.

Finally, I thank my parents for their support and encouragement all along.

R. Arun

Abstract

In chapter 1, the basic theory of radiation-matter interaction is discussed. The field quantization in a cavity, density matrix formalism, and the derivation of interaction Hamiltonian are presented. In Sec. 1.2, an overview of important atom-cavity coupling effects such as modified atomic spontaneous emission rate, vacuum field Rabi splittings, micromaser, etc. is presented. In Sec. 1.3, a general theoretical framework is introduced for studying atom-cavity interaction when the atomic motion is quantized. Interesting effects of quantized atomic motion like reflection of ultracold atoms from a cavity vacuum, micromaser pumped with ultracold atoms, etc. are also discussed.

In chapter 2, reflection and transmission of an ultracold two-level atom from the potential induced by a single mode cavity is considered. The transmission time of the atom through the cavity is calculated using the Wigner's stationary phase method. Numerically, it is shown that the peak of the transmitted wave packet occurs at the instant given by the expression for phase time. New features reported in this chapter are : (a) Negative values for the phase tunneling time, (b) Sub- and super-classical behaviors of phase time, and (c) Splitting of the atomic wave packet during propagation.

In chapter 3, transmission of an ultracold two-level atom through the potentials induced by a system of two cavities in vacuum state is analyzed. It is shown that the transmission probability of atoms exhibits new resonances for the two-cavity system in comparison to the single-cavity case. The origin of these new resonances is explained as due to resonant tunneling of atoms through the potentials induced by the cavities. Other key findings in this chapter are : (a) Demonstration of resonant tunneling of the atom through a double barrier potential induced by the two-cavity system, (b) Quantum interferences in resonant tunneling, and (c) Coupling of the cavities by the transmission of the atom.

We next investigate the maser action of ultracold atoms by considering the

interaction of a beam of ultracold atoms with a bimodal cavity. In chapter 4, Λ-type three-level atoms in the excited state are considered in the interaction. It is shown that the two fields in the bimodal cavity are strongly anti-correlated due to the stimulated one-photon emissions of the incident atoms. It is also shown that the photon emissions from the atoms can occur either by reflection or transmission of incident atoms through the cavity. In chapter 5, we consider Ξ-type three-level atoms in the excited state for the maser action in the bimodal cavity. Here it is shown that an atom can amplify the fields in the cavity either by an one-photon emission or by a two-photon emission. The key findings in this chapter are : (a) Prediction of gain regions due to the two-photon emission when the corresponding one-photon transition is forbidden in the atom-field interaction, (b) Sub- and super-Poissonian behaviors of the steady-state fields in the cavity, and (c) Generation of Poissonian photon distributions in the cavity by the stimulated two-photon emissions of incident atoms and their transmission and reflection from the cavity.

Chapter 1

Introduction

1.1 Interaction of Radiation with Matter

1.1.1 Field Quantization in a Cavity

In regions of free space where there are no charges or currents, the electric and magnetic fields are coupled by the four fundamental Maxwell equations (in M.K.S units) given by [1]

$$\begin{aligned} \vec{\nabla}.\vec{D} &= 0, \quad \vec{\nabla}.\vec{B} = 0, \\ \vec{\nabla} \times \vec{E} &= -\frac{\partial \vec{B}}{\partial t}, \\ \vec{\nabla} \times \vec{H} &= \frac{\partial \vec{D}}{\partial t}, \end{aligned} \tag{1.1}$$

where $\vec{E}$, $\vec{B}$ are the electric, magnetic-induction field vectors at the space-time point $(\vec{r}, t)$. The electric displacement $\vec{D}$ and the magnetic field $\vec{H}$ have relations $\vec{D} = \epsilon_o \vec{E}$, $\vec{B} = \mu_o \vec{H}$ through the electric permittivity ϵ_o and magnetic permeability μ_o. For the case of electromagnetic fields inside a cavity, the Maxwell equations are solved for the fields $\vec{E}$, $\vec{H}$ subject to suitable boundary conditions on the cavity walls. In this thesis, we deal with quantized electromagnetic fields in cavities by treating the electric and magnetic fields as quantum mechanical operators. The quantization of fields in the cavity requires the replacement of classical variables by quantum mechanical operators with commutation relations among them. Before this quantum - classical correspondence is made, the classical electric and magnetic fields in the cavity are first expanded in a suitable form in terms of normal mode functions of the fields. The normal mode functions (dimensionless) $\vec{U}_\alpha(\vec{r})$, $\vec{W}_\alpha(\vec{r})$ ($\alpha = 1, 2, ...$) of the cavity for the fields $\vec{E}$, $\vec{H}$ satisfy the Helmholtz equations

$$\begin{aligned} \vec{\nabla}^2 \vec{U}_\alpha(\vec{r}) \ + \ \frac{\omega_\alpha^2}{c^2}\,\vec{U}_\alpha(\vec{r}) &= 0 \ , \\ \vec{\nabla}^2 \vec{W}_\alpha(\vec{r}) \ + \ \frac{\omega_\alpha^2}{c^2}\,\vec{W}_\alpha(\vec{r}) &= 0 \ , \end{aligned} \tag{1.2}$$

subjected to the boundary conditions that the tangential component of $\vec{E}$ and the normal component of $\vec{H}$ vanish on the cavity walls. The frequency of the α-th cavity mode is denoted by ω_α and $c \equiv 1/\sqrt{\epsilon_o \mu_o}$ is the velocity of light in vacuum. In general, there exists a discrete set of modes $\{\alpha\}$ for the fields depending on the cavity geometry and its size. The electric and magnetic field modes are related by simple curl equations [2]

$$\vec{\nabla} \times \vec{U}_\alpha \ = \ \frac{\omega_\alpha}{c}\,\vec{W}_\alpha \ , \qquad \vec{\nabla} \times \vec{W}_\alpha \ = \ \frac{\omega_\alpha}{c}\,\vec{U}_\alpha \ . \tag{1.3}$$

The functions $\vec{U}_\alpha$, $\vec{W}_\alpha$ (dimensionless) have orthogonality properties of the form

$$\begin{aligned} \int_V \vec{U}_\alpha(\vec{r}).\vec{U}_\beta(\vec{r})\ d^3\vec{r} &= V\ \delta_{\alpha,\beta} \ , \\ \int_V \vec{W}_\alpha(\vec{r}).\vec{W}_\beta(\vec{r})\ d^3\vec{r} &= V\ \delta_{\alpha,\beta} \ , \end{aligned} \tag{1.4}$$

where the integration extends over the cavity volume V and the Kronecker delta function $\delta_{\alpha,\beta}$ is unity if $\alpha = \beta$, zero if $\alpha \neq \beta$. The normal mode functions $\vec{U}_\alpha$, $\vec{W}_\alpha$ also form a complete set in the sense that any arbitrary fields $\vec{E}$, $\vec{H}$ in the cavity can be expanded as a sum over all the modes :

$$\begin{aligned} \vec{E}(\vec{r}, t) &= \frac{1}{\sqrt{\epsilon_o V}} \sum_\alpha p_\alpha(t) \vec{U}_\alpha(\vec{r}) \ , \\ \vec{H}(\vec{r}, t) &= -\frac{1}{\sqrt{\mu_o V}} \sum_\alpha \omega_\alpha q_\alpha(t) \vec{W}_\alpha(\vec{r}) \ . \end{aligned} \tag{1.5}$$

Here the time dependent amplitudes $p_\alpha(t)$, $q_\alpha(t)$ accounts for the temporal variation of the fields in the cavity.

The total energy $H(t)$ stored in the cavity is

$$\begin{aligned} H(t) &= \frac{1}{2} \int_V \left(\epsilon_o \vec{E}^2(\vec{r}, t) + \mu_o \vec{H}^2(\vec{r}, t) \right)\ d^3\vec{r} \ , \\ &= \frac{1}{2} \sum_\alpha \left(p_\alpha^2(t) + \omega_\alpha^2 q_\alpha^2(t) \right) \ . \end{aligned} \tag{1.6}$$

This equation expresses the total energy of radiation field as a sum of independent, one-dimensional harmonic oscillator energies. Each mode α of the field therefore behaves dynamically similar to a classical harmonic oscillator of unit mass with position $q_\alpha(t)$ and momentum $p_\alpha(t)$. In quantum mechanics, the quantum state of fields in the cavity is described by converting classical oscillators into quantum oscillators. Then, the classical functions $q_\alpha(t)$, $p_\alpha(t)$ become Hermitian operators in the Heisenberg picture with the following commutation relations among them :

$$\begin{aligned} [q_\alpha(t), q_\beta(t)] &= [p_\alpha(t), p_\beta(t)] = 0 \ , \\ [q_\alpha(t), p_\beta(t)] &= i\hbar\delta_{\alpha,\beta} \ . \end{aligned} \tag{1.7}$$

Note that the operators $q_\alpha(t)$, $p_\alpha(t)$ are time dependent only in the Heisenberg picture of quantum evolution of the field. In the Schrödinger picture, all the operators are fixed in time and only quantum state of the system evolves with time. We follow this convention in all the following discussions that unless otherwise stated, all the operators without time dependence are in the Schrödinger picture. The Hamiltonian operator for the total energy in the cavity obtained from Eq. (1.6) becomes the sum of energy operators for harmonic oscillators in all the modes. Since the allowed energies of quantum harmonic oscillators are discrete, the field in the cavity takes only discrete values of energy on quantization. The discreteness in the energy of radiation field is a distinct feature of quantum theory from the classical theory of radiation which admits all possible non-negative values of energy. For the quantum harmonic oscillators, the energy eigenstates are known to be eigenstates of the number operator $a_\alpha^\dagger(t)a_\alpha(t)$ where the operators $a_\alpha(t)$ and its Hermitian conjugate $a_\alpha^\dagger(t)$ are defined as

$$\begin{aligned} a_\alpha(t) &= \sqrt{\frac{\omega_\alpha}{2\hbar}}\, q_\alpha(t) + \frac{i}{\sqrt{2\hbar\omega_\alpha}}\, p_\alpha(t) \ , \\ a_\alpha^\dagger(t) &= \sqrt{\frac{\omega_\alpha}{2\hbar}}\, q_\alpha(t) - \frac{i}{\sqrt{2\hbar\omega_\alpha}}\, p_\alpha(t) \ . \end{aligned} \tag{1.8}$$

With these non-Hermitian operators $a_\alpha(t)$, $a_\alpha^\dagger(t)$ the Hamiltonian operator for the total energy stored in the cavity is obtained using Eq. (1.6) to be

$$H = \sum_\alpha \hbar\omega_\alpha \left(a_\alpha^\dagger(t)a_\alpha(t) + \frac{1}{2} \right) \ . \tag{1.9}$$

The energy eigenstate $|..., n_\alpha...., n_\beta...\rangle$ (Dirac notation) in which the numbers n_α can take values from the set of non-negative integers $\{0, 1, 2, ...\infty\}$, are eigenstates of the harmonic oscillator number operator $a_\alpha^\dagger(t)a_\alpha(t)$ in each mode α with the properties

$$
\begin{aligned}
a_\alpha\ |....0, ...0, ...\rangle = 0 &= \langle ..., 0...0, ...|\ a_\alpha^\dagger\ , \\
a_\alpha\ |.....n_\alpha, ...n_\beta, ...\rangle &= \sqrt{n_\alpha}\ |.....n_\alpha - 1, ...n_\beta, ...\rangle\ , \\
a_\alpha^\dagger\ |.....n_\alpha, ...n_\beta, ...\rangle &= \sqrt{n_\alpha + 1}\ |.....n_\alpha + 1, ...n_\beta, ...\rangle\ , \\
a_\alpha^\dagger a_\alpha\ |....n_\alpha, ...n_\beta, ...\rangle &= n_\alpha\ |....n_\alpha, ...n_\beta, ...\rangle\ , \\
H\ |....n_\alpha, ...n_\beta, ...\rangle &\equiv \sum_\alpha \hbar\omega_\alpha \left(a_\alpha^\dagger a_\alpha + \frac{1}{2}\right)\ |....n_\alpha, ...n_\beta, ...\rangle\ , \\
&= \left[\sum_\alpha \hbar\omega_\alpha \left(n_\alpha + \frac{1}{2}\right)\right]\ |....n_\alpha, ...n_\beta, ...\rangle\ . \qquad (1.10)
\end{aligned}
$$

Here we have neglected the time argument for the operators a_α, $a_\alpha^\dagger$ which refers to the Schrödinger picture operators. Since the operators a_α and $a_\alpha^\dagger$ decrease and increase the photon occupation number in the mode α by one, they are known respectively as annihilation and creation operators.

When the occupation numbers $n_\alpha = 0$ in all the modes α, the cavity field is in the vacuum state with the lowest energy $\sum_\alpha \hbar\omega_\alpha/2$. For the purpose of studying the time evolution of the field and its interaction with atoms, this vacuum contribution to energy of the cavity can be neglected by setting the energy minimum to zero. The atom-field interaction in the cavity will be dominantly through electric-dipole coupling which is a coupling between the atomic dipole and the quantized electric field in the cavity. The quantized electric field in the cavity is obtained using Eqs. (1.5) and (1.8) to be

$$\vec{E}(\vec{r}) = \sum_\alpha (-i)\left(\frac{\hbar\omega_\alpha}{2\epsilon_o V}\right)^{\frac{1}{2}} \left(a_\alpha - a_\alpha^\dagger\right) \vec{U}_\alpha(\vec{r}) \qquad (1.11)$$

Since the electric field operator is linear in the operators a_α and $a_\alpha^\dagger$, quantum expectation value of the electric field in vacuum state ($|0\rangle \equiv |....0, ...0, ...\rangle$) is zero. But variance of the field operator in vacuum state, which is defined as $\Delta\vec{E}^2(\vec{r}) \equiv \langle 0|\vec{E}^2(\vec{r})|0\rangle - \langle 0|\vec{E}(\vec{r})|0\rangle^2$, can be shown to be non-zero and even infinite for an unbounded set of modes $\{\alpha\}$. The infinite fluctuations of the fields in vacuum state is a difficulty in quantum electrodynamics (QED), the resolution of which is discussed extensively in text books. In free space, the vacuum fluctuations of the fields account for the Spontaneous decay of an excited atom, Lamb shift, and Casimir force between conductors [3]. We consider the interaction of atoms with single and two mode cavities which have only finite fluctuations of the fields in vacuum state. This feature indicates that an excited atom inside a cavity can be induced for photon emission even when the cavity is initially in vacuum state. The change in state of the cavity field after the atom-field interaction will be obtained either in the probability amplitude approach or in the density matrix treatment of the atom-field dynamics. In the density matrix approach, it is relatively easier to include the cavity losses which occur in practice due to leakage of photons, inelastic collisions of photons with the cavity walls, etc,.

1.1.2 Density Matrix Formalism

A given physical system is characterized by a state vector $|\Psi(t)\rangle$ whose time evolution is governed by the Schrödinger wave equation

$$i\hbar\frac{\partial|\Psi(t)\rangle}{\partial t} = H|\Psi(t)\rangle \ . \tag{1.12}$$

Here H is the total Hamiltonian operator for the system which include all its interaction with external agencies. The interactions may be explicitly time dependent like the interaction of an atom with a classical, monochromatic wave and therefore the Hamiltonian depends explicitly on time in general. The state vector $|\Psi(t)\rangle = \sum_i C_i(t)|i\rangle$ of the system is usually expanded in terms of eigenstates $\{|i\rangle,\ i = 1, 2, ..\}$ of the non-interacting free part of the Hamiltonian. The expectation value of an operator A at the instant t is given by

$$\langle A\rangle_t = \langle\Psi(t)|A|\Psi(t)\rangle = \sum_{n,p} C_n^*(t)C_p(t)A_{np} \ , \tag{1.13}$$

where $A_{np} = \langle n|A|p\rangle$ are the matrix elements of the operator A in the basis $\{|i\rangle,\ i = 1, 2, ..\}$. The coefficients $C_n^*(t)C_p(t)$ in the above sum can be interpreted as the matrix element of an operator $|\Psi(t)\rangle\langle\Psi(t)|$ between the states $|p\rangle$ and $|n\rangle$, i.e., $C_n^*(t)C_p(t) = \langle p|\Psi(t)\rangle\langle\Psi(t)|n\rangle$. The operator $\rho(t) \equiv |\Psi(t)\rangle\langle\Psi(t)|$ thus defined is known as the density operator of the system. The matrix formed by the matrix elements

$\rho_{np}(t)$ of the density operator is called the density matrix with the properties (a) it is hermitian, (b) Tr$\rho(t) = 1$, and (c) positive definite operator, i.e., all its eigenvalues λ_α are such that $\lambda_\alpha \geq 0$. The expectation value of any operator A in terms of $\rho(t)$ is given by

$$\langle A \rangle_t = \langle \Psi(t)|A|\Psi(t)\rangle = \text{Tr}(\rho(t)A) = \text{Tr}(A\rho(t)) \ . \tag{1.14}$$

Note that $\rho^2(t) = \rho(t)$ and Tr $\left[\rho^2(t)\right] = 1$ in a pure state $|\Psi(t)\rangle$ of the system.

In many physical situations of practical interest, the state $|\Psi(t)\rangle$ of the system is not known but only the probability p_l for the system to be in the state $|\Psi_l(t)\rangle$ is known. For example, the state of radiation field in a cavity which is in equilibrium with a finite temperature thermal reservoir, can be characterized only by a statistical distribution of photon numbers. The density operator of the system in this mixed state (ensemble of states) is written as

$$\rho(t) = \sum_l p_l |\Psi_l(t)\rangle\langle\Psi_l(t)| \ , \tag{1.15}$$

with $\sum_l p_l = 1$. When $p_l = \delta_{lm}$ for some m, the density operator reduces to the pure state (deterministic) density operator $|\Psi_m(t)\rangle\langle\Psi_m(t)|$. The expectation value of an operator A is still given by Eq. (1.14) but the average $\langle A\rangle_t$ would imply an ensemble average in the mixed state. Also for the mixed state $\rho^2(t) \neq \rho(t)$ and Tr$\rho^2 < 1$ with Tr$\rho(t) = 1$. It can be shown further from the Schrödinger equation that mixed state density operator in Eq. (1.15) satisfies the differential equation

$$\dot{\rho}(t) = -\frac{i}{\hbar}[H, \rho] \ . \tag{1.16}$$

Equation (1.16) is often called as Liouville or Von Neumann equation of motion for the density matrix. It is more generally applicable than the Schrödinger Eq. (1.12) as it contains both the statistical as well as quantum description of the system. The density operator approach is particularly helpful when the system plus a reservoir interaction involves quantized variables of both the system and the reservoir. In this case, the density operator in Eq. (1.16) describes a combined state of the system plus reservoir and the density operator of the system alone can be obtained by reduced density operator techniques. For the radiation field in a cavity interacting with a thermal reservoir, the total reduced density operator $\rho(t)$ of the cavity field factories into the product $\rho(t) = \prod_\alpha \rho_\alpha(t)$ of the density

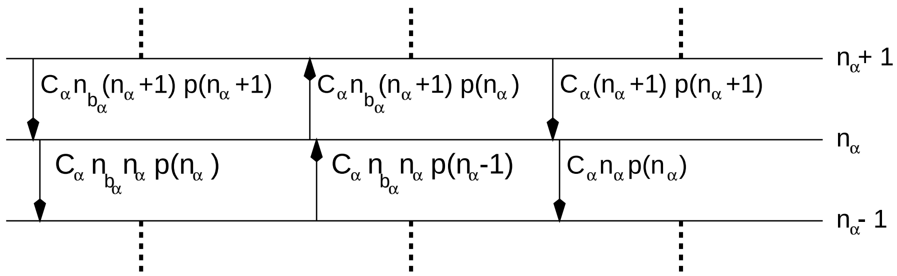

Figure 1.1: Probability flow diagram for a damped cavity mode

operators for all the modes. This implies that all the modes of the cavity behave independently during interaction with the reservoir. The reduced density operator $\rho_\alpha(t)$ describing the field in mode α is obtained by the action of a Liouville operator L_α on the total density operator $\rho(t)$ and then tracing over the other mode photon states :

$$\begin{aligned}\dot{\rho}_\alpha(t) = \mathrm{Tr}[L_\alpha\rho(t)] \;\equiv\; & \frac{1}{2}C_\alpha(n_{b_\alpha}+1)(2a_\alpha\rho_\alpha a_\alpha^\dagger - a_\alpha^\dagger a_\alpha\rho_\alpha - \rho_\alpha a_\alpha^\dagger a_\alpha) \\ & + \frac{1}{2}C_\alpha n_{b_\alpha}(2a_\alpha^\dagger\rho_\alpha a_\alpha - a_\alpha a_\alpha^\dagger\rho_\alpha - \rho_\alpha a_\alpha a_\alpha^\dagger)\ , \qquad (1.17)\end{aligned}$$

where n_{b_α} is the number of thermal photons in mode α which depends upon the temperature of the reservoir and C_α is the damping rate of this mode. The photon probability distribution $p(n_\alpha)$ in mode α defined as $p(n_\alpha) \equiv \langle n_\alpha|\rho_\alpha(t)|n_\alpha\rangle$ evolves in time as

$$\begin{aligned}\dot{p}(n_\alpha) \;=\; & C_\alpha(n_{b_\alpha}+1)[(n_\alpha+1)p(n_\alpha+1) - n_\alpha p(n_\alpha)] \\ & + C_\alpha n_{b_\alpha}[n_\alpha p(n_\alpha-1) - (n_\alpha+1)p(n_\alpha)]\ . \qquad (1.18)\end{aligned}$$

This equation behaves similar to the rate equation for a probability and the various terms on the right hand side represent the probability flow into and out of the number state $|n_\alpha\rangle$ of fixed photon number n_α as shown in Fig. 1.1. The term $C_\alpha(n_\alpha+1)p(n_\alpha+1)$ represents the flow the probability from the state $|n_\alpha+1\rangle$ to the state $|n_\alpha\rangle$ due to field decays through the cavity walls. Since the probability flows into the state $|n_\alpha\rangle$, this term is positive in Eq. (1.18). The other terms (n_{b_α} terms) indicate the random leakage of photons into and out of the cavity due to interaction with the thermal reservoir. They induce probability flows in both the directions $|n_\alpha+1\rangle \leftrightarrow |n_\alpha\rangle \leftrightarrow |n_\alpha-1\rangle$ as indicated in the probability flow diagram (Fig. 1.1).

1.1.3 Interaction Hamiltonian

Consider an one electron atom with its nucleus at position $\vec{r}_o$ in interaction with quantized fields in a cavity. The Hamiltonian of the atom-cavity field interaction is obtained by replacing the classical functions with quantum mechanical operators in the classical Hamiltonian of the system. The quantum mechanical Hamiltonian of the atom-cavity interaction including the quantization of cavity fields is thus obtained in the Schrödinger picture to be

$$H = \sum_{\alpha} \hbar\omega_\alpha a_\alpha^\dagger a_\alpha + \frac{1}{2m_e}[\vec{p}_e - e\vec{A}(\vec{r}_o + \vec{r})]^2 + V(r) + e\Phi(\vec{r}_o + \vec{r}) \ , \tag{1.19}$$

where m_e is the mass of the electron of charge e and p_e is its canonical momentum. The electron is bound to the atomic nucleus by a binding potential $V(r)$ and its position relative to the nucleus is described by the vector operator $\vec{r}$. The operator $\vec{A}(\vec{r})$ $[\Phi(\vec{r})]$ represents the vector [scalar] potentials for the quantized fields in the cavity which are dependent on the gauge chosen. The gauge independent quantities are the electric $\vec{E}(\vec{r})$ and magnetic $\vec{H}(\vec{r})$ fields. Generally, it is convenient to work in the Coulomb gauge in which $\Phi = 0$ and $\vec{\nabla}.\vec{A} = 0$. The vector potential operator $\vec{A}(\vec{r})$ can be expanded in terms of normal modes similar to Eq. (1.11). Further, one can make dipole approximation to the Hamiltonian when the size of the atom is much smaller than the wavelengths involved in the normal mode expansion of operator $\vec{A}(\vec{r})$. In this case, it is a good approximation to substitute $\vec{A}(\vec{r}_o + \vec{r}) = \vec{A}(\vec{r}_o)$ for the vector potential in Eq. (1.19), where $\vec{r}_o$ is the position of the atomic nucleus. Physically, this means that in the dipole approximation, the fields acting on the whole atom are uniform about the nucleus at position $\vec{r}_o$. The Hamiltonian H together with the state $|\Psi(\vec{r}, t)\rangle$ obeys the Schrödinger equation (1.12). The interaction Hamiltonian Eq. (1.19) expressed in terms of the vector potential $\vec{A}(\vec{r}_o)$ is called as the minimal coupling form of the atom-field interaction. Besides this, another form known as multipolar Hamiltonian is found to be more convenient for treating the interaction between the atom and quantized fields. This form can be derived in the dipole approximation from Eq. (1.19) by a unitary transformation [4]

$$|\Psi(\vec{r}, t)\rangle = \exp\left[\frac{i}{\hbar}\vec{d}.\vec{A}(\vec{r}_o)\right] |\chi(\vec{r}, t)\rangle \ . \tag{1.20}$$

Here $\vec{d} = e\vec{r}$ is the dipole moment operator of the atom. Substituting this into the Schrödinger equation (1.12) and after doing some algebras, the equation for the time evolution of state $|\chi(\vec{r},t)\rangle$ can be found to be

$$\begin{aligned} i\hbar\frac{\partial}{\partial t}|\chi(\vec{r},t)\rangle &= \left(\sum_\alpha \hbar\omega_\alpha a^\dagger_\alpha a_\alpha + \frac{\vec{p}_e^{\,2}}{2m_e} + V(r) - \vec{d}.\vec{E}(\vec{r}_o)\right)|\chi(\vec{r},t)\rangle \ , \\ &= (H_o + H_I)\,|\chi(\vec{r},t)\rangle \ , \end{aligned} \tag{1.21}$$

where $H_o = \sum_\alpha \hbar\omega_\alpha a^\dagger_\alpha a_\alpha + \frac{\vec{p}_e^{\,2}}{2m_e} + V(r)$ is the free Hamiltonian of the atom-cavity system, $H_I = -\vec{d}.\vec{E}(\vec{r}_o)$ with $\vec{E}(\vec{r}_o)$ being the electric field in Eq. (1.11) . In deriving Eq. (1.21), we have omitted a constant term in the Hamiltonian. Note that in this multipolar Hamiltonian, the interaction part H_I takes the form of a dipole coupling with the electric field in the dipole approximation. We shall use this dipolar interaction and the transformed Schrödinger equation (1.21) in all subsequent studies of atom-field interaction in cavities.

1.2 Atom-Field Interaction in a Cavity

The interaction of atoms with quantized, electromagnetic fields lead to many remarkable effects such as irreversible atomic decay, Lamb shift, Casimir effects, etc. Spontaneous decay of an atom, which is a manifestation of vacuum fluctuations, depends also on the mode structure of the electromagnetic vacuum in which the atom is placed. In free space vacuum, the spontaneous emission of radiation from an excited level of an atom is characterized by specific decay rates to lower lying levels of the atomic transitions. However, the situation becomes different when the atom is confined inside a cavity. The density of field modes available for the interaction of the atom gets modified inside the cavity. The spontaneous photon emission from the atom can be made faster or slower by manipulating the density of modes of the cavity field. It can even be made reversible leading to a periodic exchange of photons between the atom and the cavity field. The most fundamental and underlying model for all these studies is a two-level atom interacting with a single mode cavity also known as Jaynes-Cummings (JC) model. In what follows, we will discuss some of the properties of this model and review some experiments done. In the JC model, the center-of-mass position and motion of the atom are treated classically while the atom's interaction with the cavity depends on quantized variables of both the atom and the cavity field.

1.2.1 Jaynes-Cummings Model

When an atom is inside a single mode cavity, only those two atomic levels with transition frequency close to the frequency of the cavity, take part in the interaction. In this case, the atom becomes a two-level atom and the presence of other levels in the atom can be ignored for studying the dynamics of interaction. The interaction of the two-level atom with the single mode cavity was first studied by Jaynes and Cummings [5]. Let $|e\rangle$ and $|g\rangle$ represent the excited and ground energy states of the atom respectively. Using the closure relation $|e\rangle\langle e|+|g\rangle\langle g| = 1$, the free Hamiltonian H_A of the atom and its dipole moment operator $\vec{d}$ can be expanded in the energy basis states $|e\rangle$, $|g\rangle$:

$$\begin{aligned} H_A &= (|e\rangle\langle e| + |g\rangle\langle g|)\, H_A\, (|e\rangle\langle e| + |g\rangle\langle g|) \\ &= E_e|e\rangle\langle e| + E_g|g\rangle\langle g| \ , \\ \vec{d} &= \vec{d}_{eg}|e\rangle\langle g| + \vec{d}_{ge}|g\rangle\langle e| \ , \end{aligned} \tag{1.22}$$

where E_e and E_g are the energies of excited and ground states respectively. In the expansion of dipole moment, diagonal elements $\vec{d}_{ee}$, $\vec{d}_{gg}$ vanish due to parity reasons and the non-diagonal terms $\vec{d}_{eg}$, $\vec{d}_{ge}$ represent the electric dipole matrix elements between the states $|e\rangle$ and $|g\rangle$. The atom interacts with the single mode field in the cavity through its dipole coupling with the quantized, electric field [cf. Eq. (1.11)]

$$\vec{E}(\vec{r}) = (-i)\left(\frac{\hbar\omega}{2\epsilon_o V}\right)^{\frac{1}{2}} \left(a - a^\dagger\right) \vec{U}(\vec{r}) \ . \tag{1.23}$$

The total Hamiltonian of the atom-field interaction in the dipole approximation will be

$$H = \frac{\hbar\nu}{2}\,(|e\rangle\langle e| - |g\rangle\langle g|) + \hbar\omega a^\dagger a - \vec{d}.\vec{E}(\vec{r}_o) \ , \tag{1.24}$$

where $E_e = \hbar\nu/2$ ($E_g = -\hbar\nu/2$) has been assumed for the excited (ground) state energies of the atom and the frequency ω of the cavity is close to the transition frequency $\nu = (E_e - E_g)/\hbar$ of the atom. The interaction term in Eq. (1.24) depends on the atomic position $\vec{r}_o$ through the mode function $\vec{U}(\vec{r}_o)$ of the cavity. It contains four terms of which those corresponding to operators $(a\ |e\rangle\langle g|)$ and $(a^\dagger\ |g\rangle\langle e|)$ represent energy conserving processes. In both the terms, the atom is taken between the states $|e\rangle$ and $|g\rangle$ with an equivalent increase or decrease in the energy of cavity field. The other terms having the operators $(a\ |g\rangle\langle e|)$ and $(a^\dagger\ |e\rangle\langle g|)$ represent energy non-conserving processes. They result in loss or gain of approximately $2\hbar\omega$ in the energy of atom-field system. Dropping these energy non-conserving terms amounts to rotating wave approximation. Thus, the simplified Hamiltonian in the dipole and rotating wave approximations for the atom-field interaction [6] reads as

$$
\begin{aligned}
H &= \frac{\hbar\nu}{2}\left(|e\rangle\langle e| - |g\rangle\langle g|\right) + \hbar\omega a^\dagger a + \hbar\Omega(\vec{r}_o)\Big(|e\rangle\langle g|a + a^\dagger|g\rangle\langle e|\Big)\ , \\
\Omega(\vec{r}_o) &= i\left(\frac{\hbar\omega}{2\epsilon_o V}\right)^{\frac{1}{2}} \frac{\vec{d}_{eg}.\vec{U}(\vec{r}_o)}{\hbar}\ ,
\end{aligned}
\tag{1.25}
$$

in which the coupling strength $\Omega(\vec{r}_o)$ has been set to be real by adjusting the phase of states $|e\rangle$ and $|g\rangle$. The position dependence $\vec{r}_o$ of the coupling strength leads to a dipole force acting on the atom which will be discussed later. The Hamiltonian (1.25) and the state $|\Psi(t)\rangle$ of the atom-cavity system satisfy the Schrödinger equation (1.12). The time evolution of the atom-cavity system can be obtained easily using the eigenstates of the Hamiltonian H and the probability amplitude method. Let $|e,n\rangle$ and $|g,n\rangle$ represent the excited and ground states of the atom with $'n'$ photons present in the cavity field. The exact eigenstates of the Hamiltonian (1.25) can be found to be [5]

$$
\begin{aligned}
\begin{pmatrix} |\phi^+_{n+1}\rangle \\ |\phi^-_{n+1}\rangle \end{pmatrix} &= \begin{pmatrix} \cos\theta_n \\ -\sin\theta_n \end{pmatrix} |g, n+1\rangle + \begin{pmatrix} \sin\theta_n \\ \cos\theta_n \end{pmatrix} |e,n\rangle\ , \\
\tan\theta_n &= 2\Omega\sqrt{(n+1)}\Big/(\Omega_{n,\Delta} - \Delta)\ , \quad \Delta = \nu - \omega\ , \\
\Omega_{n,\Delta} &= \sqrt{(\Delta^2 + 4\Omega^2(n+1))}\ , \quad n = 0, 1, 2, ...,
\end{aligned}
\tag{1.26}
$$

with the corresponding eigenvalues

$$
\hbar\lambda^\pm_{n+1} = \hbar\omega(n+\frac{1}{2}) \pm \frac{\hbar\Omega_{n,\Delta}}{2}\ . \tag{1.27}
$$

The states (1.26) are called the dressed states for the quantized atom-field system. In addition the state $|\phi_0\rangle = |g, 0\rangle$ is also an eigenstate of H with eigen-energy value $-\hbar\nu/2$.

The dressed states $|\phi^{\pm}_{n+1}\rangle$ for atom-field interaction in the cavity form a two-state manifold with 'n' labeling each element. They also serve as a set of basis states in expanding a general state of the atom-cavity system. Since the interaction term in the Hamiltonian (1.25) couples only the states $|e, n\rangle$ and $|g, n+1\rangle$, the dressed states are linear superpositions of these states. For an initial atom-field state $|e, n\rangle$, the state $|\Psi(t)\rangle$ of the atom-cavity system can be expanded in the dressed state basis as

$$|\Psi(t)\rangle = C^{+}_{n}(t)|\phi^{+}_{n+1}\rangle + C^{-}_{n}(t)|\phi^{-}_{n+1}\rangle \ , \tag{1.28}$$

where the coefficients obey $C^{+}_{n}(0) = \sin\theta_n$, $C^{-}_{n}(0) = \cos\theta_n$, the initial conditions at time $t = 0$. Solving for the amplitudes $C^{\pm}_{n}(t)$ using Schrödinger equation (1.12) with these initial conditions and then using Eq. (1.26), the probability $P_{e,n}$ that the atom remains in the initial excited state at time t after the interaction is found to be

$$P_{e,n}(t) = \cos^2\left(\frac{\Omega_{n,\Delta}\ t}{2}\right) + \frac{\Delta^2}{\Omega^2_{n,\Delta}}\sin^2\left(\frac{\Omega_{n,\Delta}\ t}{2}\right) \ . \tag{1.29}$$

The probability $P_{g,n+1}(t)$ that the atom goes to the ground state with an emission of one photon into the cavity is given by $P_{g,n+1}(t) = 1 - P_{e,n}(t)$ due to probability conservation. The solution (1.29) shows that the excited state probability oscillates with an angular frequency $2\Omega\sqrt{n+1}$ for the resonant case $(\Delta = 0)$. As the detuning Δ is increased, the frequency of oscillation increases, but the amplitude decreases. For an initial vacuum $(n = 0)$ field in the cavity, the frequency 2Ω for the resonant case is called as vacuum Rabi frequency - an analogue of frequency in magnetic resonance described by I. I. Rabi [7]. The oscillations in the excited or ground state probability are also known as Rabi oscillations. The Rabi oscillations of the excited state probability for the initial vacuum state is the simplest example of the spontaneous emission of an atom inside the cavity in which the spontaneously emitted photon contributes to the single mode of the cavity. The spectrum of spontaneous emission was shown to exhibit a doublet rather than a single Lorentzian line of free space atom [8]. The splitting of this single line is called as *vacuum field Rabi splitting*. The emission spectrum is also very sensitive to the number of atoms interacting with the cavity and many new lines were predicted even for two atoms [9]. Eberly et al [10] showed that for an initial coherent field in the cavity, the spontaneous and stimulated processes of atomic emission leads to a periodic collapse and revival behavior in the atomic inversion. This was later verified experimentally in Rydberg atomic transitions by Rempe et al [11].

Atom in a damped cavity : In the above analysis, we have not taken the decay of cavity field into account. The approximation of lossless cavity holds good only when the interaction time of atom with the cavity is much less than the decay time of cavity field. In practical situations, one has to consider the damping of field into account and the atom interaction with the cavity can be treated either perturbatively or non-perturbatively depending on the atom-field coupling strength [12, 13]. The perturbative regime of atom-field interaction corresponds to cavities of low quality factor $Q \equiv \omega/C$, where ω and C are the frequency and damping rate of the cavity field. Here, the excited atom is coupled to many field modes in the cavity which leads to an exponential decay in the probability of excited state. The spontaneous emission rate can be calculated perturbatively using Fermi-Golden rule and can be controlled by the proper design of cavity geometry, its quality factor etc. In this low Q regime, a number of experiments have demonstrated the inhibition [14, 15, 16, 17, 18] or enhancement [19, 20, 21] of atomic spontaneous emission inside the cavity. On the other hand, in a cavity of high quality factor, the atom is strongly coupled to the cavity with the atom-field coupling strength much larger than the cavity decay rate. In this case, the perturbative treatment ceases to be valid and one has to consider the atom-cavity as a single system. The spontaneous emission spectrum of an atom exhibits vacuum field Rabi splittings similar to the case of atom in a lossless cavity. For Rydberg atomic transitions in a microwave cavity, theoretical [22] and experimental [23] analysis showed that the excited state probability of the atom exhibits damped Rabi oscillations instead of exponential decay. Agarwal [24] provided yet another elegant approach to demonstrate the effects of strong atom-field couplings in Rydberg atomic transitions. He showed that the absorption spectrum of a weak probe beam passing through the atom-cavity vacuum system exhibits vacuum field Rabi splitting. He also gave a physical understanding of this behavior in terms of dressed states of the atom-field system. Agarwal's work led further to a series of theoretical [25, 26, 27, 28, 29, 30, 31] and experimental investigations on vacuum field Rabi splittings in the optical [32, 33, 34, 35] as well as microwave domain [36]. Furthermore, Varada, Sanjay kumar and Agarwal [37] showed that the cavity damping leads to subnatural line widths in the emission spectrum of an atom. Puri and Agarwal [38, 39] studied the effects of cavity damping in the strong coupling regime on the collapse and revival behavior of a two-level atom operating on one- and two-photon transitions. Besides these significant publications in the study of strong atom-field couplings, the subject has seen a rapid growth after the experimental realization of one-atom maser or Micromaser by Meschede, Walther and Muller. In the next subsection, we will discuss about these developments which are the cumulative effects of many atomic interactions with the cavity.

1.2.2 Micromaser

One of the most elaborately studied effects of strong interaction between atoms and quantized fields in a cavity is the micromaser in which a beam of excited atoms is sent through a microwave cavity. The motion of the atoms through the cavity is one-dimensional (assumed to be in z-direction) and is treated classically in the semiclassical theory of atom-field interaction. The atom-field coupling strength $\Omega(z)$ in Eq. (1.25) is assumed to be independent of the atomic position z along the propagation axis. The flux of the atomic beam is so adjusted that only one atom interacts with the cavity field at a time. The cavity has a very high quality factor in the micromaser and hence the decay of cavity field can be ignored during the time of atom-field interaction. Atoms in the beam are prepared in the highly excited states called as Rydberg states [40] before entering into the cavity. The reason for using Rydberg atoms is two fold - First, the Rydberg states have very long life time and hence the spontaneous decay of the atom can be ignored during the time of atom-field interaction. Secondly, the probability of induced transitions between neighboring states is relatively very large for Rydberg states. These situations make the micromaser ideal for realizing the basic model of a single atom interacting with a quantized field treated by Jaynes and Cummings. The operation of the micromaser is based on these series of single atom interactions with the cavity. The cavity field also damps in the time interval between two successive atoms entering into the cavity. When the mean time interval between the atoms injected into the cavity is shorter than the cavity decay time, a steady state field is built up in the cavity due to the balance among the stimulated photon emissions from the pumping atoms and cavity field decays. The first experimental realization of micromaser was reported by Meschede, Walther and Muller [41].

The early theoretical studies on micromaser showed that the steady state features of the cavity field depend in an important manner on parameters like flux (r) of the incident atoms, atom-cavity interaction time (τ), atom-field coupling constant (Ω), quality factor (Q) and decay rate (C) of the cavity, etc.. Two different approaches were developed to study the steady state features : a microscopic theory based on the Jaynes-Cummings model [42] and a macroscopic theory based on the quantum theory of the laser [43]. In the macroscopic theory which we follow, the probability $p(n)$ of finding n photons in the single mode micromaser cavity pumped by two-level atoms evolves in time t as follows :

$$\begin{aligned} \frac{dp(n)}{dt} \quad = \quad & G_{n-1}p(n-1) - G_n p(n) \\ & -C(n_b+1)\left[np(n) - (n+1)p(n+1)\right] \\ & +Cn_b\left[np(n-1) - (n+1)p(n)\right] \ , \end{aligned} \tag{1.30}$$

with $G_n = r\sin^2(\Omega\tau\sqrt{n+1})$ being the gain coefficient for the atomic transition and n_b the number of thermal photons in the cavity. The terms containing the decay rate of the cavity are just the diagonal elements of the density operator as given in Eq. (1.18) for the single mode field. The other terms containing the gain coefficients represent the photon emissions from the incident atoms. They can be given a physical meaning in terms of probability flow rate between the state $|n\rangle$ of fixed photon number (n) and the states $|n \pm 1\rangle$ with photon number $(n \pm 1)$ of the cavity field as shown in Fig. 1.2. It is to be noted that the gain terms (G_n terms) can make only upward transitions $|n-1\rangle \rightarrow |n\rangle \rightarrow |n+1\rangle$ and the damping terms (C terms) can make only downward transitions $|n+1\rangle \rightarrow |n\rangle \rightarrow |n-1\rangle$. The thermal photon terms (n_b terms) can induce both the upward and downward transitions $|n-1\rangle \leftrightarrow |n\rangle \leftrightarrow |n+1\rangle$. Since the cavity field in an initial state $|n\rangle$ can induce stimulated photon emissions from the incident atoms at the rate G_n, the term containing $G_n p(n)$ is negative in Eq. (1.30). It represents $|n\rangle \rightarrow |n+1\rangle$ transition in the cavity-field state with a decrease in the probability $p(n)$ and an equivalent increase in the probability $p(n+1)$. Similar physical meaning holds for all other terms in Eq. (1.30) as indicated in the probability flow diagram (Fig. 1.2).

After these early publications on the time development of micromaser field, a number of theoretical investigations had been carried out in connection with two-photon micromaser theory [44], state reduction of excited atoms [45], trapping states [46], number state generation by velocity control of pumping atoms [47], atomic beam noise suppression [48], semi-classical micromaser theory [49], quantum non-demolition measurement of photon numbers [50], cavity field noise reduction by regulating pump statistics [51], cavity QED analog of Raman scattering [52], micromaser with intra-cavity kerr nonlinearity [53], micromaser spectrum [54, 55, 56, 57, 58, 59] and its time evolution [60], effect of finite atomic life time on micromaser field state [61], generation of macroscopic and submacroscopic fields in the micromaser [62], quantum measurements in the micromaser [63], effect of cavity decay on micromaser field state [64], intensity-intensity correlations [65], generation of correlated fields by Raman transitions [66], two-mode three-level micromaser [67], micromaser with non-Poissonian pumping [68], pure states in micromaser [69], detection statistics [70], coherently pumped micromaser [71], etc,. On the experimental side, demonstrations of collapse and revival of Rabi oscillations [11, 72], two-photon maser oscillator [73] and sub-Poissonian photon statistics [74] were the significant developments. Further, Scully, Englert and Walther demonstrated that micromaser set-up can be used as which-path detectors to verify the principle of complementarity in quantum mechanics [75]. The micromaser was even extended to optical regime and the realization of microlaser was also reported [76]. The subject had been reviewed in many different journals [77].

In all these studies, the steady state behavior of the micromaser was generally considered. The steady state probability $p(n)$ is obtained by setting the time derivative equal to zero in Eq. (1.30). The solution can then be obtained in analytical form by applying the principle of detailed balance to the probability flow diagram in Fig. 1.2. The principle of detailed balance states that the net down-

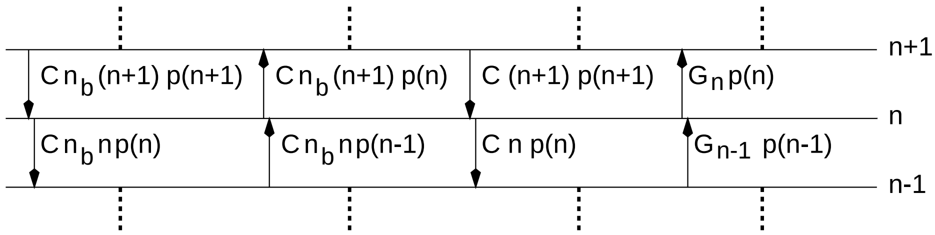

Figure 1.2: Probability flow diagram for a single mode micromaser

ward and upward probability flow rate between the states $|n\rangle$ and $|n-1\rangle$ of fixed photon numbers in the cavity are equal, that is

$$[Cn_b n + Cn]p(n) = [Cn_b n + G_{n-1}]p(n-1) \ , \tag{1.31}$$

which on successive iterations, leads to the steady state solution

$$p(n) = p(0) \prod_{m=1}^{n} \frac{Cn_b + r\sin^2(\Omega\tau\sqrt{m})/m}{C(n_b+1)} \ . \tag{1.32}$$

The probability of finding zero photon $p(0)$ is determined by the normalization condition $\sum_n p(n) = 1$. A remarkable steady state behavior of the micromaser is that the photon distribution $p(n)$ can be narrower than a Poissonian distribution [42, 43]. This is termed as sub-Poissonian photon statistics which can be exhibited only by quantized fields. The experimental observations of non-classical features such as sub-Poissonian photon statistics [78], photon antibunching [79] and squeezing [80] were the early demonstrations for the field quantization. In micromaser, the experiments on quantum Rabi oscillations [11, 72] and sub-Poissonian photon statistics [74] provided further the evidence for the non-classical characters of quantized field in the cavity. The most basic quantum mechanical states for the quantized cavity field are those with fixed photon number also known as number (or Fock) states. Various theoretical schemes using state reduction of excited atoms [45], trapping states [46] and velocity control of pumping atoms [47] were proposed to create a number state in the micromaser cavity. Recently, Walther's group have realized the number state in the micromaser experimentally both by trapping states [81, 82] and state reduction [83] methods. With the realization of the sub-Poissonian and number state of the radiation field, the micromaser has now become an important non-classical field generator.

1.2.3 Mechanical Forces in Cavity QED

It is known that laser lights can cool and trap atoms in optical-wavelength-sized regions. The stronger the intensity of the trapping laser, the deeper is the optical potential that holds the atom. Moreover, it was the development of advanced laser cooling techniques [84] that made the optical trapping of atoms possible. In cavity QED, dipole forces for trapping of atoms were first predicted for Rydberg atomic systems by Haroche and coworkers [85]. They considered a two-level, Rydberg atom moving into a high finesse, microwave cavity in the adiabatic limit. For small detuning of the cavity field which satisfy the adiabaticity criteria, they showed that an excited atom can be attracted to the cavity center even in vacuum state of the cavity. Just like optical potentials are created by the atom-laser interaction in optical traps, in cavity vacuum traps, the dressed states of atom-vacuum field interaction creates a potential well for trapping the atom. For Rydberg atomic transitions induced in a high quality cavity, the effects of spontaneous atomic decay and cavity losses can be ignored during the time of atom-field interaction. Still, the trapping force created by the photon exchange between the atom and the cavity field is at least 10 times smaller than gravity, thus severely limiting experiments.

On the other hand, in the optical domain of atomic transitions, the cavity mediated dipole forces on atoms are stronger enough to overcome gravity. Recently, Kimble's group [86] have demonstrated the evidence for the mechanical forces on atoms in an optical cavity. Although optical photons provide forces of sufficient magnitude, the atomic and cavity decays become much faster in the optical domain. The cavity is therefore continuously pumped with an external laser to replace the lost photons from the atom-cavity system. The transmission of the external laser through the cavity has been used as a direct measure for the strength of the atom-field coupling [87, 88, 89, 90]. In the kimble's experiment [86], the transmission measurement on the laser provided the real time detection of the atomic position in the cavity. The force operator $\vec{F}$ which represents the dipole forces on atom is defined as the time derivative of atomic momentum operator $\vec{P}$:

$$\vec{F} = \frac{d\vec{P}}{dt} = \frac{i}{\hbar}\left[H, \vec{P}\right] = -\vec{\nabla}_{\vec{R}} H \ . \tag{1.33}$$

Here H is the Hamiltonian of the atom-field interaction which depends on the atomic position operator $\vec{R}$. In the semiclassical treatment of atomic motion, the position operator $\vec{R}$ is replaced by its average value $\vec{r}_o$ of the atomic position. The position dependence $\vec{r}_o$ of the Hamiltonian through the atom-field coupling strength $\Omega(\vec{r}_o)$ discussed in Sec. 1.2.1, thus leads to a dipole force acting on the atom. For the Hamiltonian (1.25), the average force acting on the atom is given by

$$\langle \vec{F} \rangle = -\hbar \vec{\nabla}_{\vec{r}_o} \Omega(\vec{r}_o) \left\langle \ |e\rangle\langle g|a + a^{\dagger}|g\rangle\langle e| \ \right\rangle . \tag{1.34}$$

In the optical cavity trap, the average in the above equation is taken over the atom and photon states including the interaction of the external laser, the losses due to spontaneous emission of atom and leakage of photons through cavity walls. This averaging can be done easily in the density matrix framework for low intensity limit of the external laser driving the cavity. Based on the density matrix treatment, an average force proportional to the atomic velocity (friction force) has been predicted for a standing wave mode field in the cavity [91]. Analogously to Sisyphus cooling mechanism for the movement of atom in a classical standing wave, this friction force which acts mainly along the cavity axis, can lead to cooling of the atom under suitable operating conditions. The first experimental demonstration of cooling and heating of atoms through cavity mediated velocity dependent force inside an optical cavity was reported by G. Rempe and his coworkers [92]. Trapping of an atom inside the cavity requires a restoring force transverse to the cavity standing wave in addition to the friction force on the atom along the cavity axis. Evidence for the trapping force has been reported in recent experiments by Rempe [93] and Kimble [94] groups. In these experiments, the atom entering into the cavity triggers an external feedback switch which then increases the intensity of the external laser to provide the trapping force. It is remarkable to see that atoms can be trapped in this way by a cavity field containing less than one photon on an average contrary to highly intense (large number of photons) trapping lasers used in optical traps.

1.3 Ultracold Atoms in a Cavity - Quantization of the Atomic Motion

In all the theoretical and experimental studies discussed above, the atomic motion was considered classically while the atom-field interaction was treated by quantum electrodynamics. This semiclassical treatment of atom-field interaction is valid as long as the atomic wave packet's spatial extension, and therefore its de Broglie wavelength, are small when compared with the cavity size. The quantum effects of atomic motion become significant only when the atom's de Broglie wavelength is comparable to or larger than the cavity dimensions. This condition is met for laser cooled atoms since the atoms have very low kinetic momentum and therefore high de Broglie wavelength at ultra-low temperatures. By considering the ultracold atoms, Englert et al [95] discovered that the interaction of an atom with the cavity induces a quantum mechanical potential for the quantized, external motion of the atom. In this section, we explain the general theoretical framework for studying atom-cavity interaction when the atomic motion is quantized and review some theoretical developments in the context of micromasers pumped by ultracold atoms. Regarding experiments, realization of quantized atomic motion in cavity QED has to wait for the technical advances in the form of large atom-field coupling strength, control over parameters like cavity length, flux and velocity of atoms, etc,.

1.3.1 Atom-Field Interaction as a Scattering of a Wave packet

Consider an ultracold, two-level atom to be passing through a single mode cavity of length L . The atomic motion is assumed to be one-dimensional both inside and outside the cavity which we fix to be in the z direction. The atom passing along the axis of the cylindrical cavity in micromaser experiments is an example of this. The Hamiltonian describing the atom-field interaction including the quantized motion of center-of-mass (c.m.) of the atom along the z-axis, is then given from Eq. (1.25) to be

$$H = \frac{p_z^2}{2m} + \frac{\hbar\nu}{2}\left(|e\rangle\langle e| - |g\rangle\langle g|\right) + \hbar\omega a^\dagger a + \hbar\Omega(z)(|e\rangle\langle g|\; a + a^\dagger\; |g\rangle\langle e|)\;, \tag{1.35}$$

where p_z is the atomic c.m. momentum operator and m is the atomic mass. The parameter $\Omega(z)$, which gives the strength of atom-field interaction, depends on the one-dimensional position z of the atom as it moves. The Hamiltonian (1.35) together with the state vector $|\Psi(z,t)\rangle$ obeys the time evolution in the Schrödinger Eq. (1.12). Now, transforming to an interaction picture with an unitary transformation on the state,

$$\begin{aligned} H_o &\equiv \frac{\hbar\omega}{2}\left(|e\rangle\langle e| - |g\rangle\langle g|\right) + \hbar\omega a^\dagger a \ , \\ |\chi(z,t)\rangle &= \exp(iH_o t/\hbar)|\Psi(z,t)\rangle \ , \end{aligned} \tag{1.36}$$

the state vector $|\chi(z,t)\rangle$ in the interaction picture obeys the following equation with an effective Hamiltonian H_I :

$$\begin{aligned} H_I &\equiv \frac{p_z^2}{2m} + \frac{\hbar\Delta}{2}\left(|e\rangle\langle e| - |g\rangle\langle g|\right) + \hbar\Omega(z)(|e\rangle\langle g| \ a + a^\dagger \ |g\rangle\langle e|) \ , \\ i\hbar\frac{\partial}{\partial t}|\chi(z,t)\rangle &= H_I|\chi(z,t)\rangle \ . \end{aligned} \tag{1.37}$$

The detuning $\Delta = \nu - \omega$ represents the mismatch of the atomic frequency from the cavity frequency. The state vector $|\chi(z,t)\rangle$ contains information about the internal state of the atom and the field as well as the external motion of the atomic wave packet.

Potential Induced by a Resonant Cavity : Since the total energy of the atom-cavity system is conserved, the external motion of the atom is influenced by both the internal atomic and photon states in the cavity. This is easily seen in the simplest case when the cavity frequency is tuned on resonance with the atomic frequency ($\Delta = 0$). It can be verified that the atom-field states $|\phi^{\pm}_{n+1}\rangle = \frac{1}{\sqrt{2}}\left(|e,n\rangle \pm |g,n+1\rangle\right)$ in Eq. (1.26) are eigenstates of the interaction picture operator H_I with eigenvalues $h_{\pm} = \frac{p_z^2}{2m} \pm \hbar\Omega(z)\sqrt{n+1}$ for the resonance case ($\Delta = 0$). The interest here is to find the effect of quantized atomic motion on the time evolution of the initial atom-field state $|e,n\rangle$. Similar to Eq. (1.28), the state of the atom-field system can be expanded as

$$|\chi(z,t)\rangle = C_n^+(z,t)|\phi^+_{n+1}\rangle + C_n^-(z,t)|\phi^-_{n+1}\rangle \ , \tag{1.38}$$

with the coefficients $C_n^{\pm}$ now depending on the position z of the atom. With this expansion, the time dependent Schrödinger equation (1.37) for $\Delta = 0$, becomes

$$i\hbar\frac{\partial C_n^{\alpha}(z,t)}{\partial t} = h_{\alpha}C_n^{\alpha}(z,t) \ , \qquad \alpha = \pm \ , \tag{1.39}$$

where the operators $h_{\pm}$ act on the c.m. wave functions of the atom. The effect of the cavity with fixed initial number (n) of photons is thus seen to produce potential terms in $h_{\pm}$ as first discussed by Englert et al [95]. Thus, the problem of atom-field interaction is reduced to that of a scattering of a wave packet from the cavity induced potentials $V_{n+1}^{\pm} = \pm\hbar\Omega(z)\sqrt{n+1}$ in the eigenstates $|\phi_{n+1}^{\pm}\rangle$. For the external motion of the atom in the initial atom-field state $|e,n\rangle$, the cavity acts like a potential which is a coherent combination of the barrier (V_{n+1}^{+}) and well (V_{n+1}^{-}) components. These potentials are quite analogous to those induced in the interaction of a spin-half particle with a classical magnetic-field when the motion of the particle is quantized [96].

Distinction from Optical Potentials : In the scattering process of an atom from a resonant cavity discussed above, the potentials are created for the external motion of the atom by photon exchange between the atom and the cavity field. The potentials experienced by the atom in the dressed states $|\phi_{n+1}^{\pm}\rangle$ can be viewed as due to a force mediated by the atomic transitions $|e\rangle \leftrightarrow |g\rangle$ inside the cavity. These potentials should be distinguished from those experienced by an atom interacting with a far-detuned classical field. In the classical treatment of the monochromatic field, the operators a and $a^{\dagger}$ in the Hamiltonian (1.37) are treated as c-numbers which can be set to be unity by redefining the coupling strength $\Omega(z)$. For a far detuned field $(\Delta >> \Omega(z))$, the perturbation theory then gives a shift $\hbar\ \delta E(z) \equiv \pm 4\hbar\Omega^2(z)/\Delta$ in the energy levels of the excited and ground states of the atom. The Hamiltonian (1.37), in the leading order of perturbation, becomes

$$H_I \approx \frac{p_z^2}{2m} + \hbar(\frac{\Delta}{2} + \delta E)\,(|e\rangle\langle e| - |g\rangle\langle g|) \ . \tag{1.40}$$

The bare atomic state $|e\rangle$ $(|g\rangle)$ thus induces a potential barrier (well) with the potential energy $4\hbar\Omega^2(z)/\Delta$ for the external motion of the atom. With a sinusoidal coupling strength $\Omega(z) \propto \sin(\omega z/c)$, the atom moves in a periodic potential due to these non-resonant light shifts. This principle is being used in optical lattices to cool and trap atoms [97].

1.3.2 Reflection and Transmission

In comparison to semiclassical treatment, the quantum treatment of atomic motion leads to reflection of the incident atoms from the cavity induced potentials besides partial transmission. This reflection or the transmission of the atom is very similar to that of a particle interacting with potential barriers or wells. The interaction of the atom with the cavity can also change the electronic states of the atom. Consider a resonant cavity of length L to be located in the region $z = 0 \rightarrow L$. The cavity region can be specified by the mesa function $\theta(z)\theta(L-z)$ where $\theta(z)$ is the Heaviside's unit step function, i.e., $\theta(z)$ is zero if $z < 0$, unity if $z > 0$. The incident wave packet of the free moving atom in the left region $(z < 0)$ has a decomposition in the momentum domain (wavenumber k) of the form $\exp\left(-ip_z^2 t/2m\hbar\right) \int dk A(k) e^{ikz} = \int dk A(k) e^{-i\left(\hbar k^2/2m\right)t} e^{ikz}$. Each plane wave component (momentum $\hbar k$) in the incident wave packet gets reflected or transmitted through the cavity with amplitudes $\rho_n^{\pm}(k)$, $\tau_n^{\pm}(k)$, respectively, in the dressed states $|\phi_{n+1}^{\pm}\rangle$. In the long time limit, when the atom has left the cavity after its interaction, the reflected and transmitted wave packets in regions to the left $(z < 0)$ and the right $(z > L)$ of the cavity are given by solving equations (1.38) and (1.39) to be

$$\begin{aligned} |\chi(z,t)\rangle \quad = \quad & \int dk A(k) e^{-i\left(\hbar k^2/2m\right)t} \left\{ \left[R_{e,n}(k) e^{-ikz} \theta(-z) + T_{e,n}(k) e^{ikz} \theta(z-L) \right] |e,n\rangle \right. \\ & \left. + \left[R_{g,n+1}(k) e^{-ikz} \theta(-z) + T_{g,n+1}(k) e^{ikz} \theta(z-L) \right] |g,n+1\rangle \right\} , \qquad (1.41) \end{aligned}$$

where

$$R_{e,n} = \frac{1}{2}(\rho_n^+ + \rho_n^-), \qquad T_{e,n} = \frac{1}{2}(\tau_n^+ + \tau_n^-) \ , \qquad (1.42)$$

are the reflection and transmission amplitudes for the excited state of the atom and

$$R_{g,n+1} = \frac{1}{2}(\rho_n^+ - \rho_n^-), \qquad T_{g,n+1} = \frac{1}{2}(\tau_n^+ - \tau_n^-) \ , \qquad (1.43)$$

are the reflection and transmission amplitudes for the ground state of the atom with an emission of a photon from the atom. These reflection and transmission amplitudes depend on the mode function of the field in the cavity through the coupling strength $\Omega(z)$. For a mesa mode coupling strength $\Omega(z)$ which represents z-independent atom-field coupling inside the cavity, the amplitudes ρ_n^+, τ_n^+ correspond to the reflection and transmission amplitudes of an atom interacting with a potential barrier of height $V_{n+1}^{+} = \hbar\Omega\sqrt{n+1}$. Similarly, the amplitudes ρ_n^-, τ_n^- describe the reflection and transmission of the atom incident on a potential well of depth $V_{n+1}^{-} = -\hbar\Omega\sqrt{n+1}$. The lengths of the induced barrier - well components are given by the interaction length L of the cavity region. The influence of the barrier - well components on the atomic motion become significant only when the average energy $\bar{E} \equiv \hbar^2\bar{k}^2/2m$ of the incident atom is lesser or comparable to the atom-field interaction energy $\hbar\Omega\sqrt{n+1}$. Further, for higher interaction lengths, the barrier component can only reflect the atom from the cavity, i.e., $\rho_n^+(\bar{k}) \approx \pm 1$, $\tau_n^+(\bar{k}) \approx 0$. The reflection and transmission coefficients, which are defined as $|R_{e,n}(\bar{k})|^2$, $|R_{g,n+1}(\bar{k})|^2$, $|T_{e,n}(\bar{k})|^2$ and $|T_{g,n+1}(\bar{k})|^2$ in the excited or ground state of the atom, exhibit resonances as a function of the average energy $\bar{E}$ for ultracold atoms ($\bar{E} < \hbar\Omega\sqrt{n+1}$). The resonances in transmission will occur when the cavity length is an integer multiple of half the mean de Broglie wavelength of the atom inside the potential well component. For the case of fast moving atoms with average energy $\bar{E} >> \hbar\Omega\sqrt{n+1}$, the reflection coefficients vanish because of the null reflections from both the barrier and well components. The transmission coefficients exhibit Rabi oscillations as a function of the energy $\bar{E}$ similar to that discussed in the Jaynes-Cummings model (Sec. 1.2.1).

Micromazer : A very important result of quantized atomic motion is the micromaser pumped with ultracold (slow moving) atoms instead of thermal (fast moving) atoms. When the single mode micromaser is pumped by ultracold two-level atoms, the gain coefficient G_n in the master equation (1.30) will now depend upon reflection and transmission amplitudes in Eqs. (1.42) and (1.43). Considering the mesa mode coupling strength, Scully et al [98, 99] have treated this problem in detail. They showed that the steady state photon distribution exhibits a mixture of thermal and shifted thermal distributions. Since the quantized motion of atoms along the z-axis influences the photon statistics, they termed the micromaser as micromazer with the letter z indicating the quantized z-motion in micromazer. The experimental strategies and the spectrum of micromaser pumped by cold atoms were also discussed [100, 101]. Further, the steady state field in the micromazer cavity has been shown to be nonclassical [102]. Zhang et al [103] have developed the theory for two-photon micromazer and generalized the idea of quantized, atomic motion to study the interaction of three-level atoms with a single mode field [104]. Retamal et al studied the effects of periodic potentials on the steady state photon distribution in micromazer by considering sinusoidal mode function [105].

Chapter 2

Tunneling Time of Ultracold Atoms Through Vacuum Induced Potential

An important question of great interest in several disciplines of physics has been - what is the tunneling time or traversal time of a quantum mechanical particle through a potential. Various definitions have been proposed and the subject has been reviewed extensively [106, 107, 108, 109, 110, 111, 112]. Mainly, three different approaches have been proposed to evaluate the tunneling time of a particle passing through a potential barrier: (i) the Wigner time [108, 109]; (ii) the Büttiker - Landauer time [110]; (iii) the Larmor time [111].

In Wigner's method, one calculates how much time the peak of the particle's wave packet takes to travel the potential. The tunneling time is simply the derivative of the transmission amplitude's phase with respect to the energy of the particle. This time is also known as *phase time* for tunneling or traversal of the particle through the potential. The phase tunneling time of the particle passing through a potential barrier was shown to be positive and lesser than the free-space traversal time by Hartman [109]. This means that the peak of tunneling wave packet appears on the far exit-side of the barrier much earlier than if it had propagated the same distance in free space. Single-photon and optical-pulse transmission experiments by Steinberg [113] et al. and Spielman et al. [114] have actually demonstrated a similar superluminal tunneling of electromagnetic wave packets through the forbidden mid-gap region of a photonic band-gap material. The passage time of the wave packets were found to be consistent with the Wigner's phase time calculated theoretically. Recently, closed analytic-formulas have also been derived for the phase time associated with the passage of electrons or photons through a finite superlattice [112].

For the barrier tunneling time, the other approach by Büttiker and Landauer [110] considered the case in which either the height of the potential barrier or the amplitude of the incident wave varies sinusoidally with time. They found that, if the frequency of the sinusoidal modulation is very low, the transmission of the particle adiabatically follows the modulation. However, as the frequency of the modulation increases, the transmitted waves begin to depart from the adiabatic behavior. In this method, the tunneling time is defined as the modulation period at which the crossover from adiabatic to non-adiabatic behavior occurs in the transmission of the particle.

In the Larmor method [111], the particle tunneling through the barrier is subjected to an additional, weak magnetic-field in the barrier region. The Larmor precession of the particle's spin in the magnetic field serves as a clock to measure the time spent by the particle in the barrier region. Since the particles with spin parallel to the magnetic field have higher probability of transmission through the barrier than those with anti-parallel spin, the magnetic field tries to align the spin of the particle in its direction. These lead to three characteristic times for transmission of the particle through the barrier. The total angular change in the spin of the tunneling particle divided by the Larmor frequency is the Larmor time. The literature also invokes a different quantity dwell time [115] within the barrier which is defined as the ratio of integrated probability density over the barrier region to the incident flux. The dwell time measures the average time spent by the particle in the barrier region irrespective of the reflection or transmission at the end of its stay. Recently, the dwell time for a particle interacting with an arbitrary potential has been obtained and a new interpretation of the Büttiker-Landauer barrier tunneling time has been given within the framework of quantum measurement theory [116].

In this chapter, we examine the passage of a cold atom through a high quality cavity. In particular, we enquire what is the passage time of the atomic wave packet through the cavity. The question is a complicated one as we have here a coupling with three different types of the degrees of freedom - (a) atom's center-of-mass (c.m.) motion, (b) atom's electronic states and (c) photons. As shown in Sec. 1.3, this coupling induces a quantum mechanical potential for the external motion of the atoms. We refer to the potential induced by the vacuum field in the cavity as *Vacuum Induced Potential*. We have found that the passage time of the atom through the vacuum induced potential can be defined through the phase tunneling time of the wave packet.

2.1 Atom-Field Dynamics and Its Basic Equations

We consider an ultracold, two-level atom in the excited state to be passing through a single mode cavity of length L as shown in Fig. 2.1. The motion of the atom is assumed to be one-dimensional which we fix to be along the z-axis. As described in Sec. 1.3, the interaction of the atom couples the excited $|e\rangle$ and the ground $|g\rangle$ states either by reflection or transmission through a potential induced by the cavity. The nature and strength of the potential induced by the cavity depend on

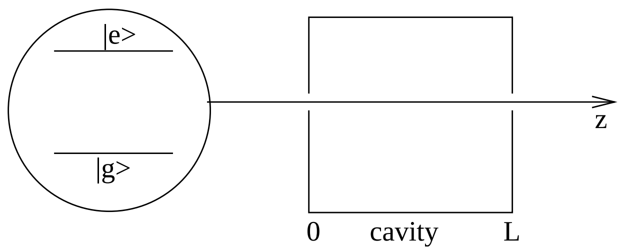

Figure 2.1: The scheme of the high quality cavity with which the ultracold atom interacts.

the mode function of the cavity field through the coupling strength $\Omega(z)$. It also depends on the initial number n of photons in the cavity. The potential energy is given by $V_{n+1}^{\pm} = \pm\hbar\Omega(z)\sqrt{n+1}$ in the dressed states $|\phi_{n+1}^{\pm}\rangle$. We consider the cavity to be initially in vacuum $(n = 0)$ state and the atom-field coupling to be a mesa mode coupling $\Omega(z) = \Omega\theta(z)\theta(L - z)$ where $\theta(z)$ is the Heaviside's unit step function. Thus, the atom-field coupling is z-independent inside the cavity region and zero outside the cavity region as indicated by the Heaviside unit step function. In this case, the incident atom experiences the cavity as a coherent addition of

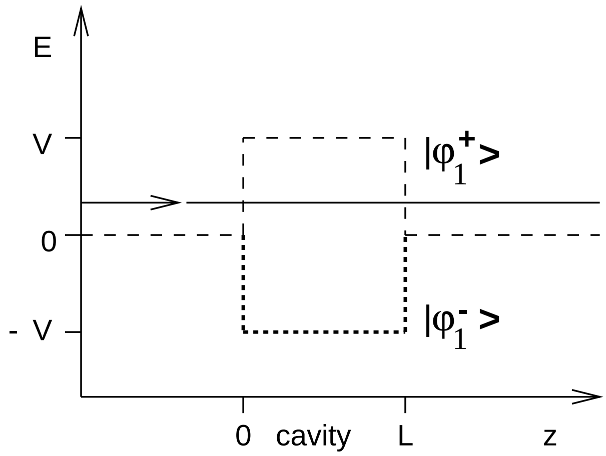

Figure 2.2: Schematic representation of the energy E of the excited two-level atom incident upon a single mode cavity in vacuum state. The interaction is equivalent to reflection and transmission of the atom through a potential barrier (dashed) or potential well (dotted) with a potential energy $V = \hbar\Omega$. The atom can be reflected or transmitted in either of the states $|e, 0\rangle$ and $|g, 1\rangle$.

a potential barrier and a potential well with potential energy $\hbar\Omega$ which we term as vacuum induced potential. The barrier and well components in this vacuum induced potential are shown in Fig. 2.2. The initial wave packet of the moving free atom (mass m) can be written in the form $\psi(z,t) = \exp\left(-ip_z^2 t/2m\hbar\right)\int dkA(k)e^{ikz} = \int dkA(k)e^{-i\left(\hbar k^2/2m\right)t}e^{ikz}$. We assume that $A(k)$'s are such that $\psi(z,t)$ at $z = 0$ peaks in time at the instant $t = 0$. Thus, in the presence of the cavity, the wave packet at $z = 0$ (entry of the cavity) has its peak (in time) at $t = 0$. We therefore write the initial wave function of the atom-field system as $|\Psi(z,0)\rangle = \psi(z,0)|e,0\rangle$. Then, using Eq. (1.41), the wave function of the atom-field system after the interaction is given in the left $(z \leq 0)$ and right $(z \geq L)$ regions to be

$$\begin{aligned}|\Psi(z,t)\rangle &= \int dkA(k)e^{-i\left(\hbar k^2/2m\right)t}\Big\{\Big[R_{e,0}(k)e^{-ikz}\theta(-z) + T_{e,0}(k)e^{ikz}\theta(z-L)\Big]|e,0\rangle \\ &\quad + \Big[R_{g,1}(k)e^{-ikz}\theta(-z) + T_{g,1}(k)e^{ikz}\theta(z-L)\Big]|g,1\rangle\Big\}\ , \qquad (2.1)\end{aligned}$$

where

$$R_{e,0} = \frac{1}{2}(\rho_0^+ + \rho_0^-), \qquad T_{e,0} = \frac{1}{2}(\tau_0^+ + \tau_0^-)\ , \tag{2.2}$$

are the reflection and transmission amplitudes for the excited state of the atom and

$$R_{g,1} = \frac{1}{2}(\rho_0^+ - \rho_0^-), \qquad T_{g,1} = \frac{1}{2}(\tau_0^+ - \tau_0^-)\ , \tag{2.3}$$

are the reflection and transmission amplitudes for the ground state of the atom with an emission of a photon from the atom. The probability amplitudes $\rho_0^{\pm}$, $\tau_0^{\pm}$ for reflection and transmission of the atom through barrier (superscript +) and well (superscript -) components are given by

$$\rho_0^{\pm} = i\Delta_0^{\pm}\sin(k_0^{\pm}L)\exp(ikL)\tau_0^{\pm} \ , \tag{2.4}$$

$$\tau_0^{\pm} = \exp(-ikL)\left[\cos(k_0^{\pm}L) - i\Sigma_0^{\pm}\sin(k_0^{\pm}L)\right]^{-1} \ , \tag{2.5}$$

$$\begin{aligned} \Delta_0^{\pm} &= \frac{1}{2}\left(\frac{k_0^{\pm}}{k} - \frac{k}{k_0^{\pm}}\right) \ , \\ \Sigma_0^{\pm} &= \frac{1}{2}\left(\frac{k_0^{\pm}}{k} + \frac{k}{k_0^{\pm}}\right) \ , \end{aligned} \tag{2.6}$$

$$\begin{aligned} k_0^{\pm} &= \sqrt{\left(k^2 \mp \frac{2m\Omega}{\hbar}\right)} \\ &= \sqrt{(k^2 \mp \kappa^2)} \ . \end{aligned} \tag{2.7}$$

Here $\hbar k$ is the c.m. momentum of the incident atom and $\hbar^2\kappa^2/2m \equiv \hbar\Omega$ is the vacuum coupling energy. Note that the reflection and transmission amplitudes $\rho_0^{\pm}$, $\tau_0^{\pm}$ depend on the momentum $\hbar k$ of the atom and the atom-vacuum field coupling strength Ω. For the wave packet $\psi(z, 0)$ of the incident atom, the different momentum (wave number k) components have different amplitudes for reflection and transmission through the cavity. The incident wave packet is split into reflected and transmitted wave packets both for excited and ground states of the atom.

2.2 Phase Tunneling Time of a Gaussian Wave Packet

In the previous section, we have seen that dynamics of an ultracold atom passing through the cavity is reduced to the problem of reflection and transmission of the atomic wave packet incident on vacuum induced potential. In this section, we study in detail the transmission of the atom in its initial excited state through the cavity. The transmission amplitude $T_{e,0} \equiv |T_{e,0}(k)|e^{i\phi(k)}$, given by Eq. (2.2), depends on the coherent addition of amplitudes for transmission through barrier and well components. We consider a Gaussian wave packet $A(k) = \exp\left(-(k-\bar{k})^2/\sigma^2\right)$ of width σ and mean momentum $\bar{k}$ for the incident atom. With this substitution for $A(k)$, the transmitted wave function in Eq. (2.1) including the normalization factor, becomes for $z \geq L$

$$|\Psi_T(z,t)\rangle = \frac{1}{(2\pi)^{3/4}} \sqrt{\frac{2}{\sigma}} \int_{-\infty}^{\infty} dk\ \exp\left(-(k-\bar{k})^2/\sigma^2\right)\ e^{-i\left(\hbar k^2/2m\right)t}\ |T_{e,0}|\ e^{i\phi(k)}\ e^{ikz}\ |e,0\rangle\ . \tag{2.8}$$

For small width σ, the integrand in Eq. (2.8) has non vanishing value only in a small range of wave numbers k centered about the mean $\bar{k}$. Then, the envelope of the transmitted wave packet $|\langle e,0|\Psi_T(z,t)\rangle|^2$ will be maximum when the total phase $\Theta(k)$ of the integrand exhibits extremum at the wave number $k = \bar{k}$. Since we have assumed that the center of incident wave packet enters the cavity at time $t = 0$, this stationary phase condition at the exit of the cavity $(z = L)$, gives the time the wave packet takes to tunnel or traverse through the cavity :

$$\left.\frac{\partial \Theta(k)}{\partial k}\right|_{k=\bar{k}} = \left.\frac{\partial}{\partial k}\left[kL + \phi(k) - \left(\hbar k^2/2m\right)t\right]\right|_{k=\bar{k}} = 0\ , \tag{2.9}$$

which yields the phase tunneling time t_{ph}

$$t_{ph} = \left[\frac{m}{\hbar k}\left(\frac{\partial \phi}{\partial k} + L\right)\right]_{k=\bar{k}}\ . \tag{2.10}$$

The integral in Eq. (2.8) can be evaluated approximately by making the Taylor expansion of the phase of transmission amplitude about the mean wave number $k = \bar{k}$. Keeping terms up to second order in the expansion and assuming $\sigma << \bar{k}$ to approximate $|T_{e,0}(k)| \approx |T_{e,0}(\bar{k})|$, the transmitted wave function is given at $z = L$ by

$$\begin{aligned} |\Psi_T(z,t)\rangle\ |_{z=L} \ &\approx\ \frac{1}{(2\pi)^{3/4}} \sqrt{\frac{2}{\sigma}}\ \exp\left[i(\bar{k}L + \phi(\bar{k}) - \bar{E}t/\hbar)\right]\ |T_{e,0}(\bar{k})| \\ &\times \sqrt{\frac{2\pi}{\left(\frac{2}{\sigma^2} + i\alpha\right)}}\exp\left(\frac{-\bar{E}(t-t_{ph})^2}{m\left(\frac{2}{\sigma^2} + i\alpha\right)}\right)\ |e,0\rangle\ , \end{aligned} \tag{2.11}$$

where $\bar{E} = \hbar^2\bar{k}^2/2m$ is the average energy of the incident atom and the parameter $\alpha = \frac{\hbar t}{m} - \left.\frac{\partial^2\phi}{\partial k^2}\right|_{k=\bar{k}}$ accounts for the spreading of the wave packet as it propagates. The maximum amplitude of the transmitted wave packet occurs at time $t = t_{ph}$ given by the stationary phase assumption. It is very important to note that the phase time has no significance when either the Taylor expansion of the phase does not converge or additional terms more than the second order term are important in the expansion. In this general case, the transmitted wave packet will be deformed from the Gaussian shape and the concept of following the peak of the wave packet is meaningless. When there is no cavity $|T_{e,0}(k)| = 1$, $\phi(k) = 0$, then the phase time in Eq. (2.10) becomes $t_{ph} = mL/\hbar\bar{k} \equiv t_{cl}$, which is the classical time needed for the center of a free-atomic wave packet to traverse a distance of length L. The phase tunneling time which a particle takes to traverse a *potential barrier*, has been studied extensively by Hartman [109]. The tunneling time for a barrier is less than the time a free particle takes to traverse the same distance in free space. Here, we report such a superclassical traversal of the ultracold atom through the vacuum induced potential. Note that the temperature of the atom will be in the range 10^{-7}-10^{-8} K if the coupling constant Ω $(\equiv \hbar\kappa^2/2m)$ is in the range of 100-10 kHz and if the mean momentum $\bar{k}/\kappa = 0.1$. It should be borne in mind

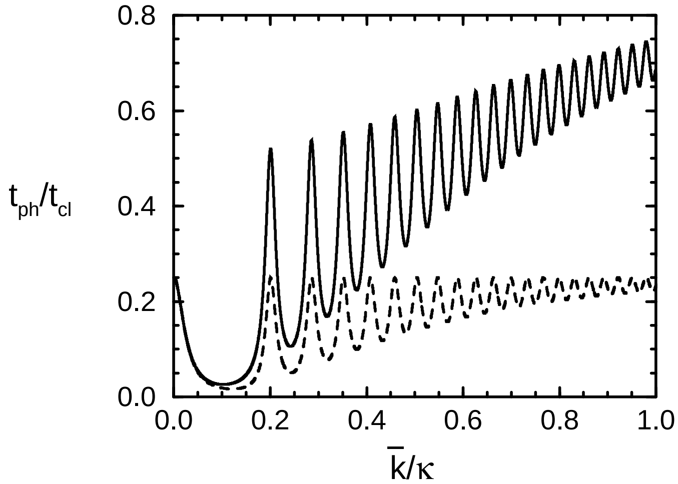

Figure 2.3: The dependence of the dimensionless phase time (solid curve) for transmission in the excited state on the mean wave number $\bar{k}/\kappa$ of the incident atom for the parameter $\kappa L = 50\pi$. The phase time follows the resonant behavior of the transmission probability $|T_{e,0}|^2$ (dashed curve).

that both barrier and well contribute to the traversal time of ultracold atoms. Using Eq. (2.10), we plot in Fig. 2.3 the phase time as a function of the mean wave number $\bar{k}$ for the length of the cavity $\kappa L = 50\pi$. The important result here is that the phase time exhibits the resonant behavior of transmission probability and that the phase time is less than the classical time t_{cl}. In a different context, viz., in the tunneling time of electrons passing through a finite superlattice, a similar resonant behavior is found [112].

Another remarkable behavior of phase time is that it can even be *negative*. Negative phase time implies that the peak of the transmitted wave packet emerges even before the peak of the incident wave packet enters the interaction region. This can be understood from the interference between the incident wave and the wave that is reflected at the end of the cavity. From Eq. (2.10), we see that when

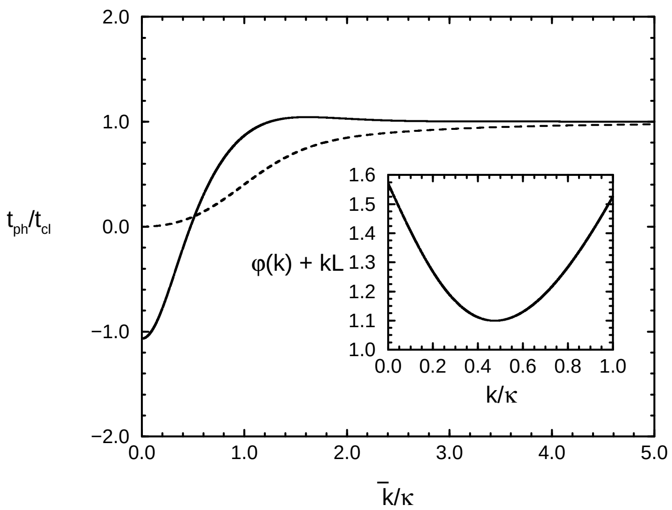

Figure 2.4: The dimensionless phase time (solid curve) for transmission in the excited state as a function of the mean wave number $\bar{k}/\kappa$ of the incident atom for the parameter $\kappa L = \pi/2$. The dashed curve represents the probability of transmission of the atom in the initial excited state $\left(|T_{e,0}|^2\right)$ through the cavity. The inset shows the phase function $\phi(k) + kL$ as a function of the wave number k/κ of the excited atom for the same parameter.

the derivative of the phase of transmission amplitude is negative and its absolute value is greater than the length L of the cavity, the phase time becomes negative. Put another way, when the phase function $\phi(k) + kL$ has negative slope, the phase time takes negative values. In Fig. 2.4, we show this behavior in the phase time for the parameter $\kappa L = \pi/2$. It is seen from the graph that for ultracold atoms ($\bar{k}/\kappa << 1$) the phase time is negative. For fast atoms ($\bar{k}/\kappa >> 1$), the phase time approaches the classical time as the transmission probability becomes closer to unity. The phase time being negative is very similar to the concept of negative group velocity in the case of electromagnetic pulse propagation. Here, the variation of the refractive index of the medium with respect to the frequency has a steep negative slope leading to superluminal propagation [117]. To understand the negative phase time, we have also plotted the phase function $\phi(k) + kL$ in the inset of Fig. 2.4. The graph shows the expected negative slope for ultracold atoms.

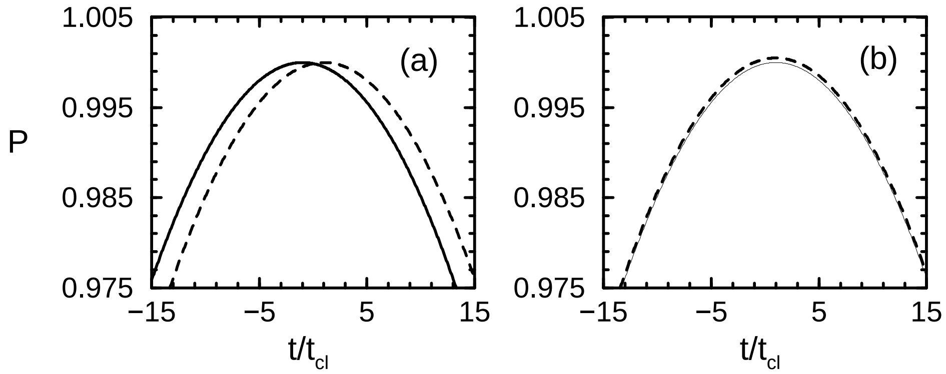

Figure 2.5: The normalized probability density $P \equiv |\langle e, 0|\Psi_T(z,t)\rangle|^2/\sigma$ at $z = L$ as a function of the dimensionless time t/t_{cl}. The solid (dashed) curve represents P after transmission through the cavity (free space). The parameters used for the calculation are $\kappa L = \pi/2$, $\sigma/\kappa = 0.01$ and $\bar{k}/\kappa = 0.1$ (a), $\bar{k}/\kappa = 10$ (b). Both the solid and dashed curves are normalized to unity.

2.3 Time Dependence of the Wave Packet for Ultracold Atoms

To study the behavior of actual envelope of the wave function, we evaluate numerically the integral Eq. (2.8) which describes the propagation of a Gaussian wave packet of an excited atom through the vacuum induced potential. Garrett and McCumber [118] carried out a similar numerical integration for the electric field amplitude of a Gaussian light pulse passing through an anamolous dispersive medium. In Fig. 2.5(a), we show the numerical results for the normalized probability density $|\langle e, 0|\Psi_T(z,t)\rangle|^2/\sigma$ at the exit of the cavity $z = L$ as a function of the time for the parameters $\kappa L = \pi/2$, $\sigma/\kappa = 0.01$, $\bar{k}/\kappa = 0.1$. The peak of the transmitted wave packet occurs at the time $t/t_{cl} \approx -0.98$, which matches with the phase time in Fig. 2.4 for the parameter $\bar{k}/\kappa = 0.1$. Thus, the wave packet appears to travel backwards in time in the sense of tracing the locus of maximum amplitude.

The peak of the transmitted wave packet is formed even before the peak of the incident wave packet enters the cavity. For comparison, we have also plotted the envelope of the wave packet which travels through the same distance of length L in free space. The peak of the free wave packet occurs at the expected classical time. From the graph, we see that for ultracold atoms ($\bar{k}/\kappa << 1$) the propagation of the atom through the cavity is faster than through the free space. In Fig. 2.5(b), we plot the envelope of the wave function for the parameters $\kappa L = \pi/2$, $\sigma/\kappa = 0.01$, $\bar{k}/\kappa = 10$. In this case of fast atoms ($\bar{k}/\kappa >> 1$), the transmitted wave packet has maximum amplitude at the classical time ($t/t_{cl} \approx 1$) as expected from Fig. 2.4. Thus, the peak of the transmitted wave packet occurs at the instant given by the expression for phase time Eq. (2.10), even if that instant is earlier than the instant at which incident wave packet enters the cavity. While this is generally true for

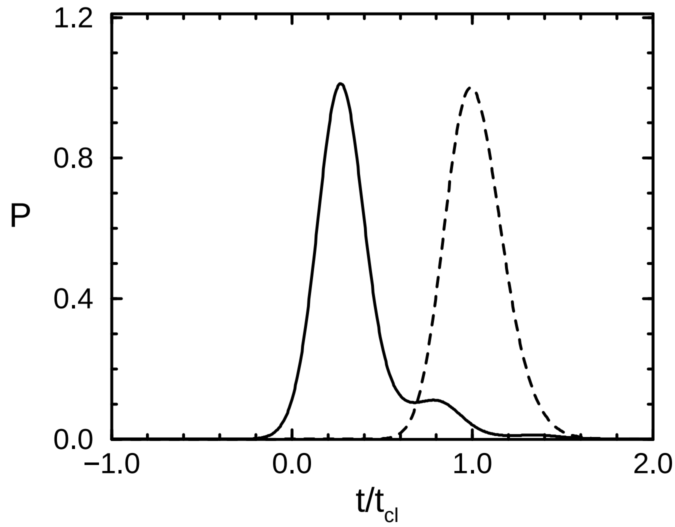

Figure 2.6: The normalized probability density $P \equiv |\langle e, 0|\Psi_T(z,t)\rangle|^2/\sigma$ at $z = L$ as a function of the dimensionless time t/t_{cl}. The solid (dashed) curve represents P after transmission through the cavity (free space). The parameters used for the calculation are $\kappa L = 50\pi$, $\sigma/\kappa = 0.05$ and $\bar{k}/\kappa = 0.28$. Both the solid and dashed curves are normalized to unity.

a narrow momentum distribution characterized by $\sigma << \bar{k}$ of the incident atom, strong deformation of the incident wave packet sometimes makes the phase time meaningless. The deformation of the wave packet during propagation occurs generally when the mean momentum of incident atom is near a sharp resonance for transmission probability. This is because all the discussions above are based on the assumption that the modulus of the transmission amplitude is a slowly varying function of the wave number k of the incident atom. In Fig. 2.6, we show the probability density of the transmitted atom for the mean momentum $\bar{k}/\kappa = 0.28$, which is near the second resonance for transmission probability in Fig. 2.3. The transmitted wave packet seems distorted strongly from the Gaussian shape and the peak of the transmitted wave packet does not occur at the phase tunneling time for the chosen momentum in Fig. 2.3.

2.4 Splitting of the Wave Packet

We have so far considered only the propagation of the atomic wave packet in the initial excited state. But in a high-quality cavity, the atom-field interaction leads to photon emission by the excited atom. We can also study the behavior

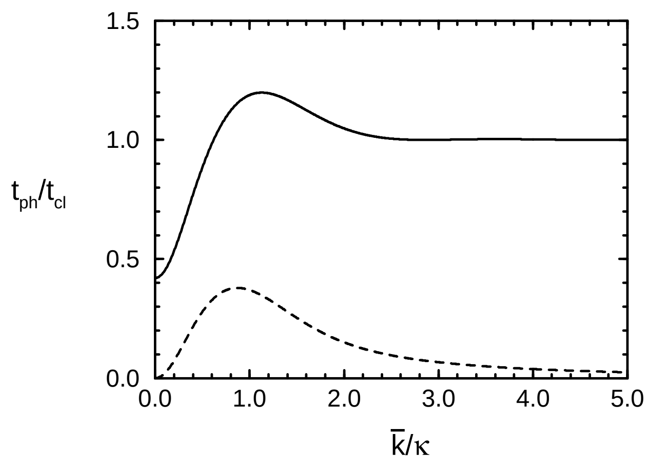

Figure 2.7: The dimensionless phase time (solid curve) for transmission in the ground state as a function of the mean wave number $\bar{k}/\kappa$ of the incident atom for the parameter $\kappa L = \pi/2$. The dashed curve represents the probability of transmission of the atom in the ground state $\left(|T_{g,1}|^2\right)$ through the cavity.

of the transmitted wave packet $|\langle g, 1|\Psi_T(z,t)\rangle|^2$ for the ground state of the atom using Eq. (2.1). For the parameters of Fig. 2.5(a), the phase time for the ground state $t_{ph}/t_{cl} \approx 0.45$ is positive but still a superclassical time. Numerical integration also gives the same time delay for the transmitted wave packet. In Fig. 2.7, we show the behavior of the phase time for the wave packet corresponding to the transmitted atom in the ground state. This behavior is to be compared with that of the phase time for the transmission in the excited state (Fig. 2.4). The two phase times differ considerably for cold atoms. Generally, the difference in phase times for the ground and excited states of the atom results in the *splitting* of the incident wave packet into two in the total transmission. But for the parameters of Fig. 2.5(a), the total transmission is dominated by the contribution from the ground state, and hence, the splitting is not seen.

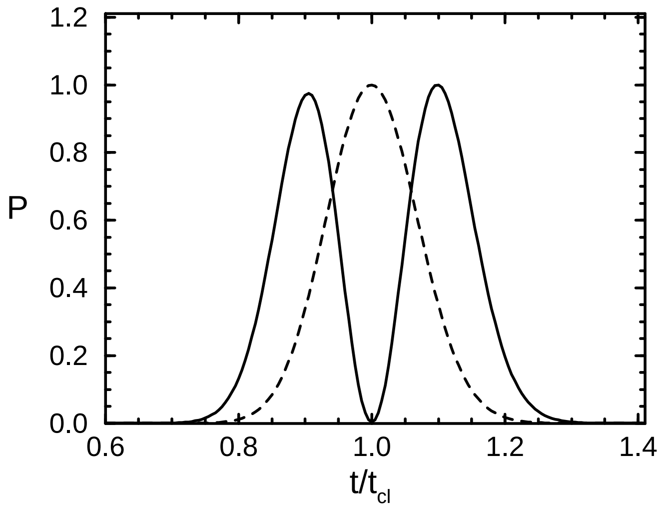

Figure 2.8: The normalized probability density $P \equiv |\langle e,0|\Psi_T(z,t)\rangle|^2/\sigma$ at $z = L$ as a function of the dimensionless time t/t_{cl}. The solid (dashed) curve represents P after transmission through the cavity (free space). The parameters used for the calculation are $\kappa L = 10\pi$, $\sigma/\kappa = 0.5$, and $\bar{k}/\kappa = 10$. Both the solid and dashed curves are normalized to unity.

The *splitting* of the incident wave packet can also occur for a different reason as shown in the Fig. 2.8 for the parameters $\kappa L = 10\pi$, $\sigma/\kappa = 0.5$, $\bar{k}/\kappa = 10$. It is seen that the probability density is zero at the classical time. This can be understood from the Rabi oscillations between the internal states of the fast atoms. For fast atoms $(k/\kappa >> 1)$, the transmission amplitude can be approximated as $T_{e,o}(k) \approx \exp(-ikL)(\exp(ik_0^+L) + \exp(ik_0^-L))/2$, where $k_0^\pm$ are given by Eq. (2.7). The transmission probability $|T_{e,0}|^2$ exhibits oscillatory behavior as a function of the momentum k of the incident atom. Moreover, at the mean wave number corresponding to the classical time, the transmission amplitude $T_{e,0}(\bar{k}) \approx \cos(gt_{cl}) = 0$.

Thus, the *correlation with the internal dynamics* (Rabi oscillations) of the atom leads to the splitting of the incident wave packet of the external motion. Obviously, since the wave packet is deformed for these parameters, the phase time $(t_{ph}/t_{cl} \approx -0.62)$ loses its physical significance and does not represent the peak to peak traversal time. Finally, we note that the vacuum field for the initial state of the cavity does not limit the study of tunneling time of the atom. In a general Fock state, the potential energy of atom-field interaction with the cavity induced potentials will be different from that of vacuum field. Still, we can redefine the atom-field coupling constant of the interaction to include this change. The super-classical tunneling and splitting of the wave packets are common features for a general Fock state of the cavity field.

2.5 Summary

In summary, we have discussed the new features in the passage time of a Gaussian wave packets of an ultracold two-level atom through a cavity which is initially empty. In Sec 2.1, we have formulated the model describing the traversal of ultracold atoms as a scattering of atoms from a potential. In Sec 2.2, we have calculated the phase tunneling time of the wave packets. It was shown that the phase tunneling time can exhibit sub- and super-classical traversal behaviors including negative values. We explained these characteristics of phase time in terms of the dispersion of the phase of transmission amplitude. In Sec 2.3, numerical results were presented for the transmitted wave packets as a function of time. The peak of the transmitted wave packet was shown to occur at the phase tunneling time calculated in Sec 2.2. Here, we have also shown that for negative phase time, the peak of the transmitted wave packet emerges the cavity even before it enters. Finally, in Sec. 2.4, we demonstrated splitting of transmitted wave packets when the effects of the atomic transitions in the cavity become important.

Chapter 3

Resonant Tunneling of Ultracold Atoms Through Vacuum Induced Potentials

It is well known that energy eigenvalues of a quantum mechanical particle fall into continuous bands separated by forbidden gaps in an infinite periodic potentials. The classic paper of Kronig and Penney [119] on this subject laid the foundation for the modern theory of solids. Extensions of the Kronig-Penney model to finite periodic potentials showed band of resonances separated by zero transmission probability in the energy eigenstates of the particle [120]. Tsu and coworkers [121] verified experimentally this resonant transmission in the context of electrons passing through semiconductor double barriers. The aim of the present chapter is to demonstrate a similar resonant tunneling of ultracold, two-level atoms through a system of potentials induced by two cavities initially in vacuum state. Unlike the semiconductor systems an important new feature of our current system is the entanglement between electronic, center-of-mass (c.m.) and the photonic degrees of freedom.

3.1 What is Resonant Tunneling ?

Consider a particle tunneling through a system of two potential barriers as shown in Fig. 3.1. The incident particle has an energy $E \equiv \hbar^2 k^2/2m$ which depends on its momentum $\hbar k$ and the mass m. Quantum mechanically, the particle can either be reflected or transmitted through the barrier potentials. We assume the particle's

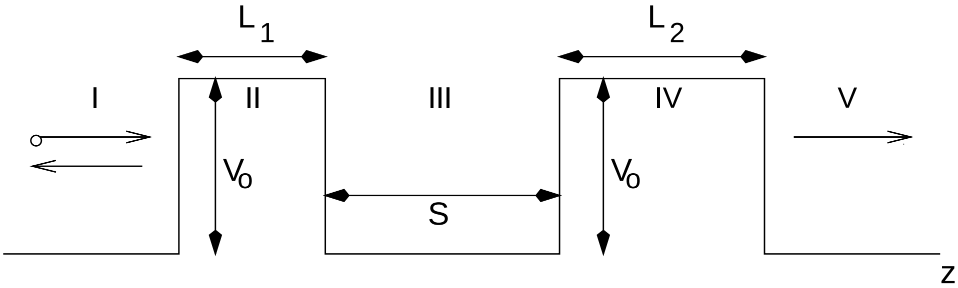

Figure 3.1: A particle tunneling through a two-barrier potential

energy to be below the top of the barrier and study its probability of tunneling from left to right regions as a function of the energy E. To keep the analysis simple, we have assumed equal potential energy V_o for each barrier and the inter-barrier separation is denoted by S. The lengths L_1 and L_2 denote the widths of the barriers in regions II and IV. The stationary wave functions of the particle in different regions are

$$\begin{aligned} \Psi_{\mathrm{I}}(z) &= A_1 e^{ikz} + B_1 e^{-ikz} , \\ \Psi_{\mathrm{II}}(z) &= A_2 e^{qz} + B_2 e^{-qz} , \\ \Psi_{\mathrm{III}}(z) &= A_3 e^{ikz} + B_3 e^{-ikz} , \\ \Psi_{\mathrm{IV}}(z) &= A_4 e^{qz} + B_4 e^{-qz} , \\ \Psi_{\mathrm{V}}(z) &= A_5 e^{ikz} + B_5 e^{-ikz} , \end{aligned} \tag{3.1}$$

where $q = \sqrt{(2m/\hbar^2)(V_o - E)}$ represents the wave number for the amplifying and decaying waves in the barrier regions. The wave functions and its derivatives should match at all the interfaces in different regions. These boundary conditions yield eight coupled equations for the coefficients A_i, B_i of the waves. We set $B_5 = 0$ which corresponds to only transmitted waves in region V. The coupled equations can be solved easily by the transfer matrix method to give the probability amplitude $B_k^{(2)} \equiv A_5/A_1$ for transmission of the particle through the two-barrier system. The absolute square of the complex quantity $B_k^{(2)}$ gives the probability $T(E)$ of transmission of the particle as a function of the energy E.

In Fig. 3.2, we compare the probability $T(E)$ for transmission of the particle through a single-barrier ($L_2 \equiv 0$) versus two-barrier ($L_2 = L_1 \neq 0$) system. The graph shows that the transmission probability of the particle exhibits new reso-

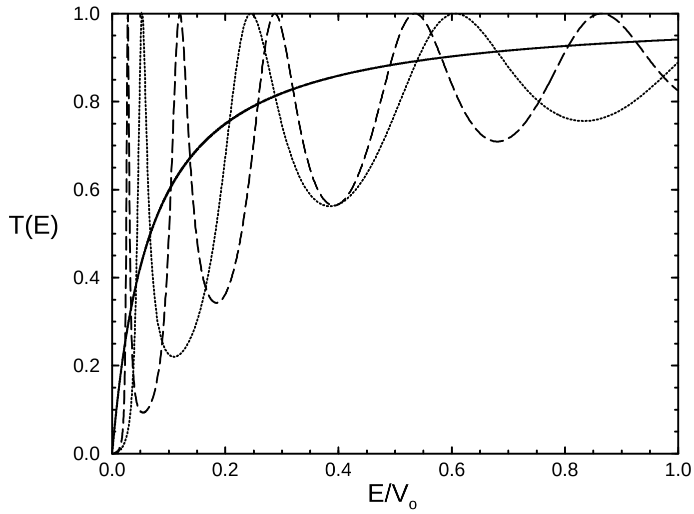

Figure 3.2: The probability of transmission $T(E)$ as a function of the energy E of a particle tunneling through a single barrier ($L_2 \equiv 0$) and double barrier ($L_2 = L_1 \neq 0$) potentials. The solid curve represents the transmission probability for the single barrier potential with length $L_1 = L$ given by $\sqrt{2mV_oL^2/\hbar^2} = 0.5$. The other two graphs correspond to particle's transmission through the two-barrier system of the same lengths $L_1 = L_2 = L$ with the inter-barrier separation S given by $\sqrt{2mV_oS^2/\hbar^2} = 10$ (dotted curve) and $\sqrt{2mV_oS^2/\hbar^2} = 15$ (long-dashed curve).

nances for the two-barrier system when compared with the single-barrier case. Also, the number of resonances in the two-barrier transmission increases with the inter-barrier separation. The origin of these transmission resonances can be understood from the fact that the presence of a potential well formed in region III between the barriers supports bound states. The bound states are defined by the poles of the transmission amplitude $B_k^{(2)}$ when viewed as a complex function of the energy E. The real and imaginary parts of the poles (complex E values) give the positions and half-widths of the resonances in transmission. These bound states are also known as quasi-bound states which corresponds to decaying solutions of time dependent Schrödinger equation solved with one of these complex E values. The perfect transmission of the particle in the quasi-bound state through the two-barrier system is termed as *resonant tunneling*. Historically, Tsu and coworkers [121] were the first to verify resonant tunneling of electrons through the two-barrier system. They considered the potential barriers made of a semiconductor material GaAlAs. A different material GaAs was sandwiched between the barriers to form the potential well. To demonstrate resonant tunneling, they measured the tunneling current of electrons through the system as a function of an applied voltage. The resonant tunneling manifested itself as peaks or humps in the tunneling current at voltages corresponding to the quasi-bound states of the potential well.

3.2 Model System

Consider an ultracold, two-level atom to be incident on a system of two cavities in vacuum state as shown in Fig. 3.3. Each cavity has a length L and the intercavity separation is denoted by S. The frequency ω of the single mode field in each cavity has been tuned to the frequency $\nu = (E_e - E_g)/\hbar$ of the atomic transition between the excited state $|e\rangle$ (energy E_e) and the ground state (energy E_g). We assume the atom (mass m) to be in the excited state initially. After the interaction, the atom

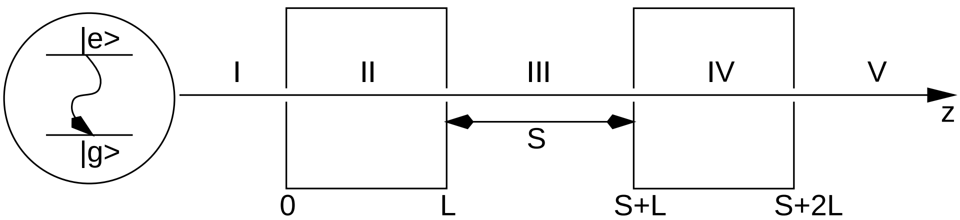

Figure 3.3: Schematic arrangement of two high quality cavities with which the ultracold atom interacts.

can exit, besides being reflected, from the two cavities either in the excited state or in the ground state. The total Hamiltonian for the atom (including the quantized motion of its center-of-mass) interacting with the two cavities is

$$\begin{aligned} H &= E_e|e\rangle\langle e| + E_g|g\rangle\langle g| + \hbar\omega(a^\dagger a + b^\dagger b) + \frac{p_z^2}{2m} \\ &\quad + \hbar\Omega_a(z)(|e\rangle\langle g|a + a^\dagger|g\rangle\langle e|) \\ &\quad + \hbar\Omega_b(z)(|e\rangle\langle g|b + b^\dagger|g\rangle\langle e|) \qquad . \end{aligned} \tag{3.2}$$

Here, operators a, b are the annihilation operators for the photons in the two cavities. The functions $\Omega_a(z)$, $\Omega_b(z)$ describe the atom-field coupling strengths in the two cavities which we assume to be equal inside the cavities. For simplicity, we also take the coupling strengths to be mesa functions $\Omega_a(z) = \Omega u_a(z)$, $\Omega_b(z) = \Omega u_b(z)$ where u_a and u_b are the mesa functions of the cavities. In writing Eq. (3.2), the dipole and rotating wave approximations have been used.

Since the interaction operator couples only the zero and one-photon states in the cavities, the total wave function of the combined system of the atom and the cavities can be written in the form

$$|\Psi(z,t)\rangle = \Phi_e(z,t)|e,0,0\rangle + \Phi_a(z,t)|g,1,0\rangle + \Phi_b(z,t)|g,0,1\rangle \ , \tag{3.3}$$

where Φ's describe the wave functions for the c.m. motion and the atom-photon states $|g,1,0\rangle$, $|g,0,1\rangle$ represent the photon emission from the atom in either of the cavities. Combining Eqs. (3.2) and (3.3) and transforming to a frame rotating with frequency ω, the Schrödinger equation (1.12) leads to the following coupled equations for the Φ's :

$$\begin{aligned} i\hbar\frac{\partial\Phi_e}{\partial t} &= -\frac{\hbar^2}{2m}\frac{\partial^2\Phi_e}{\partial z^2} + \hbar\Omega u_a(z)\Phi_a + \hbar\Omega u_b(z)\Phi_b \ , \\ i\hbar\frac{\partial\Phi_j}{\partial t} &= -\frac{\hbar^2}{2m}\frac{\partial^2\Phi_j}{\partial z^2} + \hbar\Omega u_j(z)\Phi_e \ , \end{aligned} \tag{3.4}$$

where $j = a, b$. The coupled Eqs. (3.4) are to be solved subject to the boundary conditions on four different interfaces at $z = 0$, $z = L$, $z = L + S$, and $z = 2L + S$. We look for stationary solutions of the form $\Phi_i(z,t) = \Phi_i(z)\exp(-iEt/\hbar)$ $[i = e, a, b]$ with $E \equiv \hbar^2 k^2/2m$ being the average c.m. energy of the incident atom. Then, for the five different regions indicated in Fig. 3.3, we have in general both forward and backward waves. As discussed in Sec. 1.3, the cavity regions (II & IV) act like a coherent addition of a potential barrier and a potential well (vacuum induced potential) for the incident atom. The wave numbers $k_0^{\pm} \equiv \sqrt{k^2 \mp 2m\Omega/\hbar}$ defined by Eq. (2.7) for propagation in the barrier and well components depend on the atom-field coupling energy $\hbar\Omega$. The analytic expressions for the stationary wave functions $|\Psi(z,t)\rangle = |\Psi(z)\rangle\exp(-iEt/\hbar)$ in the different regions are

$$
\begin{aligned}
|\Psi_{\mathrm{I}}(z)\rangle &= (A_1 e^{ikz} + B_1 e^{-ikz})|e,0,0\rangle + (C_1 e^{ikz} + D_1 e^{-ikz})|g,1,0\rangle \\
&\quad + (E_1 e^{ikz} + F_1 e^{-ikz})|g,0,1\rangle \ , \\
|\Psi_{\mathrm{II}}(z)\rangle &= (A_2 e^{ik_0^+ z} + B_2 e^{-ik_0^+ z} + C_2 e^{ik_0^- z} + D_2 e^{-ik_0^- z})|e,0,0\rangle \\
&\quad + (A_2 e^{ik_0^+ z} + B_2 e^{-ik_0^+ z} - C_2 e^{ik_0^- z} - D_2 e^{-ik_0^- z})|g,1,0\rangle \\
&\quad + (E_1 e^{ikz} + F_1 e^{-ikz})|g,0,1\rangle \ , \\
|\Psi_{\mathrm{III}}(z)\rangle &= (A_3 e^{ikz} + B_3 e^{-ikz})|e,0,0\rangle + (C_5 e^{ikz} + D_5 e^{-ikz})|g,1,0\rangle \\
&\quad + (E_1 e^{ikz} + F_1 e^{-ikz})|g,0,1\rangle \ , \\
|\Psi_{\mathrm{IV}}(z)\rangle &= (A_4 e^{ik_0^+ z} + B_4 e^{-ik_0^+ z} + E_4 e^{ik_0^- z} + F_4 e^{-ik_0^- z})|e,0,0\rangle \\
&\quad + (C_5 e^{ikz} + D_5 e^{-ikz})|g,1,0\rangle \\
&\quad + (A_4 e^{ik_0^+ z} + B_4 e^{-ik_0^+ z} - E_4 e^{ik_0^- z} - F_4 e^{-ik_0^- z})|g,0,1\rangle \ , \\
|\Psi_{\mathrm{V}}(z)\rangle &= (A_5 e^{ikz} + B_5 e^{-ikz})|e,0,0\rangle + (C_5 e^{ikz} + D_5 e^{-ikz})|g,1,0\rangle \\
&\quad + (E_5 e^{ikz} + F_5 e^{-ikz})|g,0,1\rangle \ .
\end{aligned}
\tag{3.5}
$$

The boundary conditions on all the interfaces give 16 coupled equations which relate the coefficients of plane waves in different regions. We solve for the coefficients under the conditions $C_1 = E_1 = B_5 = D_5 = F_5 = 0$ which corresponds to incident atom in the excited state and only transmitted waves in region V. After solving these coupled equations, we get the analytical expression for the transmission amplitude $\tau_e(k) \equiv A_5/A_1$ which describes the transmission of the atom in its initial, excited state. In Fig. 3.4, some typical results are shown for the transmission probability $T \equiv |\tau_e(k)|^2$ of an excited atom through the two-cavity system. The figure shows the dependence of the transmission on the intercavity separation as well. For comparison, we also plot the corresponding result for transmission of the atom through a single cavity. The parameters have been scaled in terms of a wavenumber κ which is defined by the vacuum coupling energy $\hbar\Omega \equiv \hbar^2\kappa^2/2m$ of the atom. Note that the temperature of the atom will be in the range 10^{-7} - 10^{-8} K if the coupling constant Ω is in the range of $100 - 10$ kHz and if $k/\kappa = 0.1$. The graph shows that the transmission probability exhibits well defined resonances at discrete values of the momentum of the incident atom. Further, the number of resonances in transmission increases with the inter-cavity separation very sim-

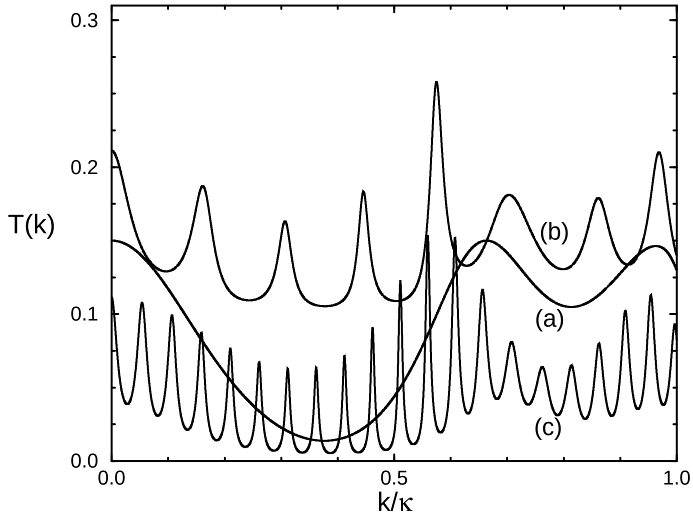

Figure 3.4: The probability T of transmitting an excited atom through a system of cavities in vacuum state as a function of the normalized momentum k/κ of the atom. The excited state of the transmitted atom is monitored. The graph (a) gives $T - 0.1$ for the single cavity case with a width given by $\kappa L = 5\pi$. The other two graphs correspond to transmission through two cavities with $\kappa L = 5\pi$, $\kappa S = 20$ [(b), plotted quantity is $T + 0.1$], $\kappa S = 60$ [(c)].

ilar to that discussed in Sec. 3.1 for a particle tunneling through a two-barrier system.

3.3 Quantum Interferences in Resonant Tunneling

In this section, we examine the origin of new resonances in the two-cavity transmission shown in Fig. 3.4 by studying the analytic structure of the transmission amplitude. We have proved that the transmission amplitude $\tau_e(k)$ can be written in a very interesting form in terms of the transmission and reflection amplitudes for the single cavity as

$$\tau_e(k) = T_{e,0}^2 \{1 - \exp(2ikS) R_{e,0}^2\}^{-1} . \tag{3.6}$$

Here $R_{e,0}$ and $T_{e,0}$ are the reflection and transmission amplitudes for the excited atom incident on a single cavity in vacuum state. As defined in section 2.1, these amplitudes can be defined in terms of single barrier (superscript +) and well (superscript -) reflection and transmission amplitudes $\rho_0^{\pm}$, $\tau_0^{\pm}$ as

$$R_{e,0} = \frac{1}{2}\left(\rho_0^{+} + \rho_0^{-}\right) \ , \tag{3.7}$$

$$T_{e,0} = \frac{1}{2}\left(\tau_0^{+} + \tau_0^{-}\right) \ . \tag{3.8}$$

The formula Eq. (3.6) is very much reminiscent of transmission of light through a Fabry-Pérot cavity where $R_{e,0}$ is the amplitude for reflection of light at the mirrors of the cavity. The formula also shows that the probability of atom transmitting through the two-cavity system is not the product of probabilities for transmission through two single cavities. The atom bounces back and forth in region III between the two cavities just like light between mirrors of the Fabry-Pérot cavity. In region III, the amplitudes for a single reflection of the atom from the first (re-

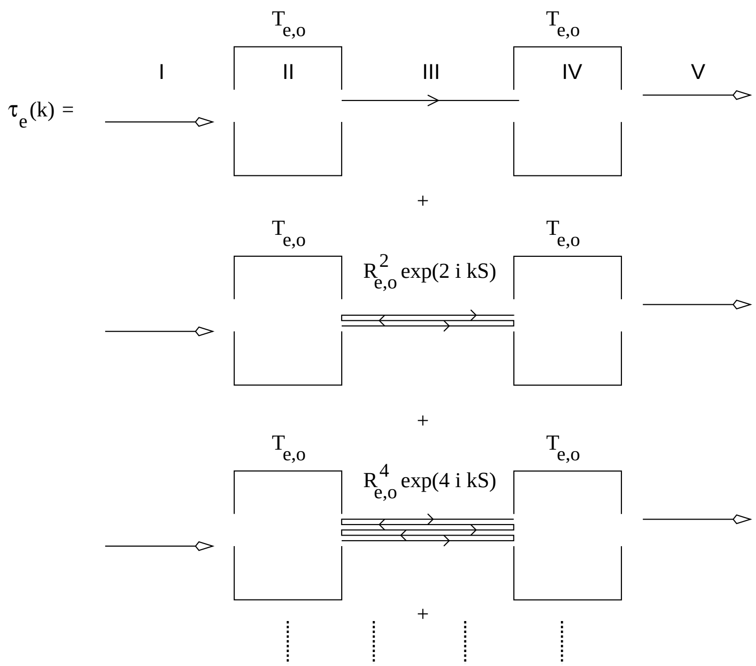

Figure 3.5: Diagrammatic representation of possible paths of the transmission of the atom through the two-cavity system.

gion II) and second (region IV) cavities are $R_{e,0}\exp(-2ikL)$ and $R_{e,0}\exp(2ik(L+S))$ respectively. Here, the additional phase factors account for the phase shifts imparted upon each reflection from both the cavities. The total amplitude for traversal of the atom in region III after a single round trip (a distance $2S$) is therefore $R_{e,0}^2\exp(2ikS)$ as shown in Fig. 3.5. A Taylor expansion of the denominator (expression in curly brackets) in Eq. (3.6) gives further the amplitudes for all possible events in the multiple reflections of the atom between the cavities as indicated in Fig. 3.5. Note that when the transmission amplitude $\tau_e(k)$ is viewed as a complex function of k, it has a discrete number of simple poles in the complex k plane. A pole of the transmission amplitude describes a self-reproducing wave, i.e., a wave that reproduces itself after a single round trip ($R_{e,0}^2 \exp(2ikS) = 1$) in region III. The real (imaginary) part of the poles (complex k values) gives the position (width) of the resonances in transmission. The transmission resonances in Fig. 3.4 are consistent with these momentum values. The quantum states corresponding to these complex momentum (k) values are known as quasi-bound states in the sense that atom in this state is not bound strictly to the potential well between the cavities. The atom can escape out of the well by tunneling through the adjacent cavities.

In order to understand further the origin of new resonances in the transmission, we also study the transmission of atoms through a double barrier potential or a double well potential. We replace each cavity region by a barrier (well) of height (depth) $\hbar\Omega$. This leads to three distinct configurations of potentials such as

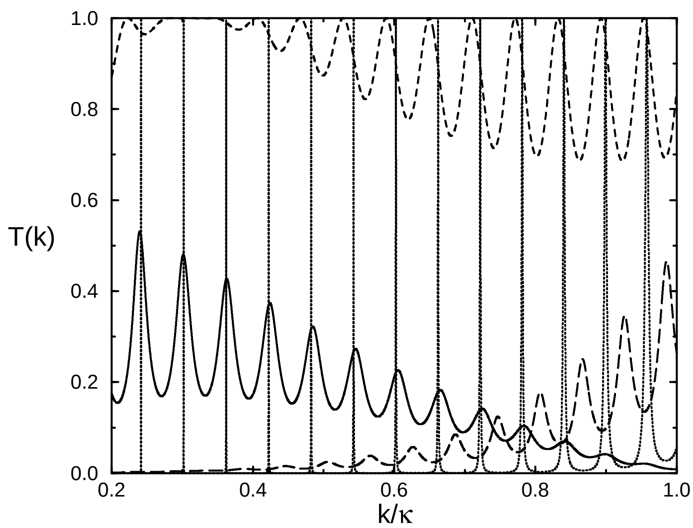

Figure 3.6: The probability of transmission T of an excited atom through a system of two cavities in vacuum state, along with transmission through double barrier (dotted curve), double well (dashed curve), single barrier - single well (long dashed curve) potentials. For all the graphs, $\kappa L = 3$, $\kappa S = 50$. The solid curve corresponds to $5T$ through the two cavity system

double barrier, double well and single barrier - single well potentials. In Fig. 3.6, we compare the transmission of atom through two-cavity system with its transmission through these potential configurations. The close relation of the two-cavity transmission to the tunneling resonances of the double barrier potential is to be noticed. Note that for an infinitely deep well between the two barriers in double barrier system, the resonances occur at $kS = n\pi$ or at $k/\kappa = n\pi/\kappa S = n\pi/50$. The resonances in the two-cavity transmission shown in Fig. 3.6 are in the vicinity of these positions. Clearly the peaks in the transmission have a definite bearing to the tunneling resonances. Thus the passage of an ultracold atom through a system of cavities exhibits tunneling resonances in a way similar to the work of Tsu and co-workers [121] on the tunneling of electrons in semiconductor double-barriers (Sec. 3.1).

3.4 Coupling of the Cavities

In the previous section, we have shown that the transmission of ultracold atoms through a two-cavity system shares some features with tunneling through double barrier potential. Though this is true, in general, all the barrier and well potential combinations contribute to the tunneling of atoms through the two-cavity system. This can be better understood if we compare the the transmission amplitude $\tau_e(k)$ with the probability amplitudes for transmission of the atom through double barrier $[B_k^{(2)}]$ and double well $[W_k^{(2)}]$ potentials given by

$$B_k^{(2)} = \tau_0^{+2}\Big\{1 - \exp(2ikS)\rho_0^{+2}\Big\}^{-1}, \tag{3.9}$$

$$W_k^{(2)} = \tau_0^{-2}\Big\{1 - \exp(2ikS)\rho_0^{-2}\Big\}^{-1}, \tag{3.10}$$

There are many similarities among the results (3.6), (3.9), and (3.10) though there are also differences. The differences arise as in each cavity we have two dressed states leading to Eqs. (3.7) and (3.8). In order to see the mixing of the barrier and well contributions to the tunneling of atoms, we show in Fig. 3.7 the transmission probability as a function of the length of each cavity for ultra-cold, incident atoms $(k/\kappa << 1)$. It is seen from the graph that each resonance curve of the single cavity is split into two for smaller kinetic energies of the incident atoms. The second

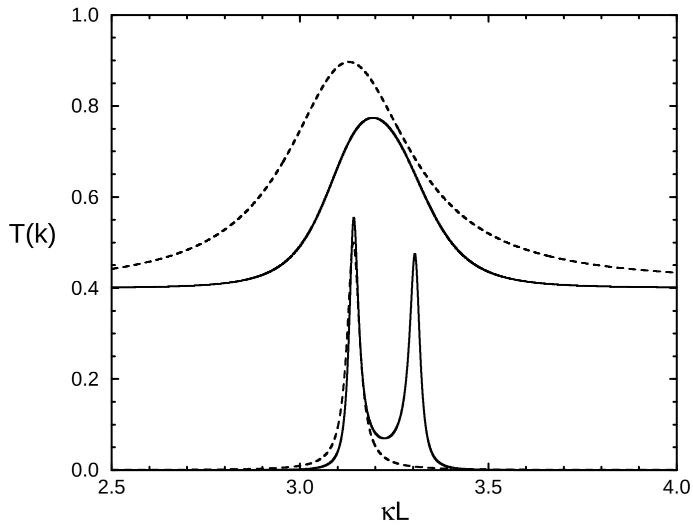

Figure 3.7: The probability of transmission T of an excited atom through a system of two cavities in vacuum state as a function of length κL of cavities for fixed intercavity separation $\kappa S = 5$. For comparison, the corresponding graph (dashed line) for single cavity has been superimposed. The two upper (bottom) curves are for $k/\kappa = 0.1$ (0.01). For clarity, we have plotted $2T$, $5T$, $5T + 0.4$, and $2T + 0.4$ in curves from bottom to top.

resonance at $\kappa L \approx 3.305$ for $k/\kappa = 0.01$ comes from the denominator expression in curly brackets in Eq. (3.6). Note that in this range of momentum and intercavity length, curly brackets in Eqs. (3.6), (3.9) and (3.10) can be simplified, respectively, to $-2ik[\kappa S + \coth(\kappa L) - \cot(\kappa L)]/\kappa$, $-2ik[\kappa S + 2\coth(\kappa L)]/\kappa$, and $-2ik[\kappa S - 2\cot(\kappa L)]/\kappa$. Clearly the coherent addition of amplitudes of the barrier and well components gives rise to the mixing of the terms $\coth(\kappa L)$ and $\cot(\kappa L)$ in the denominator of Eq. (3.6). As a result, all the resonances in the transmission through double barrier or double well can not account for the resonant transmission of atoms through two-cavity system. Further, the splitting of the resonance curve shows that the cavities do not behave like independent cavities for the incident atom. The interaction of atom couples the cavities both by emission and reabsorption of photons and by the reflection - transmission through the vacuum induced potentials. It is important to note that the atom can emit a photon in either of cavities by spontaneous emission and the transmission of atom in ground state can also be studied in a similar manner. Moreover, this work can also be extended to multicavity system where the sizes of the barrier - well potentials induced by the interaction can be manipulated by varying the lengths of each cavity and the separation between them. One can even discuss analog of field assisted tunneling discussed in the context of potential barriers [122].

3.5 Summary

In summary, we have discussed the new features in the transmission of an ultracold two-level atom through a system of two cavities in vacuum state. We have demonstrated resonant tunneling of ultracold atoms through the potentials produced by the interaction of the atom with the cavities. This resonant tunneling is very similar to the work of Tsu and coworkers on the tunneling of electrons through semiconductor superlattices [121]. In Sec 3.1, we explained the basic idea of resonant tunneling in the context of electrons passing through a double barrier potential. In Sec 3.2, we explained our model system and derived the basic working equations. Numerical results were presented for probability of transmitting the atom through the two-cavity system as a function of energy of incident atoms. The transmission probability was shown to exhibit new resonances for the two-cavity system when compared with the single cavity case. In Sec 3.3, we presented the analytical result for the transmission probability of the atom. The new resonances in transmission were interpreted as due to multiple bounces of ultracold atoms in the region between the cavities. Here, we also demonstrated the existence of quasi-bound states introduced in Sec. 3.1. Finally, in Sec. 3.4, we have discussed the possibility of coupling the cavities by the quantized motion of atoms.

Chapter 4

Generation of Correlated Fields in a Bimodal Cavity With Ultracold Atoms

In the previous chapters, we studied the dynamics of a single ultracold atom interacting with the cavity fields which have fixed initial state. In this chapter, we discuss the generation of correlated fields in a maser cavity by considering the interaction of a beam of ultracold atoms. The passage of each atom in the beam builds up the field against the losses in the cavity. We take the atomic-level configuration to be a Λ-type three-level atom resonant with the two modes of the cavity. This atomic model has been widely used in studies of lasing without inversion [123], electro-magnetically induced transperancy [124], matched photon statistics [125] and two-mode micromaser [67]. We follow very closely the work of Meyer, Scully and Walther [99] on two-level atoms.

4.1 A Three-level Atom Plus Bimodal Field

Consider an ultracold, three-level atom in the Λ-type configuration to be incident on a bimodal cavity. The energy level diagram for the analysis is shown in Fig. 4.1. The transition between the two ground levels g_1 and g_2 is dipole forbidden and the transition from the excited level e to any of the lower levels g_1 and g_2 is allowed. The frequencies of the transitions $e \rightarrow g_1$ and $e \rightarrow g_2$, coincide with those of the modes 1 and 2 of the microwave cavity so that the atom and the bimodal field in the cavity interact resonantly. The Hamiltonian for the atom-field

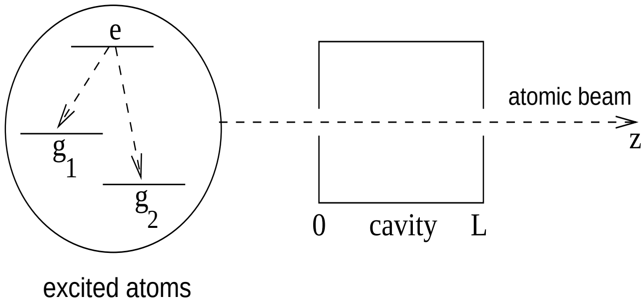

Figure 4.1: The scheme of the two-mode micromaser and the energy-level diagram for the analysis.

interaction including the quantization of the center-of-mass (c.m.) motion of the atoms, is given by

$$H = H_A + H_F + H_{AF} \ , \tag{4.1}$$

where H_A (H_F) is the Hamiltonian of the free atom (field) and H_{AF} is the interaction Hamiltonian describing the atom-field interaction in the dipole and the rotating wave approximations [cf. Eq. (1.25)] :

$$H_A = \frac{p_z^2}{2m} + \hbar\Omega_e|e\rangle\langle e| + \sum_{\alpha=1}^{2}\hbar\Omega_{g_\alpha}|g_\alpha\rangle\langle g_\alpha| \ ,$$

$$H_F = \sum_{\alpha=1}^{2}\hbar\omega_\alpha a_\alpha^\dagger a_\alpha \ , \tag{4.2}$$

$$H_{AF} = \sum_{\alpha=1}^{2}\hbar\Omega_\alpha\left(|e\rangle\langle g_\alpha|a_\alpha + a_\alpha^\dagger|g_\alpha\rangle\langle e|\right) \ .$$

The operator $|j\rangle\langle j|(j = e, g_1, g_2)$ gives the projection on to the state $|j\rangle$ with energy $\hbar\Omega_j$. The operators $|i\rangle\langle j|(i, j = e, g_1, g_2; i \neq j)$ describe the transition from level j to level i. The operators a_α ($a_\alpha^\dagger$) annihilate (create) a photon in modes α with the resonance frequencies $\omega_\alpha = \Omega_e - \Omega_{g_\alpha}$. The parameters Ω_α are the corresponding atom-field coupling constants and m is the atomic mass. The parameters Ω_α are dependent on z through the mode function of the cavity.

In a suitable interaction picture, the Hamiltonian (4.1) of the atom-field system reads as

$$H_I = \frac{p_z^2}{2m} + H_{AF} \ . \tag{4.3}$$

The operator H_{AF} is readily diagonalizable. It has eigenstates $|\phi^0_{n_1+1,n_2+1}\rangle$, $|\phi^\pm_{n_1+1,n_2+1}\rangle$ with eigenvalues 0, $\pm\hbar\sqrt{\Omega_1^2(z)(n_1+1)+\Omega_2^2(z)(n_2+1)}$, respectively, where

$$|\phi^0_{n_1+1,n_2+1}\rangle = \frac{\left[\Omega_2\sqrt{n_2+1}\;|g_1,n_1+1,n_2\rangle - \Omega_1\sqrt{n_1+1}\;|g_2,n_1,n_2+1\rangle\right]}{\left[\Omega_1^2(n_1+1)+\Omega_2^2(n_2+1)\right]^{1/2}}\;,$$

$$\begin{aligned} |\phi^\pm_{n_1+1,n_2+1}\rangle &= \frac{1}{\sqrt{2}}\left[|e,n_1,n_2\rangle \pm \frac{\Omega_1\sqrt{n_1+1}}{\sqrt{\Omega_1^2(n_1+1)+\Omega_2^2(n_2+1)}}|g_1,n_1+1,n_2\rangle\right. \\ &\left.\pm\frac{\Omega_2\sqrt{n_2+1}}{\sqrt{\Omega_1^2(n_1+1)+\Omega_2^2(n_2+1)}}|g_2,n_1,n_2+1\rangle\right]\;. \end{aligned} \tag{4.4}$$

The interaction operator H_{AF} and its eigenstates $|\phi^0_{n_1+1,n_2+1}\rangle$, $|\phi^\pm_{n_1+1,n_2+1}\rangle$ depend on the atomic position z inside the cavity through the coupling strengths $\Omega_1(z)$, $\Omega_2(z)$. Thus, it is in general difficult to carry out the time evolution of an atom-field state governed by the Hamiltonian (4.3) for the quantized motion of the atoms. So, for simplicity, we work with the mesa mode functions $\Omega_\alpha(z)=\Omega_\alpha\theta(z)\theta(L-z)$ which represent the z-independent atom-field couplings in the cavity. In this case, the eigenstates of the interaction are independent of atomic position inside the cavity and the Hamiltonian (4.3) in the eigenstates basis leads to

$$\begin{aligned} H_I|\phi^\pm_{n_1+1,n_2+1}\rangle &= h_\pm|\phi^\pm_{n_1+1,n_2+1}\rangle\;, \\ H_I|\phi^0_{n_1+1,n_2+1}\rangle &= h_0|\phi^0_{n_1+1,n_2+1}\rangle\;. \end{aligned} \tag{4.5}$$

Here $h_\pm = p_z^2/2m \pm \theta(z)\theta(L-z)\hbar\sqrt{\Omega_1^2(n_1+1)+\Omega_2^2(n_2+1)}$ and $h_0 = p_z^2/2m$. Note that $h_\pm$ and h_0 are still operators which act in the space of the c.m. variables. Clearly, the effect of the cavity is seen to produce potential terms in h_α corresponding to the dressed states $|\phi^\pm_{n_1+1,n_2+1}\rangle$ of the atom-field interaction. The dark eigenstate $|\phi^0_{n_1+1,n_2+1}\rangle$ with eigenvalue zero of the interaction Hamiltonian H_{AF} induces a reflection-less transmission for the external motion of the atom.

To study maser action, we need to consider the initial atom-field state to be $|e,n_1,n_2\rangle$, i.e., the atom is in the excited state and the cavity contains (n_1,n_2) photons in the modes (1,2) initially. Note that we can in principle work with any basis set of states to solve for the time evolution of this initial state. Thus, outside the cavity, we use (4.4). Also, it is preferable to work in the eigenbasis (4.4) inside

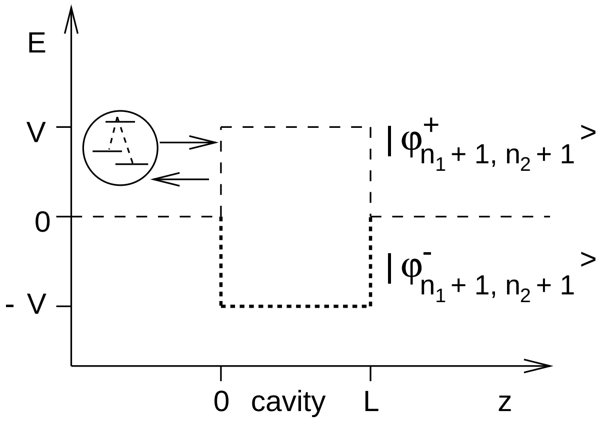

Figure 4.2: Schematic representation of the energy E of the excited atoms incident upon a two-mode micromaser cavity with (n_1, n_2) photons. The interaction is equivalent to reflection and transmission of atoms through a potential barrier (dashed) or potential well (dotted) with a potential energy $V = \hbar\sqrt{\Omega_1^2(n_1+1)+\Omega_2^2(n_2+1)}$. Thus reflection and transmission of the atom is very similar to the one in the work of Meyer et al. However, the atom can be reflected and transmitted in either of the three states $|e, n_1, n_2\rangle$, $|g_1, n_1+1, n_2\rangle$, and $|g_2, n_1, n_2+1\rangle$.

the cavity so that equations can be decoupled. The initial atom-field state $|e, n_1, n_2\rangle$ can then be expanded in terms of the dark and dressed eigenstates ;

$$|e, n_1, n_2\rangle = \frac{1}{\sqrt{2}}\left[|\phi^+_{n_1+1,n_2+1}\rangle + |\phi^-_{n_1+1,n_2+1}\rangle\right] \ . \tag{4.6}$$

Since the initial atom-field state $|e, n_1, n_2\rangle$ is orthogonal to the dark eigenstate $|\phi^0_{n_1+1,n_2+1}\rangle$, we can further expand the wave function of the combined atom-cavity system as

$$|\Psi(z,t)\rangle = \chi_+(z,t)|\phi^+_{n_1+1,n_2+1}\rangle + \chi_-(z,t)|\phi^-_{n_1+1,n_2+1}\rangle \ , \tag{4.7}$$

then the Schrödinger equation (1.12) in the interaction picture becomes

$$i\hbar\frac{\partial\chi_\alpha}{\partial t} = h_\alpha\chi_\alpha \ , \quad \alpha = \pm \ . \tag{4.8}$$

Thus, the problem is now reduced to that of an atom incident upon the barrier - well potentials $V^{\pm}_{n_1+1,n_2+1}(z) = \pm\theta(z)\theta(L-z)\hbar\sqrt{\Omega_1^2(n_1+1)+\Omega_2^2(n_2+1)}$ as shown in Fig. 4.2. Note that the dark eigenstate $|\phi^0_{n_1+1,n_2+1}\rangle$ has no influence on the atom-cavity dynamics for the initial excited state of the atom considered.

Denoting the reflection and transmission amplitudes as $\rho^{\pm}_{n_1,n_2}$,$\tau^{\pm}_{n_1,n_2}$ for the potential barrier-well problem of the dressed states $|\phi^{\pm}_{n_1+1,n_2+1}\rangle$, respectively, we have

$$\rho^{\pm}_{n_1,n_2} = i\Delta^{\pm}_{n_1,n_2} \sin(k^{\pm}_{n_1,n_2}L) \exp(ikL)\tau^{\pm}_{n_1,n_2} \ , \tag{4.9}$$

$$\tau^{\pm}_{n_1,n_2} = \exp(-ikL)\left[\cos(k^{\pm}_{n_1,n_2}L) - i\Sigma^{\pm}_{n_1,n_2} \sin(k^{\pm}_{n_1,n_2}L)\right]^{-1} \ , \tag{4.10}$$

$$\Delta^{\pm}_{n_1,n_2} = \frac{1}{2}\left(\frac{k^{\pm}_{n_1,n_2}}{k} - \frac{k}{k^{\pm}_{n_1,n_2}}\right) \ , \tag{4.11}$$

$$\Sigma^{\pm}_{n_1,n_2} = \frac{1}{2}\left(\frac{k^{\pm}_{n_1,n_2}}{k} + \frac{k}{k^{\pm}_{n_1,n_2}}\right) \ ,$$

$$k^{\pm}_{n_1,n_2} = \sqrt{\left(k^2 \mp \frac{2m}{\hbar}\sqrt{\Omega_1^2(n_1+1) + \Omega_2^2(n_2+1)}\right)} \ , \tag{4.12}$$

where $\hbar k$ is the atomic c.m. momentum and L is the length of the cavity. It is to be noted that the strengths of the barrier - well potentials (potential energy term in $k^{\pm}_{n_1,n_2}$) depend on the coupling constants Ω_1, Ω_2 as well as the occupation numbers n_1, n_2 of the photons in the cavity.

We consider the c.m. wave packet of the incident atom to be $\psi(z,0) = \int dk A(k)e^{ikz}$ where the amplitudes $A(k)$ are adjusted such that the incident wave packet $|\psi(z,0)|^2$ to the left of the cavity $(z < 0)$ does not extend into the cavity region at the initial time $t = 0$. The wave function of the atom-field system initially is therefore

$$|\Psi(z,0)\rangle = \psi(z,0)|e,n_1,n_2\rangle \ . \tag{4.13}$$

The wave function of the atom-field system at time t after the atom has left the cavity region is found by solving the Eqs. (4.7) and (4.8) subject to the above initial condition :

$$\begin{aligned} |\Psi(z,t)\rangle \quad = \quad & \int dk A(k) e^{-i(\hbar k^2/2m)t} \\ & \times \Big\{ \Big[R_{e,n_1,n_2}(k)e^{-ikz}\theta(-z) + T_{e,n_1,n_2}(k)e^{ikz}\theta(z-L)\Big] \, |e,n_1,n_2\rangle \\ & + \Big[R_{g_1,n_1+1,n_2}(k)e^{-ikz}\theta(-z) + T_{g_1,n_1+1,n_2}(k)e^{ikz}\theta(z-L)\Big] \, |g_1,n_1+1,n_2\rangle \\ & + \Big[R_{g_2,n_1,n_2+1}(k)e^{-ikz}\theta(-z) + T_{g_2,n_1,n_2+1}(k)e^{ikz}\theta(z-L)\Big] \, |g_2,n_1,n_2+1\rangle \Big\} \end{aligned} \tag{4.14}$$

where

$$
\begin{aligned}
R_{e,n_1,n_2} &= \frac{1}{2}(\rho^+_{n_1,n_2} + \rho^-_{n_1,n_2}) \ , \\
T_{e,n_1,n_2} &= \frac{1}{2}(\tau^+_{n_1,n_2} + \tau^-_{n_1,n_2}) \ ,
\end{aligned} \tag{4.15}
$$

are the probability amplitudes that the atom is reflected or transmitted with the atom-field state remaining in the same initial state as $|e, n_1, n_2\rangle$ and

$$
\begin{aligned}
R_{g_1,n_1+1,n_2} &= \frac{\Omega_1\sqrt{n_1+1}}{2\sqrt{\Omega_1^2(n_1+1)+\Omega_2^2(n_2+1)}}(\rho^+_{n_1,n_2} - \rho^-_{n_1,n_2}) \ , \\
T_{g_1,n_1+1,n_2} &= \frac{\Omega_1\sqrt{n_1+1}}{2\sqrt{\Omega_1^2(n_1+1)+\Omega_2^2(n_2+1)}}(\tau^+_{n_1,n_2} - \tau^-_{n_1,n_2}) \ ,
\end{aligned} \tag{4.16}
$$

are the probability amplitudes that the atom is reflected or transmitted when the atom-field state makes a transition from initial $|e, n_1, n_2\rangle$ to $|g_1, n_1 + 1, n_2\rangle$. Similarly, the atom is reflected or transmitted when the atom-field state changes to $|g_2, n_1, n_2 + 1\rangle$ with amplitudes

$$
\begin{aligned}
R_{g_2,n_1,n_2+1} &= \frac{\Omega_2\sqrt{n_2+1}}{2\sqrt{\Omega_1^2(n_1+1)+\Omega_2^2(n_2+1)}}(\rho^+_{n_1,n_2} - \rho^-_{n_1,n_2}) \ , \\
T_{g_2,n_1,n_2+1} &= \frac{\Omega_2\sqrt{n_2+1}}{2\sqrt{\Omega_1^2(n_1+1)+\Omega_2^2(n_2+1)}}(\tau^+_{n_1,n_2} - \tau^-_{n_1,n_2}) \ .
\end{aligned} \tag{4.17}
$$

Note that all the physical characteristics regarding the interaction of ultracold atoms with a high quality cavity can be calculated in terms of quantities defined by Eqs. (4.15)-(4.17). Let us examine the probability of emission of a photon. When an initially excited three-level atom is incident upon the cavity containing (n_1, n_2) photons in the two modes (1,2), respectively, then from Eqs. (4.16) and (4.17) the probability that the atom goes to the level g_1 and emits a photon in mode 1 is

$$
P_{n_1,n_2}(e \rightarrow g_1) = |\ R_{g_1,n_1+1,n_2}\ |^2 + |\ T_{g_1,n_1+1,n_2}\ |^2 \ , \tag{4.18}
$$

and the probability that the atom goes to the level g_2 and emits a photon in mode 2 is

$$
P_{n_1,n_2}(e \rightarrow g_2) = |\ R_{g_2,n_1,n_2+1}\ |^2 + |\ T_{g_2,n_1,n_2+1}\ |^2 \ . \tag{4.19}
$$

It is clear from the above equations that an excited atom can emit a photon in either mode 1 or mode 2 with equal probability for the case of equal coupling strengths $\Omega_1 = \Omega_2$. For the case of unequal coupling strengths $\Omega_1 \neq \Omega_2$, the photon emission probabilities in mode 1 and mode 2 are qualitatively similar except for the multiplicative factors in Eqs. (4.16) and (4.17). In Fig. 4.3, we show the probability of photon emission from an excited atom in any fixed mode for the equal parameter case $\Omega_1 = \Omega_2$. We have used a wavenumber κ defined by the vacuum coupling energy $\hbar^2\kappa^2/2m \equiv \hbar\sqrt{\Omega_1^2 + \Omega_2^2}$ to scale the parameters.

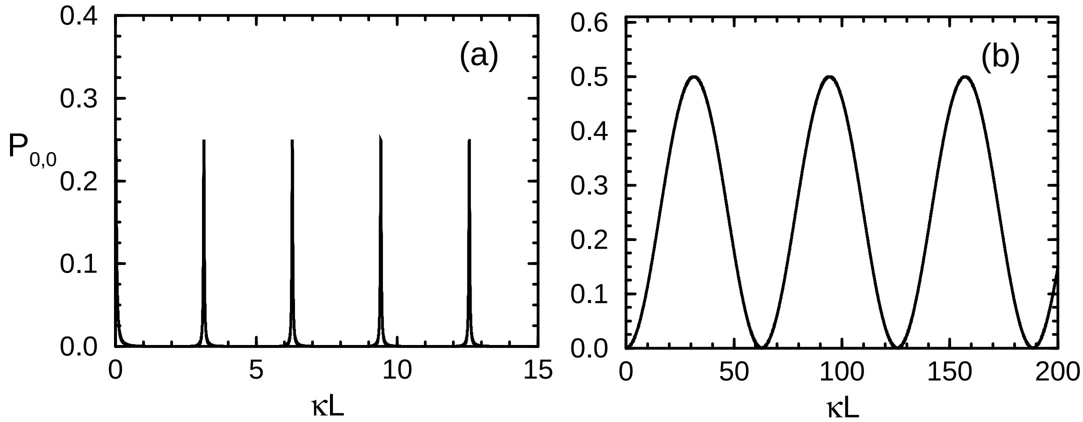

Figure 4.3: The probability of $e \to g_1$ (or) $e \to g_2$ transitions of an excited atom as a function of the length κL of the cavity. The cavity is initially in the vacuum state and the parameters used are $\Omega_2 = \Omega_1$, $k/\kappa = 0.01$ (a), $k/\kappa = 10$ (b).

The graph shows that for ultracold atoms ($k/\kappa << 1$) the probability of transition $e \to g_1$ exhibits resonances similar to that of a two-level atom incident on a single mode cavity [99]. For fast atoms ($k/\kappa >> 1$), the photon emission probability exhibits Rabi oscillations as a function of the length of the cavity. This feature resembles that of the Jaynes-Cummings model studied in Sec. 1.2.1 for a two-level atom. In fact, when the energy of the incident atom is very high ($k/\kappa >> 1$), the kinetic energy operator in the Hamiltonian (4.1) can be neglected. The time evolution of the initial atom-field state $|e, n_1, n_2\rangle$ then gives for the photon emission probabilities of an atom

$$\begin{aligned} P_{n_1,n_2}(e\to g_1) &= \frac{\Omega_1^2(n_1+1)}{\Omega^2}\sin^2(\Omega\tau) \\ P_{n_1,n_2}(e\to g_2) &= \frac{\Omega_2^2(n_2+1)}{\Omega^2}\sin^2(\Omega\tau)\ , \end{aligned} \tag{4.20}$$

where $\Omega \equiv \sqrt{\Omega_1^2(n_1+1) + \Omega_2^2(n_2+1)}$ is the Rabi frequency and τ is the interaction time of the atom with the cavity.

4.2 Buildup of the Cavity Field

In this section, we derive the master equation for the cavity field assuming that a steady atomic beam passes through the cavity. The flux of the incident atoms is so adjusted that only one atom interacts with the cavity at a time. Further, the interaction time of each atom with the cavity is so small that the cavity field damping can be neglected during atom-field interaction. The successive passage of atoms changes the field in the cavity. In the previous section, we had assumed the cavity field to be in the Fock state. However, for the dynamic evolution of the field we have to examine a more general initial state of the cavity field. Using Eq. (4.6) the wave function of the initial atom-field system is now given by

$$\begin{aligned} \langle z|\Psi(0)\rangle &= \psi(z,0)\sum_{n_1,n_2} C_{n_1,n_2} \mid e, n_1, n_2\rangle \\ &= \psi(z,0)\frac{1}{\sqrt{2}}\sum_{n_1,n_2} C_{n_1,n_2}\left(\mid \phi^{+}_{n_1+1,n_2+1}\rangle + \mid \phi^{-}_{n_1+1,n_2+1}\rangle\right) . \end{aligned} \tag{4.21}$$

Carrying out the time evolution for this initial state using Eq. (4.14), the state of atom-field system after the interaction is given by

$$\begin{aligned} |\Psi(z,t)\rangle &= \int dk A(k) e^{-i(\hbar k^2/2m)t} \sum_{n_1,n_2=0}^{\infty} C_{n_1,n_2} \\ &\times \left\{ \left[R_{e,n_1,n_2}(k)e^{-ikz}\theta(-z) + T_{e,n_1,n_2}(k)e^{ikz}\theta(z-L)\right] |e, n_1, n_2\rangle \right. \\ &+ \left[R_{g_1,n_1+1,n_2}(k)e^{-ikz}\theta(-z) + T_{g_1,n_1+1,n_2}(k)e^{ikz}\theta(z-L)\right] |g_1, n_1+1, n_2\rangle \\ &+ \left. \left[R_{g_2,n_1,n_2+1}(k)e^{-ikz}\theta(-z) + T_{g_2,n_1,n_2+1}(k)e^{ikz}\theta(z-L)\right] |g_2, n_1, n_2+1\rangle \right\} \end{aligned} \tag{4.22}$$

The state $|\Psi(z,t)\rangle$ in the above equation (4.22) can be used to find the atom-field density matrix after a single atom has passed through the cavity. By taking the trace over the atomic energy eigenstates and the position eigenstates of the center of mass of the atom, the reduced density operator $\rho(t)$ of the cavity field is then found to be

$$\rho(t) = \sum_{i=e,g_1,g_2} \int dz \langle i \mid \Psi(z,t)\rangle\langle\Psi(z,t) \mid i\rangle . \tag{4.23}$$

We consider the case in which excited atoms are injected into the cavity at random times and the time interval between successive atoms entering the cavity obeys a Poissonian distribution with an average r. As discussed in [43], the contribution of each atom passing through the cavity and the field damping lead to the following coarse grained time evolution of reduced density operator of the field in the interaction picture.

$$\dot{\rho}(t) = r\delta\rho(t) + L\rho(t) \ , \tag{4.24}$$

where $\delta\rho(t)$ is the change in $\rho(t)$ due to the passage of a single atom in the excited state. The field damping is described by the Liouville operator L which we model as due to the interaction with a thermal reservoir. Since the modes of the cavity behave independently during interaction with the thermal reservoir, the Liouville operator becomes $L = L_1 + L_2$, the sum of Liouville operators L_1 and L_2 for the two modes which are defined in Eq. (1.17). Thus, the reduced density operator of the two-mode field including damping becomes

$$\begin{aligned} L\rho \ = \ & \frac{1}{2}C_1(n_{b_1}+1)(2a_1\rho a_1^\dagger - a_1^\dagger a_1\rho - \rho a_1^\dagger a_1) \\ & + \frac{1}{2}C_1 n_{b_1}(2a_1^\dagger\rho a_1 - a_1 a_1^\dagger\rho - \rho a_1 a_1^\dagger) \\ & + \frac{1}{2}C_2(n_{b_2}+1)(2a_2\rho a_2^\dagger - a_2^\dagger a_2\rho - \rho a_2^\dagger a_2) \\ & + \frac{1}{2}C_2 n_{b_2}(2a_2^\dagger\rho a_2 - a_2 a_2^\dagger\rho - \rho a_2 a_2^\dagger) \ . \end{aligned} \tag{4.25}$$

Here n_{b_α} is the number of thermal photons in mode α and C_α is the damping rate of this mode. Using Eqs. (4.23)-(4.25) we obtain the equation governing the time evolution of the density matrix elements

$$
\begin{aligned}
\dot{\rho}(n_1, n_2; n_1', n_2') &= r\left\{(R_{e,n_1,n_2}R^{\star}_{e,n_1',n_2'} + T_{e,n_1,n_2}T^{\star}_{e,n_1',n_2'} - 1)\rho(n_1, n_2; n_1', n_2')\right. \\
&+ \; (R_{g_1,n_1,n_2}R^{\star}_{g_1,n_1',n_2'} + T_{g_1,n_1,n_2}T^{\star}_{g_1,n_1',n_2'})\rho(n_1-1, n_2; n_1'-1, n_2') \\
&+ \; \left.(R_{g_2,n_1,n_2}R^{\star}_{g_2,n_1',n_2'} + T_{g_2,n_1,n_2}T^{\star}_{g_2,n_1',n_2'})\rho(n_1, n_2-1; n_1', n_2'-1)\right\} \\
&+ \frac{1}{2}C_1(n_{b_1}+1)[2\sqrt{(n_1+1)(n_1'+1)}\rho(n_1+1, n_2; n_1'+1, n_2') \\
&- (n_1+n_1')\rho(n_1, n_2; n_1', n_2')] \\
&+ \frac{1}{2}C_1 n_{b_1}[2\sqrt{n_1 n_1'}\rho(n_1-1, n_2; n_1'-1, n_2') \\
&- (n_1+n_1'+2)\rho(n_1, n_2; n_1', n_2')] \\
&+ \frac{1}{2}C_2(n_{b_2}+1)[2\sqrt{(n_2+1)(n_2'+1)}\rho(n_1, n_2+1; n_1', n_2'+1) \\
&- (n_2+n_2')\rho(n_1, n_2; n_1', n_2')] \\
&+ \frac{1}{2}C_2 n_{b_2}[2\sqrt{n_2 n_2'}\rho(n_1, n_2-1; n_1', n_2'-1) \\
&- (n_2+n_2'+2)\rho(n_1, n_2; n_1', n_2')] \; .
\end{aligned} \tag{4.26}
$$

The diagonal elements of the density matrix $P(n_1, n_2) = \rho(n_1, n_2; n_1, n_2)$ which gives the joint distribution of photons in the two cavity modes, obeys the equation

$$
\begin{aligned}
\dot{P}(n_1, n_2) &= -\, G_{g_1,n_1,n_2}\; P(n_1, n_2) + G_{g_1,n_1-1,n_2}\; P(n_1-1, n_2) \\
&- \, G_{g_2,n_1,n_2}\; P(n_1, n_2) + G_{g_2,n_1,n_2-1}\; P(n_1, n_2-1) \\
&+ \, C_1(n_{b_1}+1)\left[(n_1+1)P(n_1+1, n_2) - n_1 P(n_1, n_2)\right] \\
&+ \, C_1 n_{b_1}\left[n_1 P(n_1-1, n_2) - (n_1+1)P(n_1, n_2)\right] \\
&+ \, C_2(n_{b_2}+1)\left[(n_2+1)P(n_1, n_2+1) - n_2 P(n_1, n_2)\right] \\
&+ \, C_2 n_{b_2}\left[n_2 P(n_1, n_2-1) - (n_2+1)P(n_1, n_2)\right] \; .
\end{aligned} \tag{4.27}
$$

Here, $G_{g_1,n_1,n_2} = r\; P_{n_1,n_2}(e \to g_1)$, $G_{g_2,n_1,n_2} = r\; P_{n_1,n_2}(e \to g_2)$ are the gain coefficients for the modes 1 and 2, respectively, with $P_{n_1,n_2}(e \to g_1)$, $P_{n_1,n_2}(e \to g_2)$ as defined in Eqs. (4.18) and (4.19). This is the master equation for the two-mode micromaser pumped with ultracold atoms. This equation has the character of rate equation for the probability and various terms on the right hand side behave as the outflow and the inflow of probabilities. This equation has also the form that one would have expected on physical grounds.

4.3 Analytical Solution of Master Equation

In this section, we derive the analytical results for the steady state photon distribution in the cavity for special choices of parameters. The steady state photon probability distribution is obtained by setting

$$\dot{P}(n_1, n_2) = 0 \ . \tag{4.28}$$

The distribution $P(n_1, n_2)$ can be obtained in analytical form by using the condition of detailed balance which states that the net inflow and outflow of probabilities are equal. This leads to

$$P(n_1, n_2) = P(n_1 - 1, n_2)\frac{1}{C_1(n_{b_1} + 1)}\left\{C_1 n_{b_1} + \frac{G_{g_1, n_1 - 1, n_2}}{n_1}\right\} \ , \tag{4.29}$$

$$P(n_1, n_2) = P(n_1, n_2 - 1)\frac{1}{C_2(n_{b_2} + 1)}\left\{C_2 n_{b_2} + \frac{G_{g_2, n_1, n_2 - 1}}{n_2}\right\} \ . \tag{4.30}$$

For the above equations to be consistent with each other, we substitute the expression for $P(n_1 - 1, n_2)$ obtained from Eq. (4.30) into Eq. (4.29) and the expression for $P(n_1, n_2 - 1)$ obtained from Eq. (4.29) into Eq. (4.30) with the results

$$\begin{aligned} P(n_1, n_2) &= P(n_1 - 1, n_2 - 1)\frac{1}{C_1(n_{b_1} + 1)}\frac{1}{C_2(n_{b_2} + 1)} \\ &\times \left(C_1 n_{b_1} + \frac{G_{g_1, n_1 - 1, n_2}}{n_1}\right) \\ &\times \left(C_2 n_{b_2} + \frac{G_{g_2, n_1 - 1, n_2 - 1}}{n_2}\right) \ , \end{aligned} \tag{4.31}$$

$$\begin{aligned} P(n_1, n_2) &= P(n_1 - 1, n_2 - 1)\frac{1}{C_1(n_{b_1} + 1)}\frac{1}{C_2(n_{b_2} + 1)} \\ &\times \left(C_2 n_{b_2} + \frac{G_{g_2, n_1, n_2 - 1}}{n_2}\right) \\ &\times \left(C_1 n_{b_1} + \frac{G_{g_1, n_1 - 1, n_2 - 1}}{n_1}\right) \ . \end{aligned} \tag{4.32}$$

It is obvious that Eqs. (4.31) and (4.32) can both be satisfied if

$$\Omega_1 = \Omega_2 \equiv \Omega, \ C_1 n_{b_1} = C_2 n_{b_2} \equiv C n_b \ . \tag{4.33}$$

Under these conditions, the steady state photon distribution has the form

$$P(n_1,n_2) = P(0,0)\left(\frac{r}{C_1+Cn_b}\right)^{n_1}\left(\frac{r}{C_2+Cn_b}\right)^{n_2}\prod_{q=1}^{n_1+n_2}\left\{\frac{Cn_b}{r}+\frac{1}{2(q+1)}\right.$$
$$\left.\times\left[1-\frac{(1+\Delta_q^+\Delta_q^-S_q^+S_q^-)(C_q^+C_q^-+\Sigma_q^+\Sigma_q^-S_q^+S_q^-)}{({C_q^+}^2+{\Sigma_q^+}^2{S_q^+}^2)({C_q^-}^2+{\Sigma_q^-}^2{S_q^-}^2)}\right]\right\}, \quad (4.34)$$

where $C_q^\pm = \cos(k_q^\pm L)$, $S_q^\pm = \sin(k_q^\pm L)$ with $k_q^\pm = \sqrt{\left(k^2 \mp \kappa^2\sqrt{\frac{q+1}{2}}\right)}$ which is the same as Eq. (4.12) with (n_1+n_2+1) replaced by q and $\Omega_1=\Omega_2=\Omega$. Similarly $\Delta_q^\pm, \Sigma_q^\pm$ are defined by equations (4.11) with $k_{n_1,n_2}^\pm$ replaced by $k_q^\pm$. The normalization condition of joint probability gives $\sum_{n_1,n_2=0}^{\infty} P(n_1,n_2)=1$. The expression (4.34) contains all the statistical informations about the steady state field. We consider the special case in which all the parameters for the two modes are equal, i.e., $\Omega_1=\Omega_2=\Omega$, $C_1=C_2=C$, $n_{b_1}=n_{b_2}=n_b$. In this case, Eq. (4.33) can be satisfied and the detailed balance steady state photon distribution has the form

$$P(n_1,n_2) = f(n_1+n_2)\ , \quad (4.35)$$

where

$$f(n) = P(0,0)\left[\frac{r}{C(n_b+1)}\right]^n\prod_{q=1}^{n}\left\{\frac{Cn_b}{r}+\frac{1}{(q+1)}\right.$$
$$\left.\times\left[\frac{1}{2}\left(1-\frac{(1+\Delta_q^+\Delta_q^-S_q^+S_q^-)(C_q^+C_q^-+\Sigma_q^+\Sigma_q^-S_q^+S_q^-)}{({C_q^+}^2+{\Sigma_q^+}^2{S_q^+}^2)({C_q^-}^2+{\Sigma_q^-}^2{S_q^-}^2)}\right)\right]\right\}. \quad (4.36)$$

It is to be noted that the square bracketed term inside the product in the above equation, is identical to the photon emission probability of an ultracold, excited two-level atom entering a single mode resonant cavity containing q photons in the single mode Mazer [99]. For comparison the steady state photon distribution of the single mode mazer operating on two-level atoms with the atom-field coupling constant Ω [99] is

$$P(n) = P(0)\left[\frac{r}{C(n_b+1)}\right]^n\prod_{q=1}^{n}\left\{\frac{Cn_b}{r}+\frac{p_e(q-1)}{q}\right\}. \quad (4.37)$$

Here $p_e(q)$ is the photon emission probability of an excited atom incident on the cavity containing q photons and is equal to the square bracketed term in Eq. (4.36)

with Ω replaced by $\Omega/\sqrt{2}$. For fast atoms i.e., when the energy of incident atoms is very large compared to the vacuum coupling energy, the square bracketed term in Eq. (4.36) can be approximated to $\sin^2(\Omega\tau\sqrt{q+1})$(see Sec. V of [99]) where $\Omega\tau = \kappa^2 L/2\sqrt{2}k$. In this case f(n) has the form

$$f(n) = P(0,0)\left[\frac{r}{C(n_b+1)}\right]^n \prod_{q=1}^{n}\left\{\frac{Cn_b}{r} + \frac{1}{(q+1)}\sin^2(\Omega\tau\sqrt{q+1})\right\} , \tag{4.38}$$

which is the same as obtained in the two-mode micromaser operating on three-level atoms [67]. As mentioned in [67], $f(n) = P(n,0) = P(0,n)$ is the joint probability of having n photons in one mode and no photons in the other mode and the probability that the cavity contains $'n'$ total number of photons is

$$P_\Sigma(n) \equiv \sum_{n_1+n_2=n} P(n_1,n_2) = f(n)(n+1) . \tag{4.39}$$

$P(0,0)$ can be determined from the normalization condition $\sum_{n=0}^{\infty} P_\Sigma(n) = 1$. For

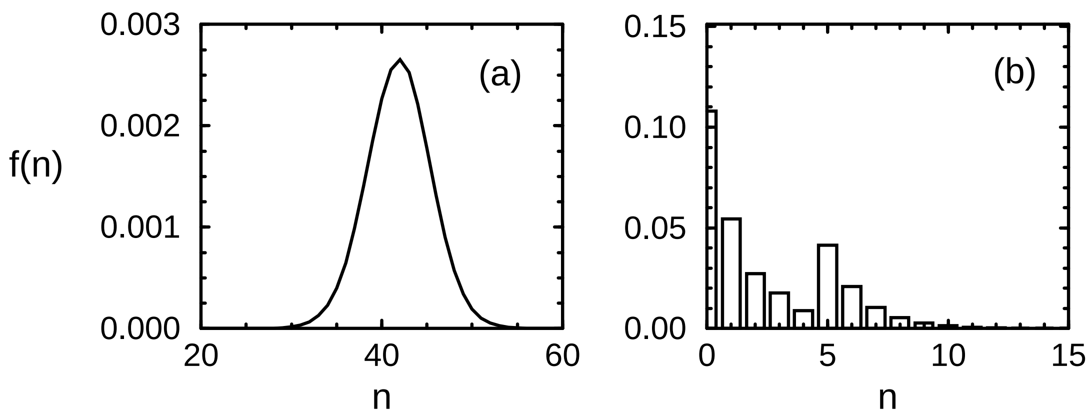

Figure 4.4: The function $f(n) = P(n,0) = P(0,n)$ for the parameters $\Omega_1 = \Omega_2 = \Omega$, $C_1 = C_2 = C$, $n_{b_1} = n_{b_2} = n_b$, $r/C = 100$, $n_b = 1$, $\kappa L = 10\pi/(3)^{1/4}$ and $k/\kappa = 10$ (a), $k/\kappa = 0.01$ (b).

fast atoms, the graph of $f(n)$ has been plotted in Fig. 4.4(a) for the parameters $r/C = 100$, $n_b = 1$, $\kappa L = 10\pi/(3)^{1/4}$, $k/\kappa = 10$. The graph shows the distribution $f(n)$ with single peak and compares well with the Ref. [67] on two-mode micromaser. In general, the function $f(n)$ can have more than one peak depending on the value of $\Omega\tau = \kappa^2 L/2\sqrt{2}k$. The joint probability distribution $f(n)$ behaves differently when the micromaser is pumped by ultracold atoms, i.e., when the energy of incident atoms is very low compared to vacuum coupling energy. For ultracold atoms, $f(n)$ is shown in Fig. 4.4(b) for the parameters $r/C = 100$, $n_b = 1$, $\kappa L = 10\pi/(3)^{1/4}$, $k/\kappa = 0.01$. The graph looks similar to a pair of thermal distributions one of which is shifted towards the larger photon number. This behavior of $f(n)$ occurs at $\kappa L = m\pi/(N)^{1/4}$ with $m = 1, 2, ...$, $N = 1, \frac{3}{2}, 2, ...$ and is similar to that of the steady state photon distribution of the single mode mazer [99] as expected on comparing Eqs. (4.36) and (4.37). When $\kappa L \neq m\pi/(N)^{1/4}$, the distribution $f(n)$ is a decreasing function of n similar to a thermal distribution for ultracold incident atoms.

4.4 Steady State Photon Statistics

We now obtain the steady state distribution of photons $P_\alpha(n)$ in any fixed mode α. From the joint probability distribution $P(n_1, n_2)$, we can get photon distribution $P_\alpha(n)$ in any fixed mode α by summing over the number of photons in the other mode. The function $P_\alpha(n)$ is defined by

$$P_1(n) = \sum_{l=0}^{\infty} P(n, l) \ , \quad P_2(n) = \sum_{l=0}^{\infty} P(l, n) \ . \tag{4.40}$$

By using Eq. (4.35) the function $P_\alpha(n)$ is found to be

$$P_\alpha(n) = \sum_{l=n}^{\infty} f(l) \ . \tag{4.41}$$

It may be noted from this equation that $P_\alpha(n)$ is independent of α since we assumed $\Omega_1 = \Omega_2 = \Omega$, $C_1 = C_2 = C$, $n_{b_1} = n_{b_2} = n_b$ and

$$P_\alpha(n+1) = P_\alpha(n) - f(n) \ . \tag{4.42}$$

The function f(n) is positive as seen from Eq. (4.36). Therefore, the photon distribution decreases monotonously with n. The probability distribution of photons in a fixed mode calculated from (4.41), is plotted both for fast atoms ($k/\kappa = 10$) and ultracold atoms ($k/\kappa = 0.01$) in Fig. 4.5 for the parameters $r/C = 100$, $n_b = 1$, $\kappa L = 10\pi/(3)^{1/4}$. The graphs show that for ultracold atoms there is a steep decrease in the curve of $P_\alpha(n)$ at the value $n = 5$ for the chosen parameters. From equation (4.41), it is clear that this decrease in the curve is due to the two-peaked

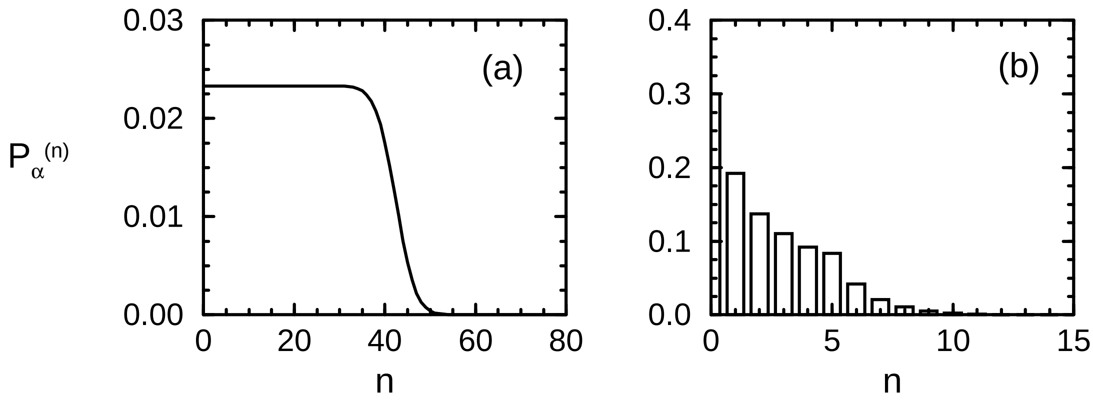

Figure 4.5: The distribution of photons in mode α for the parameters $\Omega_1 = \Omega_2 = \Omega$, $C_1 = C_2 = C$, $n_{b_1} = n_{b_2} = n_b$, $r/C = 100$, $n_b = 1$, $\kappa L = 10\pi/(3)^{1/4}$ and $k/\kappa = 10$ (a), $k/\kappa = 0.01$ (b).

nature of f(n) behaving similar to a pair of thermal distributions for ultracold incident atoms. We can examine numerically the stability and uniqueness of this steady state result derived under the condition of detailed balance. Using the fourth order Runge kutta method for direct integration of rate equation (4.27), we have plotted the photon probability distribution in Fig. 4.6 at different times for the equal parameter case when the initial state of the field for mode 1 is a thermal distribution with the mean value of photon number $< n_1 >= 1$ and vacuum state for mode 2, for the parameters of 4.5(b).

It is seen from the graphs that a steady state is reached within a time of order 10/C and the steady state photon probability distribution coincides with the analytical result obtained under the principle of detailed balance. This confirms the uniqueness and stability of detailed balance steady state solution. We next evaluate the first and second moments of the photon distribution in any fixed mode α using Eqs. (4.36) and (4.41). From Eq. (4.41), we find

$$\langle n_\alpha \rangle \equiv \sum_{n=0}^{\infty} n P_\alpha(n) = \frac{1}{2} \sum_{m=0}^{\infty} f(m) m(m+1) \ , \tag{4.43}$$

$$\langle n_\alpha^2 \rangle \equiv \sum_{n=0}^{\infty} n^2 P_\alpha(n) = \frac{1}{6} \sum_{m=0}^{\infty} f(m) m(m+1)(2m+1) \ . \tag{4.44}$$

The mean value of total photon number is found from Eqs. (4.39) and (4.43) to be

$$\langle n_\Sigma \rangle \equiv \sum_{n=0}^{\infty} n P_\Sigma(n) = \sum_{n=0}^{\infty} n f(n)(n+1) = 2\langle n_\alpha \rangle \ . \tag{4.45}$$

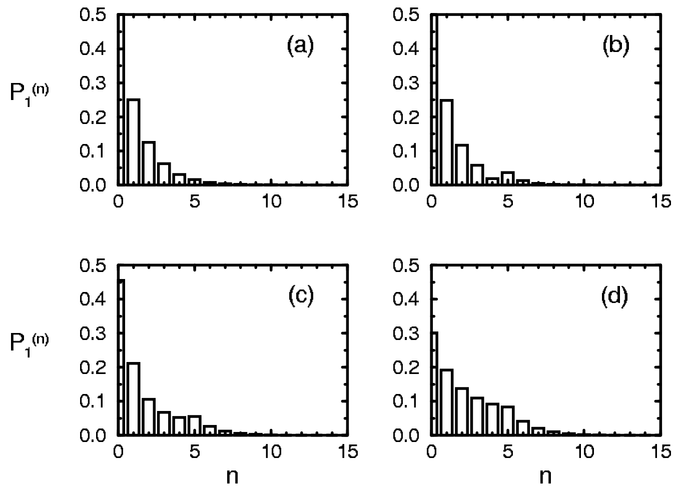

Figure 4.6: The distribution of photons in mode 1 at different times t during the evolution from the initial state. Mode 1 is initially in a thermal state with $\langle n_1 \rangle = 1$. Mode 2 is initially in the vacuum state. The parameters for the calculations are $\Omega_1 = \Omega_2 = \Omega$, $C_1 = C_2 = C$, $n_{b_1} = n_{b_2} = n_b$, $r/C = 100$, $n_b = 1$, $\kappa L = 10\pi/(3)^{1/4}$, $k/\kappa = 0.01$. Graphs (a), (b), (c), and (d) correspond to $t = 0$, $t = 0.1/C$, $t = 1/C$, and $t = 10/C$, respectively.

The normalized standard deviation σ_α is defined by

$$\sigma_\alpha^2 = \frac{\langle n_\alpha^2 \rangle - \langle n_\alpha \rangle^2}{\langle n_\alpha \rangle} \,. \tag{4.46}$$

In Figs. 4.7 and 4.8, we plot the steady state mean and normalized variance of the distribution of photons in any fixed mode for $r/C = 100$ and $n_b = 0.1$ when the micromaser is pumped by fast and cold atoms. For the case of fast atoms ($k/\kappa = 10$), each mode of the cavity field exhibits features similar to that of the single mode micromaser and the statistics of photons is super-Poissonian (${\sigma_\alpha}^2 > 1$). For the case of ultracold atoms ($k/\kappa = 0.01$), the graphs show sharp resonances at $\kappa L = m\pi/(N)^{1/4}$ with $m = 1, 2, ..$ and $N = 1, \frac{3}{2}, 2, ..$ The peaks in the normalized variance are accompanied by resonances in the mean photon number and are reminiscent of the behavior of single mode mazer [99]. For small values of N, the normalized variance ${\sigma_\alpha}^2$ is less than unity which shows that the photon statistics in each mode is sub-Poissonian. This is because the joint probability function $f(n)$ behaves as a shifted thermal distribution at those resonance positions. Shifting the thermal distribution of $f(n)$ to smaller values of N does not increase the variance of probability distribution $P_\alpha(n)$ when n_b is small. However, the normal-

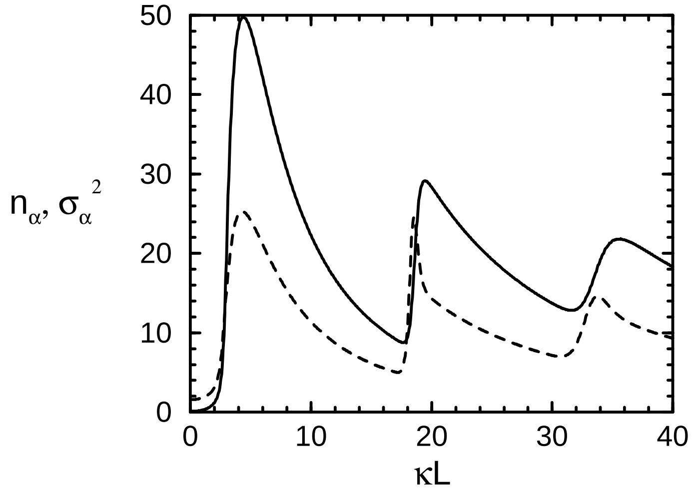

Figure 4.7: The mean (solid curve) and the normalized variance (dashed curve) of the distribution of photons in mode α as functions of the interaction length κL for the parameters $r/C = 100$, $n_b = 0.1$ and $k/\kappa = 10$. Actual values of σ_α^2 are 0.7 times those shown.

ized variance ${\sigma_\alpha}^2$ decreases below the Poissonian level because the mean value $\langle n_\alpha \rangle$ is increased. These resonances in the mean value $\langle n_\alpha \rangle$ give rise to a strong anti-correlation between the two cavity modes. A quantitative measure of this anti-correlation is given by the cross-correlation function defined by

$$\delta_{cross} \equiv \frac{\langle n_1 n_2 \rangle - \langle n_1 \rangle \langle n_2 \rangle}{\langle n_1 \rangle \langle n_2 \rangle} \ . \tag{4.47}$$

By using Eqs. (4.35) and (4.39), we can easily show that

$$\langle n_1 n_2 \rangle \equiv \sum_{n_1, n_2 = 0}^{\infty} n_1 n_2 P(n_1, n_2) = \frac{1}{6} (\langle n_\Sigma^2 \rangle - \langle n_\Sigma \rangle) \ . \tag{4.48}$$

Substituting Eqs. (4.39) and (4.48) into Eq. (4.47), we get

$$\delta_{cross} = \frac{2}{3} \left(\frac{\langle n_\Sigma^2 \rangle}{\langle n_\Sigma \rangle^2} - \frac{1}{\langle n_\Sigma \rangle} \right) - 1 \ . \tag{4.49}$$

Hence the normalized standard deviation σ_Σ and the normalized cross-correlation function δ_{cross} are related by [67]

$${\sigma_\Sigma}^2 \equiv \frac{\langle n_\Sigma^2 \rangle - \langle n_\Sigma \rangle^2}{\langle n_\Sigma \rangle} = 1 + \frac{3}{2} \langle n_\Sigma \rangle \left(\delta_{cross} + \frac{1}{3} \right) \ . \tag{4.50}$$

According to this relation, the distribution of the total number of photons in the cavity obeys sub-Poissonian statistics (${\sigma_\Sigma}^2 < 1$) when the two cavity modes are

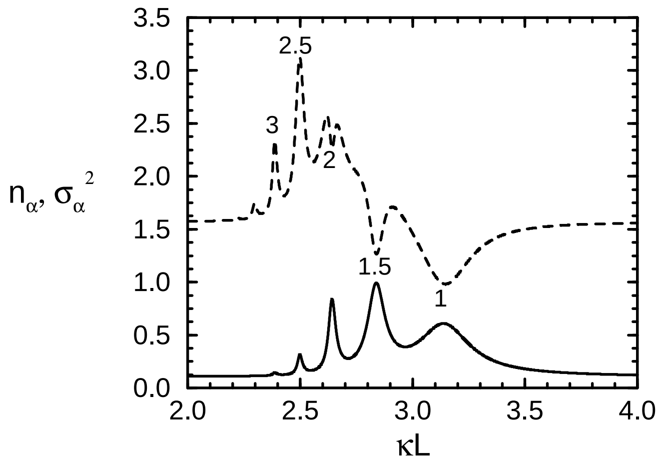

Figure 4.8: The mean (solid curve) and the normalized variance (dashed curve) of the distribution of photons in mode α as functions of the interaction length κL for the same parameters of Fig. 4.7 with $k/\kappa = 0.01$. The graphs show resonances at $\kappa L = m\pi/(N)^{1/4}$. The resonance sequence corresponding to $m = 1$ has been plotted and the peaks are labeled by N values. Actual values of σ_α^2 are 0.7 times those shown.

strongly anti-correlated ($\delta_{cross} < -\frac{1}{3}$). In Fig. 4.9, we display the normalized cross-correlation function δ_{cross} as a function of κL for the parameters $r/C = 100$, $n_b = 0.1$ both for fast atoms($k/\kappa = 10$) and for cold atoms ($k/\kappa = 0.01$). It is seen from the graph that there exists a very strong anti-correlation between the cavity modes for ultracold incident atoms compared to fast atoms when $\kappa L = m\pi$ and this leads to sub-Poissonian photon statistics for the total number of photons in the cavity.

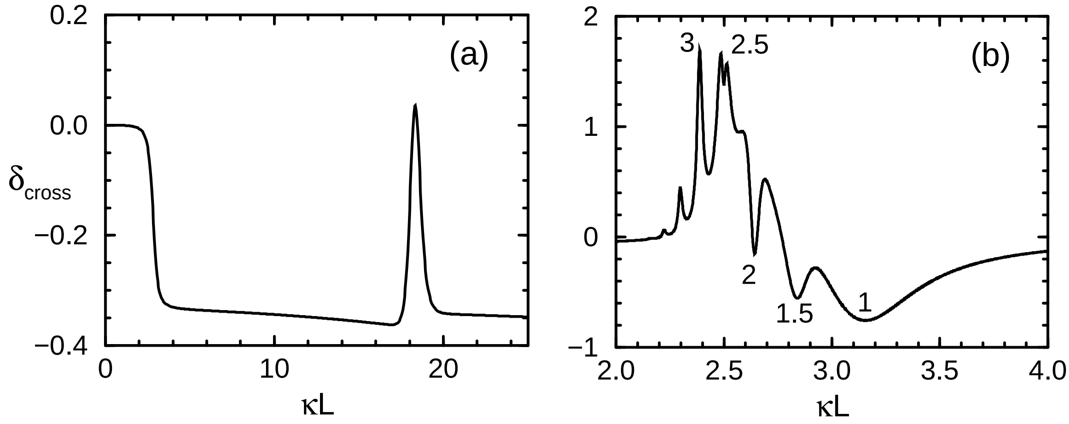

Figure 4.9: The dependence of the normalized cross-correlation function on the interaction length κL for the parameters $r/C = 100$, $n_b = 0.1$, and $k/\kappa = 10$ (a), $k/\kappa = 0.01$ (b). For the case of ultracold incident atoms, the graph show resonances at $\kappa L = m\pi/(N)^{1/4}$. The resonance sequence corresponding to $m = 1$ has been plotted and the peaks are labeled by N values.

4.5 Summary

In summary, we have discussed the new features in the photon statistics of a two-mode micromaser cavity pumped by ultracold Λ-type three level atoms. In Sec. 4.1, we described our model system and showed the correlation of external motion of atoms with the atom-photon states in the cavity. We gave the numerical result for the one-photon emission probability of atoms and discussed the similarity with the earlier work on two-level atoms [99]. In Sec. 4.2, we studied the maser action and derived the master equation for the reduced density matrix of the two-mode cavity field. In Sec. 4.3, analytical result was presented for the steady state solution of the master equation in the special case when the atom-field couplings for the two cavity-modes are equal. Finally, in Sec. 4.4, we discussed the steady state photon statistics of the fields in the cavity using the analytical formula derived in Sec. 4.3. We have presented numerical results for the mean, variance and correlation of the fields in the cavity. The results were compared with the usual case of the micromaser pumped by fast atoms. The interesting feature is that the degree of anti-correlation between the cavity modes increases when the micromaser is pumped by ultracold atoms instead of fast atoms.

Chapter 5

Maser Operating on Two-Photon Transitions in Ultracold Atoms

We have discussed in the previous chapter the maser action through one-photon emissions from Λ-type, ultracold three-level atoms. In this chapter, we extend this idea to Ξ-type, ultracold three-level atoms in the excited state. This atomic scheme has been used by Brune et al [73] to demonstrate the masing action through degenerate two-photon transitions inside a single mode cavity. Unlike Λ-type atom, an excited atom in the Ξ-type configuration can make either a one-photon transition to its middle level or a two-photon transition to its ground level inside a bimodal cavity. We study the effects of two-photon emissions from the incident atoms on the maser action in the bimodal cavity.

5.1 One- and Two- Photon Processes

We consider a bimodal cavity of length L pumped steadily by a beam of ultracold, three-level atoms in the cascade configuration. The scheme of our model is shown in Fig. 5.1. The transitions $e \to g_1$ and $g_1 \to g_2$ are dipole allowed while the direct transition $e \to g_2$ is dipole forbidden. Thus, the atom in the excited level e can reach the ground level g_2 only through the two-photon transition $e \to g_1 \to g_2$. The frequencies of the two cavity modes 1 and 2 are tuned to those of atomic transitions $e \to g_1$ and $g_1 \to g_2$ respectively.The Hamiltonian describing this resonant atom-field interaction including the quantized motion of center-of-mass

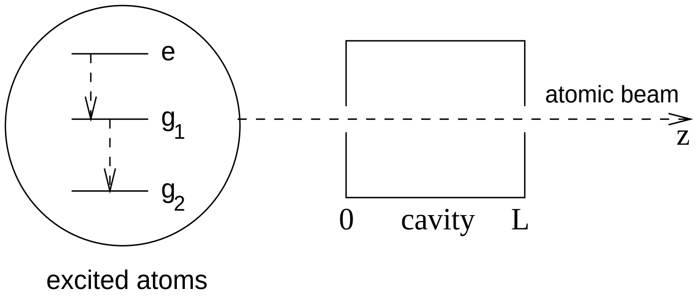

Figure 5.1: The scheme of the two-mode micromaser cavity pumped by Ξ-type three-level atoms in the excited state.

(c.m.) of the atoms along the z direction is given by

$$H = H_A + H_F + H_{AF} \ , \tag{5.1}$$

where $H_A(H_F)$ is the Hamiltonian of the free atom (field) and H_{AF} is the interaction Hamiltonian describing the atom-field interaction in the dipole and the rotating wave approximations [cf. Eq. (1.25)] :

$$H_A = \frac{p_z^2}{2m} + \hbar\Omega_e|e\rangle\langle e| + \sum_{\alpha=1}^{2} \hbar\Omega_{g_\alpha}|g_\alpha\ \rangle\langle g_\alpha| \ ,$$

$$H_F = \sum_{\alpha=1}^{2} \hbar\omega_\alpha a_\alpha^\dagger a_\alpha \ ,$$

$$H_{AF} = \hbar\Omega_1(|e\rangle\langle g_1|\ a_1 + a_1^\dagger\ |g_1\rangle\langle e|) + \hbar\Omega_2(|g_1\rangle\langle g_2|\ a_2 + a_2^\dagger\ |g_2\rangle\langle g_1|) \ . \tag{5.2}$$

The operator $|j\rangle\langle j|(j = e, g_1, g_2)$ gives the projection on to the state $|j\rangle$ with energy $\hbar\Omega_j$. The operators $|g_1\rangle\langle e|$ and $|g_1\rangle\langle g_2|$ describe the atomic transitions from the upper and lower levels to the middle level. The operators a_α ($a_\alpha^\dagger$) annihilate (create) a photon in the modes $\alpha = 1, 2$ with resonance frequencies $\omega_1 = \Omega_e - \Omega_{g_1}$ and $\omega_2 = \Omega_{g_1} - \Omega_{g_2}$ respectively. The first and second terms in the interaction operator H_{AF} represents the action of fields 1 and 2 of the cavity on the upper $(e \Leftrightarrow g_1)$ and the lower $(g_1 \Leftrightarrow g_2)$ transitions respectively. The parameters Ω_α are the corresponding atom-field coupling constants and m is the atomic mass. The parameters Ω_α are dependent on z through the mode function of the cavity.

In the interaction picture, the Hamiltonian (5.1) of the atom-field system reads

$$H_I = \frac{p_z^2}{2m} + H_{AF} \ . \tag{5.3}$$

It is useful to expand the interaction Hamiltonian H_{AF} in its diagonal basis. The operator H_{AF} has eigenstates $|\phi^0_{n_1+1,n_2+1}\rangle$, $|\phi^\pm_{n_1+1,n_2+1}\rangle$ with eigenvalues $0, \pm\hbar\sqrt{\Omega_1^2(z)(n_1+1)+\Omega_2^2(z)(n_2+1)}$, respectively, where

$$|\phi^0_{n_1+1,n_2+1}\rangle = \frac{\left[\Omega_2\sqrt{n_2+1}\ |e,n_1,n_2\rangle - \Omega_1\sqrt{n_1+1}\ |g_2,n_1+1,n_2+1\rangle\right]}{\left[\Omega_1^2(n_1+1)+\Omega_2^2(n_2+1)\right]^{1/2}}$$

$$\begin{aligned}|\phi^\pm_{n_1+1,n_2+1}\rangle \ &= \ \frac{1}{\sqrt{2}}\left[\frac{\Omega_1\sqrt{n_1+1}}{\sqrt{\Omega_1^2(n_1+1)+\Omega_2^2(n_2+1)}}|e,n_1,n_2\rangle \ \pm \ |g_1,n_1+1,n_2\rangle\right.\\ &\left. + \frac{\Omega_2\sqrt{n_2+1}}{\sqrt{\Omega_1^2(n_1+1)+\Omega_2^2(n_2+1)}}|g_2,n_1+1,n_2+1\rangle\right] \ .\end{aligned} \tag{5.4}$$

The interaction operator H_{AF} and its eigenstates $|\phi^0_{n_1+1,n_2+1}\rangle$, $|\phi^\pm_{n_1+1,n_2+1}\rangle$ depend on the position z through the coupling strengths $\Omega_1(z)$, $\Omega_2(z)$. Thus, it is in general difficult to carry out the time evolution of an atom-field state governed by the Hamiltonian (5.3) for the quantized motion of atoms. So, for simplicity, we work with the mesa mode functions $\Omega_\alpha(z) = \Omega_\alpha\ \theta(z)\theta(L-z)$ which represent the z-independent field modes in the cavity. In this case, the eigenstates of the interaction are independent of atomic position inside the cavity and the atomic motion sees free particle evolution in the dark state of interaction $|\phi^0_{n_1+1,n_2+1}\rangle$. The effect of atom's interaction with the cavity on its external motion can be realized only in the dressed state $|\phi^\pm_{n_1+1,n_2+1}\rangle$ components of the initial atom-field state. Note that we can in principle work with any basis set of states. Thus, outside the cavity, we use (5.4). Also, it is preferable to work in the eigenbasis (5.4) inside the cavity so that equations can be decoupled. We need to consider the initial atom-field state to be $|e,n_1,n_2\rangle$, i.e., the atom is in the excited state and the cavity contains (n_1,n_2) photons in the modes $(1,2)$ initially. Since we work with dark and dressed states basis inside the cavity, it is useful to expand the initial state in terms of the dark and dressed eigenstates :

$$|e,n_1,n_2\rangle = \left[\frac{\Omega_1\sqrt{(n_1+1)/2}}{\sqrt{\Omega_1^2(n_1+1)+\Omega_2^2(n_2+1)}}\left(|\phi^+_{n_1+1,n_2+1}\rangle+|\phi^-_{n_1+1,n_2+1}\rangle\right)\right.$$
$$\left.+\frac{\Omega_2\sqrt{n_2+1}}{\sqrt{\Omega_1^2(n_1+1)+\Omega_2^2(n_2+1)}}|\phi^0_{n_1+1,n_2+1}\rangle\right] . \qquad (5.5)$$

The time evolution of this initial state can be found by expanding the combined state of atom-cavity system as

$$|\Psi(z,t)\rangle = \chi_+(z,t)|\phi^+_{n_1+1,n_2+1}\rangle + \chi_-(z,t)|\phi^-_{n_1+1,n_2+1}\rangle + \chi_0(z,t)|\phi^0_{n_1+1,n_2+1}\rangle \; , \qquad (5.6)$$

then the time dependent Schrödinger equation (1.12) becomes

$$i\hbar\frac{\partial\chi_\alpha(z,t)}{\partial t} = h_\alpha\chi_\alpha(z,t) \; , \qquad \alpha = \pm, 0. \qquad (5.7)$$

Here, $h_\pm = p_z^2/2m \pm \theta(z)\theta(L-z)\hbar\sqrt{\Omega_1^2(n_1+1)+\Omega_2^2(n_2+1)}$, $h_0 = p_z^2/2m$ are operators acting in the space of c.m. variables. Thus, the effect of the cavity with fixed

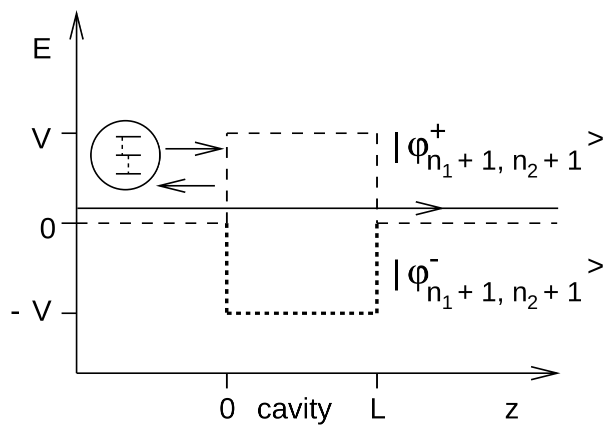

Figure 5.2: Schematic representation of the energy E of the excited atoms incident upon a two-mode micromaser cavity with (n_1, n_2) photons. The atom-field interaction creates barrier (dashed) and well (dotted) potentials with a potential energy $V = \hbar\sqrt{\Omega_1^2(n_1+1)+\Omega_2^2(n_2+1)}$ in the dressed states $|\phi^\pm_{n_1+1,n_2+1}\rangle$. The scattering from these cavity induced potentials leads to reflection or transmission of the atoms through the cavity. The interaction also induces a reflection-less transmission of the atoms in the dark state $|\phi^0_{n_1+1,n_2+1}\rangle$. However, the reflection or transmission of the atoms can occur only in one of the three states $|e,n_1,n_2\rangle$, $|g_1,n_1+1,n_2\rangle$, and $|g_2,n_1+1,n_2+1\rangle$.

number of photons produces potential terms in h_α corresponding to the dressed states $|\phi^{\pm}_{n_1+1,n_2+1}\rangle$ as discussed in Ref. [99] for two-level atoms. The barrier and well potentials induced by the interaction for the atomic motion in the states $|\phi^{\pm}_{n_1+1,n_2+1}\rangle$ are then displayed as in Fig. 5.2. It is also important to note that the external motion of atom experiences free time evolution in the dark state $|\phi^{0}_{n_1+1,n_2+1}\rangle$ for the mesa mode distribution of the cavity fields.

Denoting the reflection and transmission amplitudes as $\rho^{\pm}_{n_1,n_2}$, $\tau^{\pm}_{n_1,n_2}$ for the potential barrier-well problem of the dressed states $|\phi^{\pm}_{n_1+1,n_2+1}\rangle$, respectively, we have

$$\rho^{\pm}_{n_1,n_2} = i\Delta^{\pm}_{n_1,n_2}\sin(k^{\pm}_{n_1,n_2}L)\exp(ikL)\tau^{\pm}_{n_1,n_2} \ , \tag{5.8}$$

$$\tau^{\pm}_{n_1,n_2} = \exp(-ikL)\left[\cos(k^{\pm}_{n_1,n_2}L) - i\Sigma^{\pm}_{n_1,n_2}\sin(k^{\pm}_{n_1,n_2}L)\right]^{-1} \ , \tag{5.9}$$

$$\Delta^{\pm}_{n_1,n_2} = \frac{1}{2}\left(\frac{k^{\pm}_{n_1,n_2}}{k} - \frac{k}{k^{\pm}_{n_1,n_2}}\right) \ , \tag{5.10}$$

$$\Sigma^{\pm}_{n_1,n_2} = \frac{1}{2}\left(\frac{k^{\pm}_{n_1,n_2}}{k} + \frac{k}{k^{\pm}_{n_1,n_2}}\right) \ ,$$

$$k^{\pm}_{n_1,n_2} = \sqrt{\left(k^2 \mp \frac{2m}{\hbar}\sqrt{\Omega_1^2(n_1+1)+\Omega_2^2(n_2+1)}\right)} \ , \tag{5.11}$$

where $\hbar k$ is the atomic c.m. momentum and L is the length of the cavity. It is to be noted that the strengths of the barrier - well potentials (potential energy term in $k^{\pm}_{n_1,n_2}$) depend on the coupling constants Ω_1, Ω_2 as well as the occupation numbers n_1, n_2 of the photons in the cavity.

We consider the initial wave packet of the moving free atom to be $\psi(z,t) = \exp\left(-ip_z^2 t/2m\hbar\right)\int dkA(k)e^{ikz} = \int dkA(k)e^{-i\left(\hbar k^2/2m\right)t}e^{ikz}$. The Fourier amplitudes $A(k)$ are adjusted such that the incident wave packet $|\psi(z,0)|^2$ to the left of cavity $(z<0)$ does not extend into the cavity region at the initial time $t=0$. The combined state of the atom-cavity system at the initial time $t=0$ is therefore,

$$|\Psi(z,0)\rangle = \psi(z,0)|e,n_1,n_2\rangle \ . \tag{5.12}$$

The wave function of the atom-field system at time t after the atom has left the cavity region is found by solving the Eqs. (5.6) and (5.7) subject to the above initial condition :

$$
\begin{aligned}
|\Psi(z,t)\rangle &= \int dk A(k) e^{-i\left(\hbar k^2/2m\right)t} \\
&\times \left\{ \left[R_{e,n_1,n_2}(k) e^{-ikz}\theta(-z) + T_{e,n_1,n_2}(k) e^{ikz}\theta(z-L) \right] |e,n_1,n_2\rangle \right. \\
&+ \left[R_{g_1,n_1+1,n_2}(k) e^{-ikz}\theta(-z) + T_{g_1,n_1+1,n_2}(k) e^{ikz}\theta(z-L) \right] |g_1,n_1+1,n_2\rangle \\
&+ \left[R_{g_2,n_1+1,n_2+1}(k) e^{-ikz}\theta(-z) + T_{g_2,n_1+1,n_2+1}(k) e^{ikz}\theta(z-L) \right] \\
&\left. \times |g_2,n_1+1,n_2+1\rangle \right\} ,
\end{aligned} \tag{5.13}
$$

where

$$
\begin{aligned}
R_{e,n_1,n_2} &= \frac{\Omega_1^2(n_1+1)}{2\left(\Omega_1^2(n_1+1)+\Omega_2^2(n_2+1)\right)} \left(\rho^+_{n_1,n_2} + \rho^-_{n_1,n_2}\right) , \\
T_{e,n_1,n_2} &= \frac{\left[\Omega_1^2(n_1+1)\left(\tau^+_{n_1,n_2} + \tau^-_{n_1,n_2}\right) + 2\Omega_2^2(n_2+1)\right]}{2\left(\Omega_1^2(n_1+1)+\Omega_2^2(n_2+1)\right)} ,
\end{aligned} \tag{5.14}
$$

are the reflection and transmission amplitudes for the excited state of the atom with the initial (n_1, n_2) photons remaining in the two cavity modes and

$$
\begin{aligned}
R_{g_1,n_1+1,n_2} &= \frac{\Omega_1\sqrt{(n_1+1)}}{2\sqrt{\left(\Omega_1^2(n_1+1)+\Omega_2^2(n_2+1)\right)}} \left(\rho^+_{n_1,n_2} - \rho^-_{n_1,n_2}\right) , \\
T_{g_1,n_1+1,n_2} &= \frac{\Omega_1\sqrt{(n_1+1)}}{2\sqrt{\left(\Omega_1^2(n_1+1)+\Omega_2^2(n_2+1)\right)}} \left(\tau^+_{n_1,n_2} - \tau^-_{n_1,n_2}\right) ,
\end{aligned} \tag{5.15}
$$

are the probability amplitudes that the excited atom goes to the state $|g_1\rangle$ and emits a photon in mode 1 while getting reflected and transmitted respectively. Similarly, the excited atom is reflected or transmitted and emits a photon in both the cavity modes while making a transition to the ground state $|g_2\rangle$ via the middle state $|g_1\rangle$ with probability amplitudes

$$
\begin{aligned}
R_{g_2,n_1+1,n_2+1} &= \frac{\Omega_1\Omega_2\sqrt{(n_1+1)(n_2+1)}}{2\left(\Omega_1^2(n_1+1)+\Omega_2^2(n_2+1)\right)} \left(\rho^+_{n_1,n_2} + \rho^-_{n_1,n_2}\right) , \\
T_{g_2,n_1+1,n_2+1} &= \frac{\Omega_1\Omega_2\sqrt{(n_1+1)(n_2+1)}}{2\left(\Omega_1^2(n_1+1)+\Omega_2^2(n_2+1)\right)} \left[\tau^+_{n_1,n_2} + \tau^-_{n_1,n_2} - 2\right] .
\end{aligned} \tag{5.16}
$$

It is clear from the above equations that the effects of the barrier and well potentials induced by the dressed states $|\phi^\pm_{n_1+1,n_2+1}\rangle$ add coherently in either the reflection or transmission of the atom. The additive term to the barrier-well amplitudes in Eqs. (5.14) and (5.16) comes from the contribution of the dark state

$|\phi^0_{n_1+1,n_2+1}\rangle$ in the initial state expansion Eq. (5.5). Since the dark state is orthogonal to the middle state $|g_1\rangle$, it influences only the zero-photon and the two-photon emissions, but not the one-photon emissions of the excited atom. An important feature here is that the two-photon transition can always be induced by the field when the one-photon transition is forbidden. This can be seen by examining the probabilities for different states of the atom. When an initially excited atom is incident upon the cavity containing (n_1, n_2) photons in the two cavity modes $(1, 2)$, respectively, then from Eqs. (5.15) and (5.16) the probability that the atom makes a one-photon transition to the state $|g_1\rangle$ with the emission of a photon in mode 1 is

$$P_{n_1,n_2}(e \to g_1) = |R_{g_1,n_1+1,n_2}|^2 + |T_{g_1,n_1+1,n_2}|^2 \ , \tag{5.17}$$

and the probability that the atom makes a two-photon transition to the state $|g_2\rangle$ with the emission of a photon in each of the modes 1 and 2 of the cavity is

$$P_{n_1,n_2}(e \to g_2) = |R_{g_2,n_1+1,n_2+1}|^2 + |T_{g_2,n_1+1,n_2+1}|^2 \ . \tag{5.18}$$

When $\Omega_2 = 0$, the lower transition $g_1 \to g_2$ is forbidden and hence the two-photon transition probability $P_{n_1,n_2}(e \to g_2)$ vanishes. Then, the upper transition $e \to g_1$ behaves like a two-level atom interacting with the mode 1 of the cavity field. In Fig. 5.3, we compare the photon emission probabilities of excited, two-level $(\Omega_2 \equiv 0)$ and three-level $(\Omega_2 \neq 0)$ atoms when the cavity is initially in vacuum state. We scale the parameters in terms of a wave number κ which is defined by the vacuum coupling energy $\hbar\Omega_1 \equiv \hbar^2\kappa^2/2m$ of the two-level atom. Note that if the coupling strength is chosen as $\Omega_1 = 2\pi \times 10$ MHz, then the parameter $\kappa L = 20000\pi$ corresponds to 155 μm length of the cavity for the Rydberg ^{85}Rb atom. The temperature of the atom is of the order of 10^{-6} K for the mean momentum $k/\kappa = 0.1$ (velocity $\approx$ 30 mm/s). For ultracold, incident atoms $(k/\kappa << 1)$, the graphs in Figs. 5.3(a) and 5.3(b) show that the one-photon emission probability exhibits resonances as a function of length of the cavity for both two-level and three-level atoms. In the three-level atom, the resonances of the one-photon emission probability occur at values of κL different from those of two-level atom. The two-photon emission probability shows maxima and minima at the resonance positions of the one-photon transition. This behavior arises from the interference of the contri-

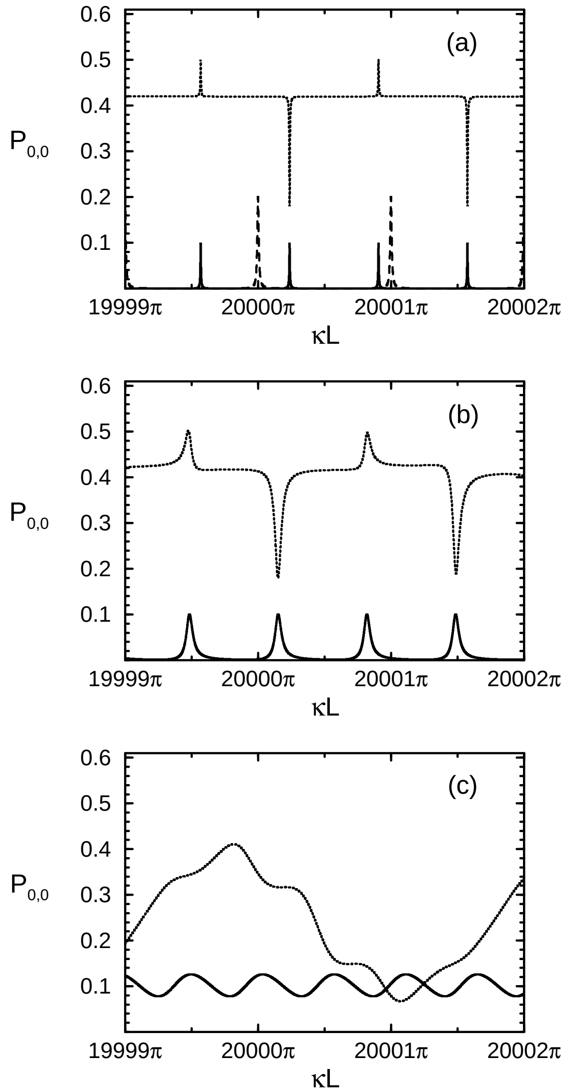

Figure 5.3: The probabilities of $e \rightarrow g_1$ (solid curve) and $e \rightarrow g_2$ (dotted curve) transitions of an excited atom as a function of the length κL of the cavity. The cavity is initially in the vacuum state and the parameters used are $\Omega_2/\Omega_1 = 2$, $k/\kappa = 0.01$ (a), $k/\kappa = 0.1$ (b), $k/\kappa = 1.1$ (c). The dashed curve in (a) represents the photon emission probability of an excited two-level atom resonant with the upper transition when $\Omega_2 = 0$. Actual values of the dashed curve are 2.5 times those shown. For clarity, the dotted curves in (a) and (b) have been displaced by 0.1 units along the Y axis.

butions coming from different dressed states in the initial state expansion Eq. (5.5). The transmission probability $|T_{g_2,n_1+1,n_2+1}|^2$ obtained from Eq. (5.16) has an interference term proportional to the phase of the amplitude $\left(\tau^{+}_{n_1,n_2} + \tau^{-}_{n_1,n_2}\right)$. This term can be constructive or destructive which leads to the enhancement or reduction of the two-photon emission probability. From the graph, we also see that $P_{0,0}(e \to g_2) \approx 0.32$ when $P_{0,0}(e \to g_1) \approx 0$. This implies that the probability of two-photon emission is not the product of the probabilities for single photon emission. This also suggests that both the field modes of the bimodal cavity can be amplified together through the two-photon transition of an excited atom. This feature is absent in the case of two-mode micromaser pumped by ultra-cold, Λ-type three-level atoms studied in the previous chapter . In the Λ-scheme micromazer, the excited atom can make only one-photon transition to either of the two ground levels. Therefore, both the cavity modes can not be populated sequentially by the photon emission from the same atom.

Next, we compare our results for ultra-cold atoms with that of fast, incident atoms in the Ξ- type configuration. In the case of fast, incident atoms $(k/\kappa >> 1)$, both one- and two- photon emission probabilities exhibit Rabi oscillations as a function of the length of the cavity. The Rabi frequency of oscillation for one-photon emission is twice that of the two-photon emission. These features can be understood from the usual Jaynes-Cummings (JC) model where one neglects the quantization of the atomic motion in atom-cavity interaction [6]. Thus, neglecting the kinetic energy operator in the Hamiltonian (5.1), the time evolution of the initial atom-field state $|e, n_1, n_2\rangle$ gives for the photon emission probabilities in the JC model:

$$P_{n_1,n_2}(e \to g_1) = \frac{\Omega_1^2(n_1+1)}{\Omega^2}\sin^2(\Omega\tau) \ ,$$

$$P_{n_1,n_2}(e \to g_2) = \frac{4\Omega_1^2\Omega_2^2(n_1+1)(n_2+1)}{\Omega^4}\sin^4(\Omega\tau/2) \ ,$$

where $\Omega \equiv \sqrt{\Omega_1^2(n_1+1) + \Omega_2^2(n_2+1)}$ is the Rabi frequency and τ is the interaction time of the atom with the cavity. Note that when $\Omega\tau$ is an odd number multiple of π, the one-photon transition is forbidden and the two-photon transition probability becomes maximum. When $\Omega\tau$ is an even number multiple of π, both one- and two-photon emission probabilities vanish. We further note that the photon emission probabilities exhibit oscillatory type behavior even for energies of the incident atom comparable to vacuum coupling energy $(k/\kappa \approx 1)$. The graphs in Fig. 5.3(c) show this behavior in the atomic transitions which is to be compared with the results for ultracold, incident atoms. Thus, one finds novel features in the atom-cavity dynamics when the motional effects of atom are taken into account. However, we add that realization of such dynamical effects has to wait for the technical advances in the form of achieving higher atom-field coupling strengths, control over parameters like cavity length, velocity of atoms, etc..

5.2 Basic Master Equation

In this section, we consider the maser action of ultracold atoms in the bimodal cavity and derive the master equation for the cavity field assuming that excited atoms are pumped steadily into the cavity. We model the random pumping of the atoms into the cavity by a Poissonian process with an average rate of pumping r. The flux of the incident atoms is adjusted so that only one atom interacts with the cavity field at a time. We neglect the cavity field damping during the time an atom interacts with the field. Since the field in the cavity changes with the passage of each atom, we need to know the time evolution of the atom-field state for a general initial state of the cavity field. The wave function of the initial atom-field system is now given by

$$|\Psi(z,0)\rangle = \psi(z,0) \sum_{n_1,n_2} C_{n_1,n_2} |e, n_1, n_2\rangle. \tag{5.19}$$

Carrying out the time evolution for this initial state using Eq. (5.13), the state of atom-field system after the interaction is given by

$$\begin{aligned} |\, \Psi(z,t)\rangle \;=\; & \int dk A(k) e^{-i(\hbar k^2/2m)t} \sum_{n_1,n_2=0}^{\infty} C_{n_1,n_2} \\ & \times \Big\{ \Big[R_{e,n_1,n_2}(k) e^{-ikz}\theta(-z) + T_{e,n_1,n_2}(k) e^{ikz}\theta(z-L) \Big] |e, n_1, n_2\rangle \\ & + \Big[R_{g_1,n_1+1,n_2}(k) e^{-ikz}\theta(-z) + T_{g_1,n_1+1,n_2}(k) e^{ikz}\theta(z-L) \Big] |g_1, n_1+1, n_2\rangle \\ & + \Big[R_{g_2,n_1+1,n_2+1}(k) e^{-ikz}\theta(-z) + T_{g_2,n_1+1,n_2+1}(k) e^{ikz}\theta(z-L) \Big] \\ & \times |g_2, n_1+1, n_2+1\rangle \Big\} \,, \end{aligned} \tag{5.20}$$

The time evolution of the reduced density operator of the field in the interaction picture is then given in the coarse graining method [43] to be

$$\dot{\rho}(t) = r\delta\rho(t) + L\rho(t) \ , \tag{5.21}$$

where $\delta\rho(t) = \rho(t) - \rho(0)$ is the change in the reduced density operator of the field due to the passage of a single atom in the excited state. This can be obtained by tracing the atom-field density matrix formed from Eqs. (5.19) and (5.20) over external and internal degrees of freedom of the atom. Field damping and the effect of thermal photons are described by the Liouville operator

$$\begin{aligned} L\rho &= \frac{1}{2}C_1(n_{b_1}+1)(2a_1\rho a_1^\dagger - a_1^\dagger a_1\rho - \rho a_1^\dagger a_1) \\ &+ \frac{1}{2}C_1 n_{b_1}(2a_1^\dagger\rho a_1 - a_1 a_1^\dagger\rho - \rho a_1 a_1^\dagger) \\ &+ \frac{1}{2}C_2(n_{b_2}+1)(2a_2\rho a_2^\dagger - a_2^\dagger a_2\rho - \rho a_2^\dagger a_2) \\ &+ \frac{1}{2}C_2 n_{b_2}(2a_2^\dagger\rho a_2 - a_2 a_2^\dagger\rho - \rho a_2 a_2^\dagger) \ . \end{aligned} \tag{5.22}$$

Here n_{b_α} is the number of thermal photons in mode α and C_α is the damping rate of this mode. Using Eqs. (5.21) and (5.22) we obtain the equation governing the time evolution of density matrix elements,

$$\begin{aligned} \dot{\rho}(n_1,n_2;n_1',n_2') &= r\left\{(R_{e,n_1,n_2}R^\star_{e,n_1',n_2'} + T_{e,n_1,n_2}T^\star_{e,n_1',n_2'} - 1)\rho(n_1,n_2;n_1',n_2')\right. \\ &+ \ (R_{g1,n_1,n_2}R^\star_{g1,n_1',n_2'} + T_{g1,n_1,n_2}T^\star_{g1,n_1',n_2'})\rho(n_1-1,n_2;n_1'-1,n_2') \\ &+ (R_{g2,n_1,n_2}R^\star_{g2,n_1',n_2'} + T_{g2,n_1,n_2}T^\star_{g2,n_1',n_2'}) \\ &\times \ \left.\rho(n_1-1,n_2-1;n_1'-1,n_2'-1)\right\} \\ &+ \frac{1}{2}C_1(n_{b_1}+1)[2\sqrt{(n_1+1)(n_1'+1)}\rho(n_1+1,n_2;n_1'+1,n_2') \\ &- (n_1+n_1')\rho(n_1,n_2;n_1',n_2')] \\ &+ \frac{1}{2}C_1 n_{b_1}[2\sqrt{n_1 n_1'}\rho(n_1-1,n_2;n_1'-1,n_2') \\ &- (n_1+n_1'+2)\rho(n_1,n_2;n_1',n_2')] \\ &+ \frac{1}{2}C_2(n_{b_2}+1)[2\sqrt{(n_2+1)(n_2'+1)}\rho(n_1,n_2+1;n_1',n_2'+1) \\ &- (n_2+n_2')\rho(n_1,n_2;n_1',n_2')] \\ &+ \frac{1}{2}C_2 n_{b_2}[2\sqrt{n_2 n_2'}\rho(n_1,n_2-1;n_1',n_2'-1) \\ &- (n_2+n_2'+2)\rho(n_1,n_2;n_1',n_2')] \ . \end{aligned} \tag{5.23}$$

The diagonal elements of the density matrix $P(n_1, n_2) = \rho(n_1, n_2; n_1, n_2)$ which gives the joint distribution of photons in the two cavity modes, obeys the following equation:

$$\begin{aligned} \dot{P}(n_1, n_2) \; = \; & - G_{g_1,n_1,n_2} P(n_1, n_2) + G_{g_1,n_1-1,n_2} P(n_1 - 1, n_2) \\ & - G_{g_2,n_1,n_2} P(n_1, n_2) + G_{g_2,n_1-1,n_2-1} P(n_1 - 1, n_2 - 1) \\ & + C_1(n_{b_1} + 1) \left[(n_1 + 1)P(n_1 + 1, n_2) - n_1 P(n_1, n_2)\right] \\ & + C_1 n_{b_1} \left[n_1 P(n_1 - 1, n_2) - (n_1 + 1)P(n_1, n_2)\right] \\ & + C_2(n_{b_2} + 1) \left[(n_2 + 1)P(n_1, n_2 + 1) - n_2 P(n_1, n_2)\right] \\ & + C_2 n_{b_2} \left[n_2 P(n_1, n_2 - 1) - (n_2 + 1)P(n_1, n_2)\right] \; , \end{aligned} \tag{5.24}$$

where $G_{g_1,n_1,n_2} = rP_{n_1,n_2}(e \to g_1)$ and $G_{g_2,n_1,n_2} = rP_{n_1,n_2}(e \to g_2)$ are the gain coefficients for the atomic transitions with $P_{n_1,n_2}(e \to g_1)$ and $P_{n_1,n_2}(e \to g_2)$ as defined in Eqs. (5.17) and (5.18). This is the master equation for the two-mode micromaser describing the time evolution of photon distribution in the cavity. This equation behaves similar to a rate equation for the probability and a simple physical meaning can be given to each term on the right hand side in terms of inflow and outflow of probabilities. The first and second terms in the equation gives the effect of one-photon transitions while the third and fourth terms correspond to the two-photon transitions of the excited atoms.

5.3 Numerical Results of Photon Distribution in Steady State

The steady state distribution of photons obeys the equation

$$\dot{P}(n_1, n_2) = 0 \tag{5.25}$$

In the limit $\Omega_2 \to 0$, the two-photon transition probability in Eq. (5.18) tends to zero and therefore we can neglect the third and fourth terms containing G_{g_2,n_1,n_2} in the master Eq. (5.24). In this case, the upper transitions $e \to g_1$ behave like two-level atoms interacting with the mode 1 of the cavity. The lower transitions $g_1 \to g_2$ and hence the two-photon transitions $e \to g_1 \to g_2$ are forbidden in the interaction. The steady state solution of the Eq. (5.25) can then be obtained in analytical form by using the principle of detailed balance as discussed by Meyer et al [99]. The photon statistics in this *two-level problem is a mixture of thermal and shifted thermal distributions*. When $\Omega_2 \neq 0$, both the one- and two-photon effects of atomic transitions contribute in building up the cavity field. The two-photon terms (third and fourth terms) in the master equation have no counterpart in the decay terms and therefore the equation is *not solvable analytically* for the steady state distribution by the principle of *detailed balance* adopted in all the previous work on micromasers. In this general case, we integrate the master equation (5.24) numerically using fourth order Runge kutta method to get the steady state solution as done in Fig. 4.6. We *do not* use any decorrelation approximation, i.e., we do not assume $P(n_1, n_2) = f(n_1)g(n_2)$. The photon distribution $P_1(n)$ and $P_2(n)$ in the cavity modes 1 and 2 are obtained respectively using

$$P_1(n) = \sum_{l=0}^{\infty} P(n,l), \qquad P_2(n) = \sum_{l=0}^{\infty} P(l,n) \ . \tag{5.26}$$

The normalized variances of photon distribution in the two cavity modes are defined by

$$\sigma_\alpha^2 = \frac{\langle n_\alpha^2 \rangle - \langle n_\alpha \rangle^2}{\langle n_\alpha \rangle} \ , \qquad \alpha = 1, 2 \ . \tag{5.27}$$

In Fig. 5.4, we present the numerical results of the photon distribution in steady state for ultra-cold, incident atoms ($k/\kappa << 1$) by assuming equal parameters for the decay terms $C_1 = C_2 = C$, $n_{b_1} = n_{b_2} = n_b$. The graph shows that for $\Omega_1 < \Omega_2$, the photon statistics in mode 1 is super-Poissonian ($\sigma_1^2 > 1$) while that of mode 2 is sub-Poissonian ($\sigma_2^2 < 1$). The photon distribution for $\Omega_1 > \Omega_2$ is identical to that of $\Omega_1 < \Omega_2$ except that modes 1 and 2 are interchanged. When $\Omega_1 = \Omega_2$, each mode of the cavity field exhibits Poissonian statistics ($\sigma_\alpha^2 \approx 1$) of mean $r/2C - 1$. To understand these numerical results, we now approximate the master equation (5.24) by dropping the first and second terms corresponding to one-photon transitions. In fact, for the parameters of Fig. 5.4, the barrier and well amplitudes are $\rho^{\pm}_{n_1,n_2} \approx -1$, $\tau^{\pm}_{n_1,n_2} \approx 0$ for wide range of n_1 and n_2 values. Therefore, the one-photon transition probability $P_{n_1,n_2}(e \to g_1)$ in Eq. (5.17) is approximately zero. The two-photon emission probability $P_{n_1,n_2}(e \to g_2)$ in Eq. (5.18) can then be approximated to be $2\Omega_1^2\Omega_2^2(n_1+1)(n_2+1)/(\Omega_1^2(n_1+1)+\Omega_2^2(n_2+1))^2$. Note that

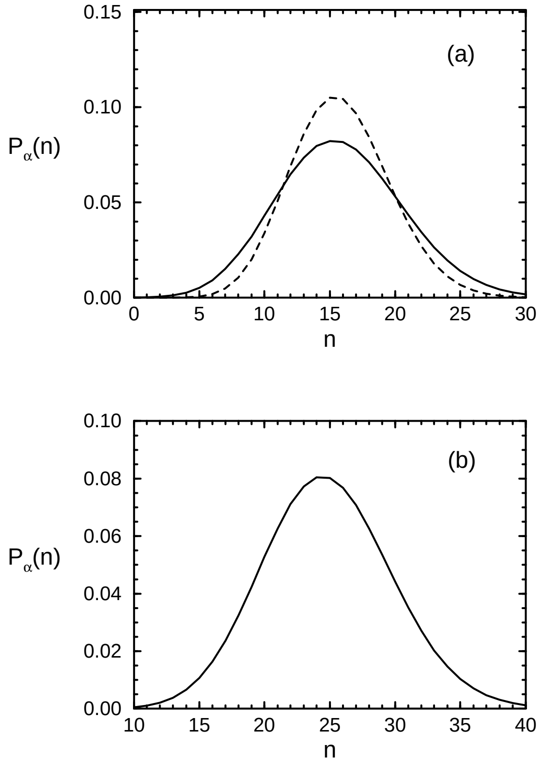

Figure 5.4: The steady-state distribution of photons in mode 1 (solid curve) and mode 2 (dashed curve). The parameters used are $C_1 = C_2 = C$, $n_{b_1} = n_{b_2} = n_b$, $r/C = 50$, $n_b = 0$, $\kappa L = 20000\pi$, $k/\kappa = 0.01$, and $\Omega_2/\Omega_1 = 2$ (a), $\Omega_2/\Omega_1 = 1$ (b). In the case of $\Omega_2 = \Omega_1$, the dashed curve is not distinguishable from the solid curve. The photon statistics for the parameter $\Omega_2/\Omega_1 = 0.5$ is approximately similar to that of $\Omega_2/\Omega_1 = 2$ except that the solid (dashed) curve corresponds to the photon distribution in mode 2 (1). The normalized variances of the photon distributions in (a) are $\sigma_1^2 = 1.47$ (solid curve) and $\sigma_2^2 = 0.9$ (dashed curve).

this approximation is also consistent with the results for ultra-cold atoms in Fig. 5.3. With these substitutions for the photon emission probabilities in gain coefficients, numerical integration of the master Eq. (5.24) again gives the same results. Moreover, in the absence of one-photon terms, the master equation is symmetric with respect to the labels 1 and 2 of the two cavity modes. Thus, the Poissonian distribution of photons in each cavity mode is purely the effect of two-photon transitions of the excited atoms. It should be emphasized that the transmission of atoms occurs only in the dark eigenstate component of the interaction during the field buildup in the cavity. The atoms interacting with the barrier-well component of the dressed states get reflected always. But both the reflected and the transmitted atoms *have equal probability* of two-photon emissions into the cavity.

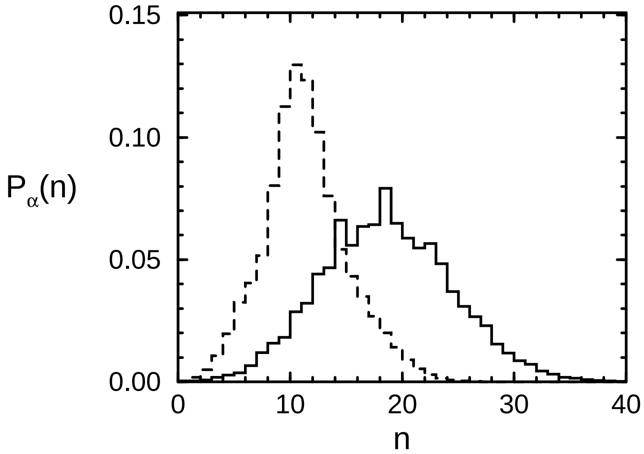

Figure 5.5: The steady-state distribution of photons in mode 1 (solid) and mode 2 (dashed) for the same parameters as in Fig. 5.4(a) with $k/\kappa = 100$.

Since the one-photon emissions are forbidden in the interaction for ultracold atoms, the photon distribution of both the cavity modes peaks around the same photon number in Fig. 5.4. In general, the photon distribution for mode 1 peaks at a higher photon number when compared with that of mode 2 . This is because the mode 1 of the cavity can be populated by both one- and two-photon emissions while the mode 2 can be populated by only two-photon emissions from the incident atoms. We have found this behavior of steady state photon distribution in the case of fast, incident atoms. In Fig. 5.5, we display the steady state photon distribution when the micromaser is pumped by fast, incident atoms $(k/\kappa >> 1)$ for the same parameters of Fig. 5.4(a). The graph shows that the field 1 is amplified more than the field 2 by the stimulated, photon emissions from the incident atoms. It is important to note that the field 2 has an influence on the field 1 in the cavity through the interaction with the atoms. The effects of field 2 such as gain enhancement or gain reduction on field 1 have been already discussed in a different context viz in a two-beam laser operating on cascade three-level atoms [126].

Next, we show the effect of thermal photons in the cavity on the steady state photon distribution in Fig. 5.6. For comparison, we have also plotted the photon

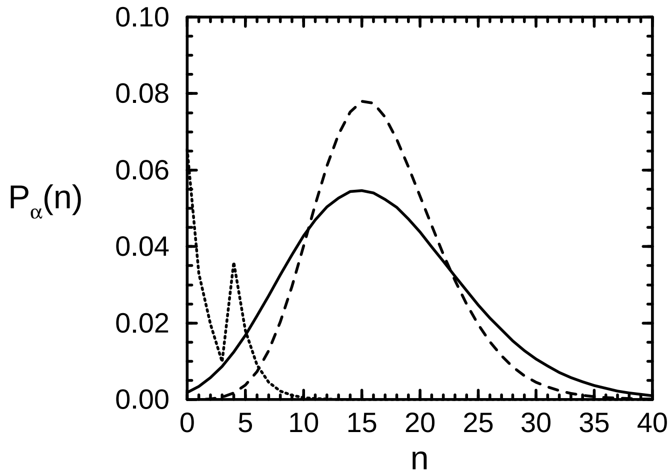

Figure 5.6: The steady-state distribution of photons in mode 1 (solid curve) and mode 2 (dashed curve). The parameters for the calculation are $C_1 = C_2 = C$, $n_{b_1} = n_{b_2} = n_b$, $r/C = 50$, $k/\kappa = 0.01$, $\Omega_2/\Omega_1 = 2$, $\kappa L = 40000\pi/(4)^{1/4}$, and $n_b = 1$. The dotted curve represents the photon distribution in mode 1 for the two-level problem when $\Omega_2 = 0$. Actual values of the dotted curve are five times those shown.

distribution for the two-level problem ($\Omega_2 \equiv 0$). The length κL of the cavity is chosen to be at a resonance of the one-photon emission probability for the initial, excited state of the two-level atom and three photons in mode 1 of the cavity. The photon distribution in the two-level problem then looks similar to a mixture of thermal and shifted thermal distributions as discussed by Meyer et al [99]. For three-level atoms, comparison with Fig. 5.4(a) shows that the photon distribution broadens because of the presence of thermal photons ($n_b \neq 0$) even though qualitative features are very similar. In particular, the two-photon emissions from the pumping atoms are still the dominant contribution to the steady state field for the chosen length of the cavity. The Poissonian-like statistics of photons in the micromaser cavity pumped by cold atoms, resembles closely the behavior of a laser operating at far above threshold [12]. Finally, we note that the two-photon effects are dominant over the one-photon transitions only in the limit ($k/\kappa << 1$) of ultra-slow motion of the incident atoms. The competition of the one-photon with the two-photon processes becomes stronger even for energies of the incident atoms ($k/\kappa \approx 1$) close to the vacuum coupling energy. In Fig. 5.7, we plot the photon distribution in the cavity for the mean momentum $k/\kappa = 1.1$ of the inci-

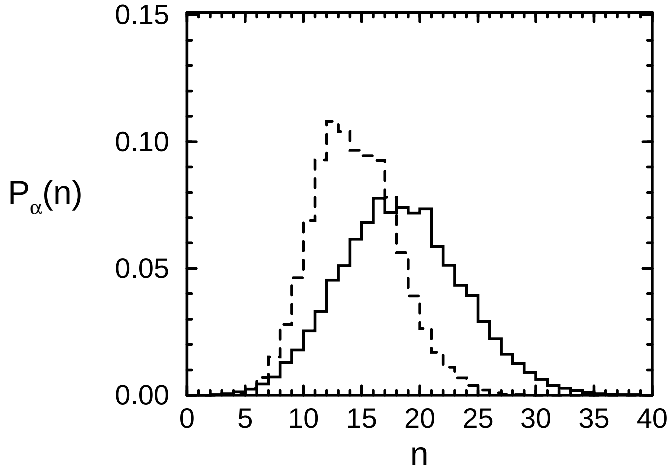

Figure 5.7: The steady-state distribution of photons in mode 1 (solid) and mode 2 (dashed) for the same parameters as in Fig. 5.4(a) with $k/\kappa = 1.1$.

dent atoms. The graph shows that the one-photon effects participate in the field build up of the cavity and these lead to unequal, average number of photons in the two modes of the mazer field. This result is also substantiated by the non-zero one-photon emission probability in Fig. 5.3(c) for the chosen parameters.

5.4 Summary

In summary, we have discussed the new features in the photon statistics of a two-mode micromaser pumped by ultracold Ξ-type three level atoms. In Sec. 5.1, we described the model system and discussed the central role played by quantizing the atomic motion. It was shown that atoms can emit photons into the cavity either by reflections or transmissions through the cavity. We presented numerical results for one-photon and two-photon emission probabilities of the atom. An important prediction was that the two-photon transition can always be induced in an excited atom when the corresponding one-photon transition is forbidden. In Sec. 5.2, we considered the maser action of ultracold atoms and derived the basic master equation for the two-mode cavity field. Finally, in Sec. 5.3, we discussed the steady state photon statistics of the cavity field using numerical results of the master equation. It was shown that, in general, the two-photon transitions dominate over the one-photon emissions in building up the steady state of the cavity fields. We also showed that this feature is absent in the usual case of micromaser pumped with fast atoms instead of ultracold atoms.

Conclusions and Future Outlook

In conclusion, this thesis reports novel features in the dynamics of ultracold atoms interacting with high-quality cavities. We show the effects of quantized motion of atoms on the passage time, tunneling probabilities through single and two cavities on one hand and on the other the maser action of ultracold atoms. Our new findings are presented with extensive numerical results which are further substantiated by physical explanations and possible analytical solutions. In the following, we present a brief summary of important conclusions of each chapter and discuss the future outlook.

In chapter 2, we have shown numerically the possibility of superclassical traversal of an ultracold two-level atom through a cavity initially in vacuum state. This implies that the peak of transmitted wave packet of the atom can emerge the cavity even before it enters it. We have explained how this behavior can be understood from the analytical formula of the phase tunneling time of the wave packet. We have also discussed the similarity of this behavior with the superluminal propagation of electromagnetic pulses through an anamolous dispersion medium. However, we have also noted that the phase time does not always account for the traversal time of the wave packet. We have shown that the wave packet gets distorted during propagation through the cavity when the average momentum of the incident atom is near a transmission resonance. This needs further explanations and analytical investigations on the transmission amplitude's behavior near the resonance.

In chapter3, we have demonstrated an analog of resonant tunneling through potential barriers in a totally new context, i.e., in the field of cavity quantum electrodynamics. We considered the transmission of an ultracold two-level atom through a system of two cavities in vacuum state. The potentials induced by the atom-cavity interaction show important bearings on the transmission of the atom. The transmission probability exhibits resonances as a function of energy of atoms corresponding to the discrete states in the potential well formed between the cavities. We have noted the similarity of this feature to the tunneling of electrons through semiconductor double barriers. Since this work shares features in common with semiconductor systems, it opens up the possibility of generalizing many ideas developed in condensed matter physics. These include, for example, extensions of this work to multi-cavity system to realize Kronig-Penney like model and considering time periodic atom-cavity coupling to realize the analog of field-assisted tunneling in potential barriers.

In chapters 4 and 5, we have discussed the maser action of ultracold atoms in bimodal cavities. The underlying theme of these studies is that the incident atoms can amplify the cavity field either by reflection or transmission through the cavity induced potentials. In chapter 4, we have considered Λ-type atoms in the excited state for interaction. Here, it has been shown that the fields in the cavity are strongly anti-correlated in steady state due to one-photon emissions from the incident atoms. In chapter 5, we have discussed the maser action of ultracold atoms with Ξ-type configuration. We have shown that atoms in this configuration can amplify the field in the cavity either by one-photon emissions or two-photon emissions. We have also shown parameter regimes where two-photon emissions from the atoms are dominant and discussed its role in the maser action. It has been shown numerically that two-photon emissions lead to sub- and super-poissonian behaviors in the photon statistics of the cavity fields. In both these chapters, we have considered the two fields in the cavity to act on different transitions of the atom. The study of cross-talk by the action of each field in the cavity on both the transitions of the atom is still an open problem. Further, we can even study cooperative effects of atomic emissions in the maser action. For example, instead of sending atoms one by one through the cavity, pairs of atoms can be injected into the cavity at a time. The interesting model to realize two-photon emissions would then be pairs of ultracold two-level atoms passing through a single mode cavity.

References

[1] J. D. Jackson, *Classical Electrodynamics*, (Wiley, New York, 1962).

[2] J. C. Slater, *Microwave Electronics*, (Van Nostrand, New York, 1950).

[3] L. Mandel and E. Wolf, *Optical Coherence and Quantum Optics*, (Cambridge Univ. Press, New York, 1995).

[4] C. Cohen-Tannoudji, J. Dupont-Roc, and G. Grynberg, *Atom-Photon Interactions*, (Wiley, New York, 1992).

[5] E. T. Jaynes and F. W. Cummings, Proc. IEEE **51**, 89 (1963).

[6] For review articles on Jaynes-Cummings model, see, P. L. Knight and P. W. Milonni, Phys. Rep. **66**, 21 (1980); H. -I. Yoo and J. H. Eberly, Phys. Rep. **118**, 239 (1985).

[7] I. I. Rabi, Phys. Rev. **51**, 652 (1937).

[8] J. J. Sanchez-Mondragon, N. B. Narozhny, and J. H. Eberly, Phys. Rev. Lett. **51**, 550 (1983).

[9] G. S. Agarwal, J. Opt. Soc. Am. B **2**, 480 (1985).

[10] J. H. Eberly, N. B. Narozhny, and J. J. Sanchez-Mondragon, Phys. Rev. Lett. **44**, 1323 (1980).

[11] G. Rempe, H. Walther, and N. Klein, Phys. Rev. Lett. **58**, 353 (1987).

[12] M. O. Scully and M. S. Zubairy, *Quantum Optics*, (Cambridge Univ. Press, New York, 1997).

[13] For a recent review, see, *Cavity Quantum Electrodynamics*, edited by P. R. Berman (Academic, Boston, 1994).

[14] D. Kleppner, Phys. Rev. Lett. **47**, 233 (1981).

[15] G. Gabrielse and H. Dehmelt, Phys. Rev. Lett. **55**, 67 (1985).

[16] R. G. Hulet, E. S. Hilfer, and D. Kleppner, Phys. Rev. Lett. **55**, 2137 (1985).

[17] W. Jhe, A. Anderson, E. A. Hinds, D. Meschede, L. Moi, and S. Haroche, Phys. Rev. Lett. **58**, 666 (1987).

[18] W. Lange and H. Walther, Phys. Rev. A **48**, 4551 (1993); A theoritical understanding of this experiment was given by G. S. Agarwal, W. Lange and H. Walther, Phys. Rev. A **48**, 4555 (1993).

[19] P. Goy, J. M. Raimond, M. Gross, and S. Haroche, Phys. Rev. Lett. **50**, 1903 (1983).

[20] D. J. Heinzen, J. J. Childs, J. E. Thomas, and M. S. Feld, Phys. Rev. Lett. **58**, 1320 (1987).

[21] F. De Martini, G. Innocenti, G. R. Jacobovitz, and P. Mataloni, Phys. Rev. Lett. **59**, 2955 (1987).

[22] S. Sachdev, Phys. Rev. A **29**, 2627 (1984).

[23] B. J. Hughey, T. R. Gentile, D. Kleppner, and T. W. Ducas, Phys. Rev. A **41**, 6245 (1990).

[24] G. S. Agarwal, Phys. Rev. Lett. **53**, 1732 (1984).

[25] G. S. Agarwal, R. K. Bullough, and G. P. Hildred, Opt. Commun. **59**, 23 (1986).

[26] G. S. Agarwal and S. Dutta Gupta, Phys. Rev. A **39**, 2961 (1989).

[27] G. S. Agarwal, Phys. Rev. A **43**, 2595 (1991).

[28] J. E. Field, Phys. Rev. A **47**, 5064 (1993).

[29] C. K. Law, S.-Y. Zhu, and M. S. Zubairy Phys. Rev. A **52**, 4095 (1995).

[30] C. Wang and R. Vyas, Phys. Rev. A **55**, 823 (1997).

[31] Hyunchul Nha, Young-Tak Chough, Wonho Jhe, and Kyungwon An, Phys. Rev. A **63**, 063814 (2001).

[32] M. G. Raizen, R. J. Thompson, R. J. Brecha, H. J. Kimble, and H. J. Carmichael, Phys. Rev. Lett. **63**, 240 (1989).

[33] Y. Zhu, D. J. Gauthier, S. E. Morin, Q. Wu, H. J. Carmichael and T. W. Mossberg, Phys. Rev. Lett. **64**, 2499 (1990).

[34] R. J. Thompson, G. Rempe and H. J. Kimble, Phys. Rev. Lett. **68**, 1132 (1992).

[35] J. Gripp, S. L. Mielke, and L. A. Orozco, Phys. Rev. A **56**, 3262 (1997).

[36] F. Bernardot, P. Nussenzveig, M. Brune, J. M. Raimond, and S. Haroche, Europhys. Lett. **17**, 33 (1992).

[37] G. V. Varada, M. Sanjay Kumar, and G. S. Agarwal, Optics Commun. **62**, 328 (1987).

[38] R. R. Puri and G. S. Agarwal, Phys. Rev. A **33**, 3610 (1986).

[39] R. R. Puri and G. S. Agarwal, Phys. Rev. A **37**, 3879 (1988).

[40] S. Haroche and J. M. Raimond, Adv. At. Mol. Phys. **20**, 347 (1985).

[41] D. Meschede, H. Walther and G. Müller, Phys. Rev. Lett. **54**, 551 (1985).

[42] P. Filipowicz, J. Javanainen, and P. Meystre, Phys. Rev. A **34**, 3077 (1986).

[43] L. A. Lugiato, M. O. Scully, and H. Walther, Phys. Rev. A **36**, 740 (1987).

[44] M. Brune, J. M. Raimond, and S. Haroche, Phys. Rev. A **35**, 154 (1987); L. Davidovich, J. M. Raimond, M. Brune, and S. Haroche, Phys. Rev. A **36**, 3771 (1987).

[45] J. Krause, M. O. Scully, and H. Walther, Phys. Rev. A **36**, 4547 (1987).

[46] P. Meystre, G. Rempe, and H. Walther, Opt. Lett. **13**, 1078 (1988).

[47] J. Krause, M. O. Scully, T. Walther, and H. Walther, Phys. Rev. A **39**, 1915 (1989).

[48] J. Bergou, L. Davidovich, M. Hillery, C. Benkert, M. Orszag, and M. O. Scully, Opt. Commun. **72**, 82 (1989); Phys. Rev. A **40**, 5073 (1989).

[49] A. M. Guzman, P. Meystre, and E. M. Wright, Phys. Rev. A **40**, 2471 (1989).

[50] M. Brune, S. Haroche, V. Lefevre, J. M. Raimond, and N. Zagury, Phys. Rev. Lett. **65**, 976 (1990); M. Brune, S. Haroche, J. M. Raimond, L. Davidovich, and N. Zagury, Phys. Rev. A **45**, 5193 (1992).

[51] E. S. Guerra, A. Z. Khoury, L. Davidovich, N. Zagury, Phys. Rev. A **44**, 7785 (1991).

[52] L. Wang, R. R. Puri, and J. H. Eberly, Phys. Rev. A **46**, 7192 (1992).

[53] B. Deb and D. S. Ray, Phys. Rev. A **48**, 3191 (1993).

[54] M. O. Scully, H. Walther, G. S. Agarwal, T. Quang, and W. Schleich, Phys. Rev. A **44**, 5992 (1991).

[55] S. Qamar and M. S. Zubairy, Phys. Rev. A **44**, 7804 (1991).

[56] T. Quang, G. S. Agarwal, J. Bergou, M. O. Scully, H. Walther, K. Vogel, and W. P. Schleich, Phys. Rev. A **48**, 803 (1993); K. Vogel, W. P. Schleich, M. O. Scully, and H. Walther, Phys. Rev. A **48**, 813 (1993).

[57] N. Lu, Phys. Rev. Lett. **70**, 912 (1993).

[58] W. C. Schieve and R. R. McGowan, Phys. Rev. A **48**, 2315 (1993).

[59] N. Lu, Phys. Rev. A **47**, 1347 (1993).

[60] B. Deb and D. S. Ray, Phys. Rev. A **49**, 5015 (1994).

[61] L. Rao, J. C. Retamal, and C. Saavedra, Phys. Rev. A **47**, 620 (1993).

[62] S. Zhu, C. Su, and A. Ma, Phys. Rev. A **47**, 2319 (1993).

[63] C. Wagner, R. J. Brecha, A. Schenzle, and H. Walther, Phys. Rev. A **47**, 5068 (1993).

[64] N. Nayak and D. Das, Phys. Rev. A **48**, 2475 (1993).

[65] S. A. Kumar and G. S. Agarwal, Phys. Rev. A **50**, 680 (1994).

[66] R. R. Puri, C. K. Law, and J. H. Eberly, Phys. Rev. A **50**, 4212 (1994).

[67] F. L. Kien, G. M. Meyer, M. O. Scully, H. Walther, and S.-Y. Zhu, Phys. Rev. A **49**, 1367 (1994).

[68] U. Herzog, Phys. Rev. A **52**, 602 (1995).

[69] N. Nayak, Phys. Rev. A **57**, 605 (1998).

[70] D. B. Johnson and W. C. Schieve, Phys. Rev. A **63**, 033808 (2001).

[71] F. Casagrande, A. Lulli, and V. Santagostino, Phys. Rev. A **65**, 023809 (2002).

[72] M. Brune, F. Schmidt-Kaler, A. Maali, J. Dreyer, E. Hagley, J. M. Raimond, and S. Haroche, Phys. Rev. Lett. **76**, 1800 (1996).

[73] M. Brune, J. M. Raimond, P. Goy, L. Davidovich, and S. Haroche, Phys. Rev. Lett. **59**, 1899 (1987).

[74] G. Rempe, F. Schmidt-Kaler, and H. Walther, Phys. Rev. Lett. **64**, 2783 (1990).

[75] M. O. Scully, B.-G. Englert, and H. Walther, Nature **351**, 111 (1991).

[76] K. An, J. J. Childs, R. R. Dasari, and M. S. Feld, Phys. Rev. Lett. **73**, 3375 (1994).

[77] D. Meschede, Phys. Rep. **211**, 201 (1992); P. Meystre, in *Progress in Optics*, edt. E. Wolf, **130**, 261 (1992); H. Walther, Phys. Scr. **T23**, 165 (1988); H. Walther, Phys. Rep. **219**, 263 (1992); For a recent review, see also, Ref. [13].

[78] R. Short and L. Mandel, Phys. Rev. Lett. **51**, 384 (1983).

[79] H. J. Kimble, M. Dagenais, and L. Mandel, Phys. Rev. Lett. **39**, 691 (1977).

[80] R. E. Slusher, L. W. Hollberg, B. Yurke, J. C. Mertz, and J. F. Valley, Phys. Rev. Lett. **55**, 2409 (1985).

[81] M. Weidinger, B. T. H. Varcoe, R. Heerlein, and H. Walther, Phys. Rev. Lett. **82**, 3795 (1999).

[82] S. Brattke, B. T. H. Varcoe, and H. Walther, Phys. Rev. Lett. **86**, 3534 (2001).

[83] B. T. H. Varcoe, S. Brattke, M. Weidinger, and H. Walther, Nature **403**, 743 (2000).

[84] Laser-cooling techniques are reviewed in *Laser Manipulation of Atoms and Ions*, edited by E. Arimondo, W. D. Phillips, and F. Strumia (North-Holland, Amsterdam, 1992).

[85] S. Haroche, M. Brune, and J. M. Raimond, Europhys. Lett. **14**, 19 (1991).

[86] C. J. Hood, M. S. Chapman, T. W. Lynn, and H. J. Kimble, Phys. Rev. Lett. **80**, 4157 (1998).

[87] G. Rempe, Appl. Phys. B, **60**, 233 (1995).

[88] R. Quadt, M. Collett, and D. F. Walls, Phys. Rev. Lett. **74**, 351 (1995).

[89] H. Mabuchi, Q. A. Turchette, M. S. Chapman, and H. J. Kimble, Opt. Lett, **21**, 1393 (1996); H. Mabuchi, J. Ye, and H. J. Kimble, Appl. Phys. B **68**, 1095 (1999).

[90] P. Münstermann, T. Fischer, P. W. H. Pinkse, and G. Rempe, Opt. Commun, **159**, 63 (1999).

[91] P. Horak, G. Hechenblaikner, K. M. Gheri, H. Stecher, and H. Ritsch, Phys. Rev. Lett. **79**, 4974 (1997); G. Hechenblaikner, M. Gangl, P. Horak, and H. Ritsch, Phys. Rev. A **58**, 3030 (1998).

[92] P. Münstermann, T. Fischer, P. Maunz, P. W. H. Pinkse, and G. Rempe, Phys. Rev. Lett. **82**, 3791 (1999).

[93] P. W. H. Pinkse, T. Fischer, P. Maunz, and G. Rempe, Nature **404**, 365 (2000).

[94] C. J. Hood, T. W. Lynn, A. C. Doherty, A. S. Parkins, and H. J. Kimble, Science **287**, 1447 (2000).

[95] B. G. Englert, J. Schwinger, A. O. Barut, and M. O. Scully, Europhys. Lett. **14**, 25 (1991).

[96] A. I. Baz, Sov. J. Nucl. Phys. **4**, 229 (1967); V. F. Rybachenko, Sov. J. Nucl. Phys. **5**, 635 (1967).

[97] P. S. Jessen and I. H. Deutsch, Adv. At. Mol. Phys. **37**, 95 (1996).

[98] M. O. Scully, G. M. Meyer, and H. Walther, Phys. Rev. Lett. **76**, 4144 (1996).

[99] G. M. Meyer, M. O. Scully, and H. Walther, Phys. Rev. A **56**, 4142 (1997).

[100] M. Löffler, G. M. Meyer, M. Schröder, M. O. Scully, and H. Walther, Phys. Rev. A **56**, 4153 (1997).

[101] M. Schröder, K. Vogel, W. P. Schleich, M. O. Scully, and H. Walther, Phys. Rev. A **56**, 4164 (1997).

[102] Ching Tsung Lee, J. Opt. Soc. Am. B **14**, 1576 (1997).

[103] Z.-M. Zhang, Z.-Y. Lu, and L.-S. He, Phys. Rev. A **59**, 808 (1999).

[104] Z.-M. Zhang and L.-S. He, Chin. Phys. Lett. **16**, 26 (1999); Z.-M. Zhang, S.-W. Xie, Y.-L. Chen, Y.-X. Xia, and S.-K. Zhou, Phys. Rev. A **60**, 3321 (1999); Z.-M. Zhang, Z.-Y. Lu, and L.-S. He, Phys. Rev. A **59**, 808 (1999).

[105] J. C. Retamal, E. Solano, and N. Zagury, Opt. Commun. **154**, 28 (1998).

[106] R. Y. Chiao and A. M. Steinberg, in *Progress in Optics*, edited by E. Wolf (Elsevier, Amsterdam, 1997), Vol. 37, p. 345 ; E. H. Hauge and J. A. Stovneng, Rev. Mod. Phys. **61**, 917 (1989); R. Landauer and Th. Martin, Rev. Mod. Phys. **66**, 217 (1994); V. S. Olkhovsky and E. Recami, Phys. Reports. **214**, 340 (1992).

[107] R. Y. Chiao, Phys. Rev. A **48**, R34 (1993); A. M. Steinberg and R. Y. Chiao, Phys. Rev. A **49**, 2071 (1994); E. Bolda, J. C. Garrison and R. Y. Chiao, Phys. Rev. A **49**, 2938 (1994).

[108] E. P. Wigner, Phys. Rev. **98**, 145 (1955).

[109] T. E. Hartmann, J. Appl. Phys. **33**, 3427 (1962).

[110] M. Büttiker and R. Landauer, Phys. Rev. Lett. **49**, 1739 (1982); M. Büttiker and R. Landauer, Phys. Scr. **32**, 429 (1985).

[111] M. Büttiker, Phys. Rev. B **27**, 6178 (1983).

[112] Pedro Pereyra, Phys. Rev. Lett. **84**, 1772 (2000).

[113] A. M. Steinberg, P. G. Kwiat, and R. Y. Chiao, Phys. Rev. Lett. **71**, 708 (1993).

[114] Ch. Spielmann, R. Szipöcs, A. Stingl, and F. Krausz, Phys. Rev. Lett. **73**, 2308 (1994).

[115] F. T. Smith, Phys. Rev. **118**, 349 (1960).

[116] H. M. Nussenzveig, Phys. Rev. A **62**, 042107 (2000).

[117] L. J. Wang, A. Kuzmich and A. Dogariu, Nature **406**, 277 (2000).

[118] C. G. B. Garrett and D. E. McCumber, Phys. Rev. A. **1**, 305 (1970).

[119] R. de L. Kronig and W. G. Penney, Proc. R. Soc. London, Ser. A **130**, 499 (1931).

[120] D. J. Griffiths and C. A. Steinke, Am. J. Phys. **69**, 137 (2001).

[121] R. Tsu and L. Esaki, Appl. Phys. Lett. **22**, 562 (1973); L. L. Chang, L. Esaki, and R. Tsu, Appl. Phys. Lett. **24**, 593 (1974).

[122] C. Perez del Valle, R. Lefebvre, and O. Atabek, Phys. Rev. A **59**, 3701 (1999).

[123] O. A. Kocharovskaya and Ya. I. Khanin, Sov. Phys. JETP Lett. **48**, 630 (1988); S. E. Harris, Phys. Rev. Lett. **62**, 1033 (1989).

[124] For a recent review, see, S. E. Harris, Phys. Today **50(7)**, 36 (1997).

[125] G. S. Agarwal, Phys. Rev. Lett. **71**, 1351 (1993).

[126] S.-Y. Zhu and M. O. Scully, Phys. Rev. A **38**, 5433 (1988).

List of Publications

I. Papers in Journals and Books:

1. *Resonant Tunneling of Ultracold Atoms through Vacuum Induced Potentials*, G. S. Agarwal and R. Arun, Phys. Rev. Lett. **84**, 5098 (2000).
2. *Mazer Action in a Bimodal Cavity*, R. Arun, G. S. Agarwal, M. O. Scully and H. Walther, Phys. Rev. A **62**, 023809 (2000).
3. *Tunneling and Traversal of Ultracold Atoms through Vacuum Induced Potentials*, R. Arun and G. S. Agarwal, Phys. Rev. A **64**, 065802 (2001).
4. *Dark States and Interferences in Cascade Transitions of Ultracold Atoms in a Cavity*, R. Arun and G. S. Agarwal, Phys. Rev. A **66**, 043812 (2002).
5. *Traversal of Ultracold Atoms through Vacuum Induced Potentials*, R. Arun and G. S. Agarwal, "7-th International Conference on Squeezed States and Uncertainity Relations (ICSSUR)", held at Boston, Massachusetts, USA, 4-8 June (2001); For details, see, http://www.physics.umd.edu/robot/

II. In Proceedings/Abstracts of International and National Conferences:

1. *Maser Action of Ultracold Atoms and Mode-Mode Correlations*, R. Arun, "Proceedings of National Laser Symposium", Pg. 265, held at University of Hyderbad, Hyderabad, India, 15-17, Dec., 1999.
2. *Tunneling of Ultracold Atoms through Vacuum Induced Potentials*, R. Arun, "International Conference on Perspectives in Theoretical Physics", Pg. 34, held at Physical Research Laboratory, Ahmedabad, India, 8-12, Jan., 2001.